3-2007

Optimal Control of a Circulare Satellite Formation Subject to Gravitational Perturbations

Jason L. Baldwin

OPTIMAL CONTROL OF A CIRCULAR SATELLITE FORMATION SUBJECT TO GRAVITATIONAL PERTURBATIONS

THESIS

Jason L. Baldwin, Captain, USAF

AFIT/GA/ENY/07-M02

DEPARTMENT OF THE AIR FORCE
AIR UNIVERSITY

AIR FORCE INSTITUTE OF TECHNOLOGY

Wright-Patterson Air Force Base, Ohio

The views expressed in this thesis are those of the author and do not reflect the official policy or position of the United States Air Force, Department of Defense, or the U.S. Government.

AFIT/GA/ENY/07-M02

OPTIMAL CONTROL OF A CIRCULAR SATELLITE FORMATION SUBJECT TO GRAVITATIONAL PERTURBATIONS

THESIS

Presented to the Faculty

Department of Aeronautics and Astronautics

Graduate School of Engineering and Management

Air Force Institute of Technology

Air University

Air Education and Training Command

In Partial Fulfillment of the Requirements for the

Degree of Master of Science in Astronautical Engineering

Jason L. Baldwin, BS

Captain, USAF

March 2007

AFIT/GA/ENY/07-M02

OPTIMAL CONTROL OF A CIRCULAR SATELLITE FORMATION SUBJECT TO GRAVITATIONAL PERTURBATIONS

Jason L. Baldwin, BS

Captain, USAF

Approved:

_____// SIGNED //_____	_____
Nathan A. Titus, Lt Col, USAF (Chairman)	Date
_____// SIGNED //_____	_____
Kerry D. Hicks, Lt Col, USAF (Member)	Date
_____// SIGNED //_____	_____
Dr. William E. Wiesel (Member)	Date

AFIT/GA/ENY/07-M02

Abstract

Satellite formations, otherwise known in the space community as satellite clusters or distributed satellite systems, have been studied extensively over the last 10 to 15 years. For use in remote sensing applications, formations consisting of smaller, simpler satellites provide numerous advantages over individual satellites. The image resolution capabilities of small-satellite formations constitute a significant technological leap in the ability to synthesize critical information.

This research utilizes the nonlinear satellite dynamics, including gravitational perturbations, to search for the optimal fuel cost for maintaining a circular formation. The system dynamics were developed in an earth-centered inertial coordinate frame using the methods of Hamiltonian dynamics. Continuous dynamic optimization theory was used to minimize fuel requirements, resulting in a continuous thrust, open-loop control law. The uncontrolled reference trajectory off which the formation is based was restricted to a circular, inclined orbit.

Given initial conditions which match the mean motion of every member of the formation, it is shown that 1-km circular formation configurations can be maintained for control costs on the order of 40-50 m/s/year at an altitude of 400 km. Additionally, further fuel savings are possible with modifications to orbit altitude, formation radius, and variations in the defined performance index.

Acknowledgements

I would like to convey my sincere thanks to Lt Col Nathan Titus, my research advisor. His insightful guidance along the way was instrumental to the success of this research effort. I would also like to thank Lt Col Kerry Hicks and Dr. William Wiesel for their help and partaking in this effort as committee members.

Jason L. Baldwin

Table of Contents

Page

List of Figures

Page

Page

List of Tables

Page

OPTIMAL CONTROL OF A CIRCULAR SATELLITE
FORMATION SUBJECT TO GRAVITATIONAL PERTURBATIONS

I. Introduction

Background

The study of satellite formations, otherwise known in the space community as satellite clusters or distributed satellite systems, has exploded over the last 10 to 15 years. For use in remote sensing applications, formations consisting of smaller, simpler satellites provide numerous advantages over their traditional counterpart, the bulky individual satellite. The image resolution capabilities of small-satellite formations constitute a significant technological leap in the ability to synthesize critical information.

Miller and Sedwick perform a thorough analysis of the various advantages achieved through the utilization of spacecraft formations (14:1-6). For example, employing smaller, simpler satellites will reduce the production and launch costs of putting vital assets in space. The need for multiple satellites that perform similar functions will also lead to mass production of these satellites, further reducing production costs. In addition to reducing costs, having multiple satellites performing the same mission provides redundancy, a luxury not often associated with space missions. The dropout or failure of one of the satellites within a cluster no longer signifies the end of the mission, as the remaining satellites within the formation can be reconfigured to compensate for the lost satellite. Finally, satellite formations provide an improvement to ground imaging applications as a direct result of the sparse aperture they create. In a

current ground-observing satellite, the resolution capabilities are restricted by the size of the mirror installed on the sensor. Satellite formations introduce sparse apertures whose data can be synthesized, resulting in much higher image resolutions. Miller and Sedwick go into further detail explaining these and many other advantages achieved with satellite formations.

Despite all the advantages satellite formations possess over individual satellites, the one disadvantage that has hindered the use of satellite formations is the excessive fuel requirements that go into maintaining the formation. The use of smaller satellites also leads to less capacity for formation-keeping fuel reserves. Until it is shown that formation-keeping fuel expenditures can be dramatically reduced through more efficient control techniques, individual satellites that can conduct the mission without the need for these fuel expenditures will continue to be employed for remote sensing applications.

An overwhelming amount of research has gone into the search for fuel efficient and minimum-fuel formation control, which will be discussed in Chapter II. Despite all this effort, very little research has been focused on studying the "true" or nonlinear dynamics when considering the optimization of this problem. One could argue that the linearized dynamics, especially in the realm of space flight, portray a very accurate representation of the actual dynamics. The study of these linearized systems has far more analytical tools than its nonlinear counterpart and produces excellent approximations over relatively short time periods when compared to the actual dynamics. For these reasons, linearizing the dynamics has been the popular approach amongst most in this field of study.

Problem Statement

This research uses the nonlinear satellite dynamics to search for an optimal solution to the minimum-fuel circular formation problem. The system dynamics will be developed in an Earth-Centered Inertial (ECI) coordinate frame using the methods of Hamiltonian dynamics. With the system dynamics in place, continuous dynamic optimization theory will be used to solve for an optimal solution to the minimum-fuel problem, and an open-loop control law based on a continuous thrust input will be developed. The uncontrolled reference trajectory off which the formation is based will be restricted to a circular, inclined orbit. In an effort to examine the long-term behavior of the formation, the search for periodic or quasi-periodic solutions to the optimization of one period of the motion will be the focus of this research.

Problem Description

This section will discuss the basics of satellite formation flight. The necessary coordinate frames are introduced and their importance to the setup of the relative motion problem is discussed. Also, circular satellite formations will be described, to include their geometry requirements and their importance to satellite formation imaging applications.

Coordinate Frames

As mentioned in the problem statement, an ECI-coordinate frame will be used to develop the equations of motion. This is a non-rotating frame which is fixed at the center of the earth as shown in Figure 1. Along with the ECI frame, another coordinate frame that is extensively used to describe the relative motion of spacecraft is the Hill frame (7).

This coordinate frame is centered on a reference trajectory, and the position and velocity of the deputy (or follower) satellites orbiting near this reference trajectory are described using this "relative" Hill frame. The Hill frame, shown and described in Figure 2, is important when discussing geometry requirements within a formation, as well as providing an excellent alternative to describing the dynamics of the formation.

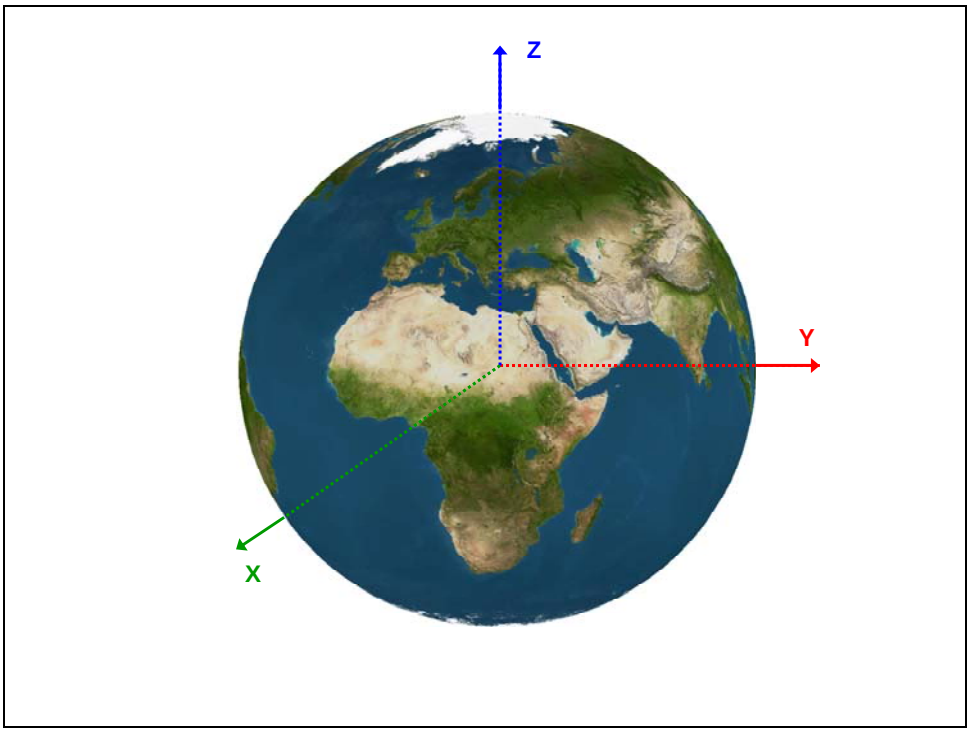

Figure 1. Earth-Centered Inertial Coordinate Frame

The need to describe the equations of motion in the ECI frame arose from the desire to include earth oblateness effects, which are a function of a satellite's geocentric latitude. These effects and their description in the dynamic model will be developed later in the paper. Initially, it was desired to derive the equations of motion in the Hill frame utilizing Hamiltonian dynamics. Unfortunately, the inertial Z-position needed to describe

the satellite's latitude induced a cross-coupling of the relative and inertial coordinates in the Hamiltonian system. Because of this, Hamilton's equations could not be developed in the relative frame, leading to the necessary development of an inertial set of equations of motion.

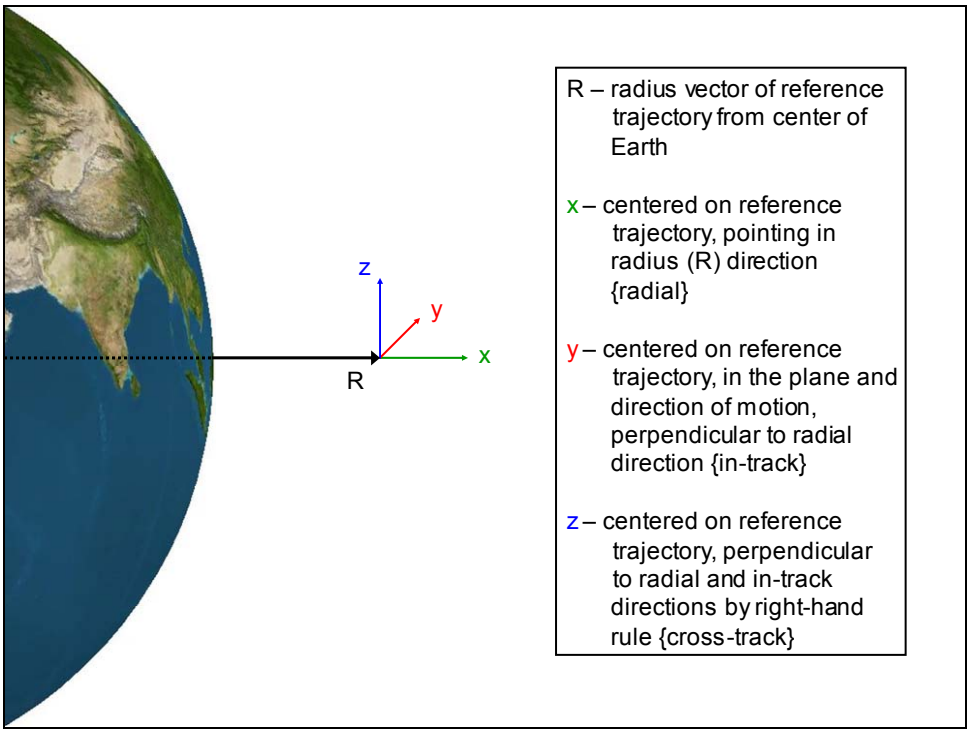

Figure 2. Relative Hill Frame

Circular Formations

There are two common circular formations currently being studied, circular and projected circular. These formations are populated by the chief satellite, which is located at the center of the circular formation, and any number of deputy satellites which are in an apparent circular orbit around the chief. The center of the circular orbit need not be a satellite, as imaging applications have no requirement for such a centered satellite.

Instead, the center of the formation is a reference trajectory that the deputies are formed about. An illustration of this type of formation can be seen in Figure 4. This research considers the formation center to be a reference trajectory.

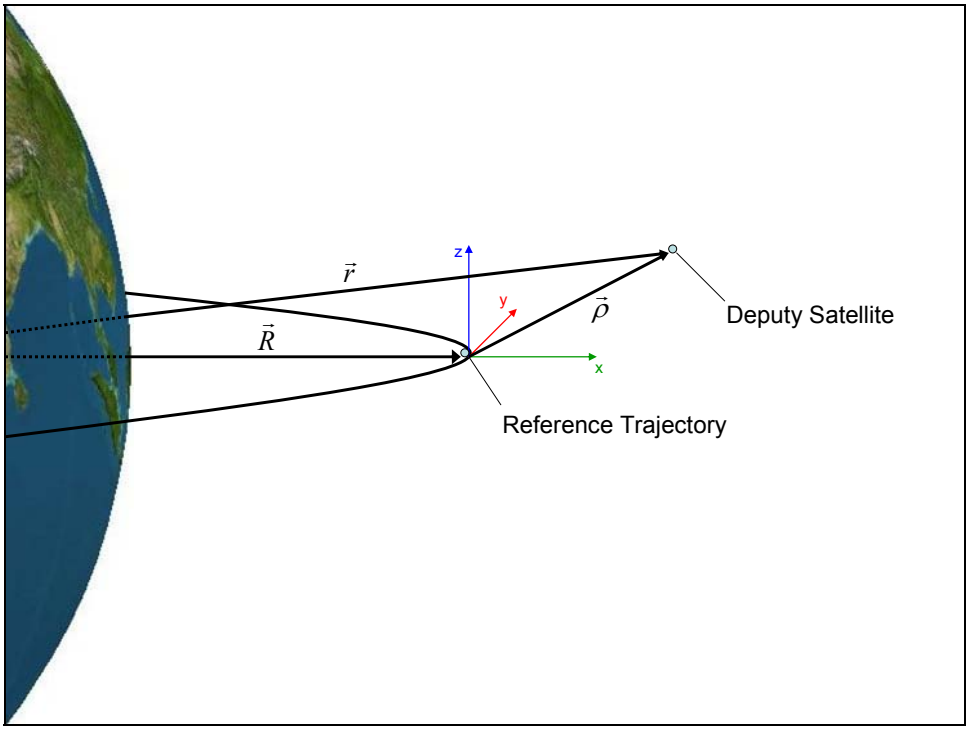

Figure 3. Formation Geometry

Sabol et al. discuss the geometry requirements in the Hill frame associated with each formation type (15:272-273). The satellite formation geometry is given by Figure 3, where $\vec{r}$ is the radius vector of a deputy satellite from the center of the earth, and $\vec{\rho}$ is the relative radius vector of the deputy with respect to the reference trajectory. A circular formation maintains a constant magnitude of the relative radius vector:

$$\rho^2 = x^2 + y^2 + z^2 \tag{1}$$

As described by this relationship, the deputy satellites maintain a constant distance from the reference trajectory. This formation structure creates a two-dimensional array whose imaging information can be synthesized, resulting in a higher resolution than each individual sensor is capable of producing. A projected circular formation is a special case of the circular formation in which a constant distance from the reference trajectory is required in the relative y-z plane:

$$\rho^2 = y^2 + z^2 \tag{2}$$

This relationship maintains a constant circular geometry projected on the surface of the earth, which also has numerous remote sensing applications.

This research is focused on the circular formation. One of the limiting factors of projected circular formations is the need to use relative coordinates in the optimization process due to the dependence on motion in the relative y-z plane. A circular formation requires a constant total distance, which can be formulated in either inertial or relative coordinates.

Perturbations and Assumptions

The existence of small perturbations, or external forces, can drastically influence the motion of orbiting space systems. This deviation from two-body motion comes in many forms to include solar radiation pressure, third-body gravity perturbations (from the Sun or Moon for example), and the zonal, sectoral, and tesseral harmonics created by non-uniformities of the orbited mass (in this case earth). These perturbations, while small in magnitude, quickly complicate the analytical representation of the system dynamics. Especially in the case of optimal control, when not only are the system states

of importance, but also the co-states, the derivation of the equations of motion can become rather intensive. Many of these external perturbations will be ignored in this formulation, keeping only those with the most significant effects on the motion of the satellite formation. Only the zonal harmonic created by the earth's equatorial bulge (J_2 perturbation) will be included in the equations of motion for this research.

Another prevalent perturbation in low-earth orbit is atmospheric drag. Drag effects induce the need for corrective thrusting for both formation keeping (maintaining the formation geometry) and station keeping (overcoming drag to maintain the satellite's orbit altitude). Assuming that each satellite in the formation has the same ballistic coefficient and that the formations are limited to relatively small separations, the drag effect on each satellite will be essentially identical, and little to no formation-keeping corrections will be required. Also, the altitude of each satellite will decay at approximately the same rate assuming small formation separation. Under these presumptions, drag effects will be ignored for this research.

II. Literature Review

Overview

Within the last 10 to 15 years, an immense amount of research has gone into the field of satellite formations. The Air Force as early as the mid 1990's began to see the possible advantages of employing a formation of satellites for sparse aperture sensing missions. In 1995, the Air Force decided to push forward with the exploration of these technologies, and in 1997, the Air Force Research Lab (AFRL) developed a space mission concept for these applications (12:1). As the Air Force began to see the importance of harnessing this new technological challenge, they began to sponsor numerous research efforts.

Along with the efforts of the Air Force, various other efforts have also gone into the study of satellite formations. Here in the United States and abroad, individuals and project teams alike have strived to understand the intricacies of this technology and in their efforts have shown that the uses for this capability are endless, yet more work is needed to show that this new method of performing space sensing and surveillance will be beneficial over current single-sensor practices.

Research

The fundamental reference in the study of the dynamics of close-proximity spacecraft is the paper by Clohessy and Wiltshire (5). In this work, the linear dynamics for a satellite rendezvous problem are derived, which are now commonly known as either the Clohessy-Wiltshire (CW) equations or Hill's equations after G.W. Hill (7). The

intrinsic value of these differential equations is the existence of a closed form solution, allowing for a description of the dynamics as functions of time. Currently, most applications involving either spacecraft rendezvous or satellite formations utilize the CW equations when developing the dynamic model, as they provide an extremely precise approximation to the actual dynamics over short time periods.

Figure 4. TechSat 21 Sparse Aperture Formation

Perhaps the most significant effort to study and understand the possibilities and capabilities of a formation of microsatellites was the TechSat 21 flight experiment conducted by AFRL in the late 1990's and early 2000's. The goal of the experiment was to launch three 150 kg satellites into a 550 km low-earth orbit (LEO) to test our current knowledge and capabilities in autonomous formation flying and sparse aperture sensing (12:2). Figure 4 is a depiction of the TechSat 21 sparse aperture formation with eight satellites in the cluster (12:1). Martin and Kilberg perform a comprehensive overview of

all the satellite systems, including the power, propulsion, and attitude control systems among others (12:5-9). Hill's equations were used to develop a dynamic model for simulation. Burns et al. also cover the propulsion and control concepts that TechSat 21 was developing (4:20-23). Unfortunately, the TechSat 21 program was canceled before it ever flew, but the research programs that spawned from its development drastically improved the state-of-the-art for formation dynamics and control.

The vast majority of the formation theory used in this paper was provided by Sabol et al. (15). This paper introduced the four main formation flying designs studied in current literature, those being the in-plane, in-track, circular, and projected circular formations. The initial conditions necessary to employ each formation design were also derived. The DSST Averaged Orbit Generator was used to propagate each formation design for one year in the presence of realistic dynamics and perturbations, and the results were presented. The advantage of using DSST is its use of mean orbital elements, which allows for quick integration over extended time periods. Once an idea of the extended behavior of each design was obtained, an analytic approach was used to solve for the fuel requirements for both formation keeping and station keeping.

Sedwick et al. conducted a comprehensive overview of the numerous sources of perturbations acting on an earth-orbiting formation (19). These forces include perturbations from the non-uniformity of the earth's mass, atmospheric drag, solar pressure, and electromagnetism. It was found that the most significant perturbation acting on an object in LEO was caused by the earth's non-uniform mass distribution, more specifically the perturbation caused by the bulging of the earth at the equator known

as the J_2 perturbation. The fuel requirements for overcoming J_2 are significantly larger than the drag requirement, and solar pressure and electromagnetic effects are minimal in LEO.

Sparks (20) used the CW equations to develop a feedback control law for projected circular formations. The methodology behind the control law consisted of a state feedback, linear quadratic controller applied to the CW equations for formation keeping of the projected circular formation. Tracking errors for the control law were limited to 50 meters over a period of three days, and the baseline propellant needed for impulsive control was given.

In addition to the numerous aspects of formation flight that have been undertaken in research, there are also several different coordinate systems and representations that have been developed in an attempt to simplify the analytic overhead of describing formation flight. The majority of these representations is linear or is accurate to first or second order at the most. These analytic developments lend themselves to closed-form solutions, as did the Clohessy-Wiltshire development. When the nonlinear approach is undertaken, the numeric integration of differential equations is nearly unavoidable.

Alfriend and Schaub (1;16) used mean Delaunay orbit elements to develop constraints that provide J_2-invariant relative orbits which are accurate to first order. These constraints implicitly restrict the values of semi-major axis, eccentricity, and inclination to eliminate the secular drift between the satellites. Schaub et al. used these mean orbital elements to develop two nonlinear feedback control laws which are shown to perform well in minimizing the tracking errors over multiple orbits (17). Vadali et al.

used the mean orbital element theory formulated by Alfriend and Schaub to develop initial conditions that result in periodic motion, and then developed a fuel-optimal, impulsive control law to maintain the formation (21).

Schweighart and Sedwick capture the effects of J_2 in a set of linear equations of motion (18). They go on to show that given the correct initial conditions, these equations have only small errors when compared to the actual nonlinear dynamics over all formation configurations. A closed-form solution to the differential equations of motion is found. This provides an excellent tool for analyzing the periodic and secular effects caused by the J_2 perturbation while also maintaining the ability to use the tools of linear theory for optimization and control applications.

Kechichian developed a full set of nonlinear differential equations to include both drag and oblateness effects (9). The derived differential equations can be numerically integrated to exactly describe relative satellite motion in the presence of only the J_2 perturbation and atmospheric drag. These equations are valid for circular and eccentric motion of the reference trajectory, although they are extremely geometry intensive.

Lovell and Tragesser (11) develop what they term "relative orbital elements," which are a change of coordinates derived from the CW equations. Both single-burn and multiple-burn impulsive guidance strategies are developed based on the relative orbital elements. The authors also look at limiting cases in the control strategies, which are a direct result of the system yielding more parameters than equations.

Wiesel uses Hamiltonian dynamics and Floquet theory to derive a description of the relative motion problem (23). This solution contains all zonal harmonics, which

makes it a much more accurate representation than the unperturbed CW equations. Very accurate comparisons are shown between the Floquet solution and numerical integrations of the actual dynamics including zonal harmonics through order and degree 14. Wiesel also shows that additional harmonics, to include sectoral and tesseral harmonics, as well as air drag can be incorporated as particular solutions to the Floquet problem. These solutions also compare very well with numerical integrations of the actual dynamics.

Kasdin and Gurfil (8) study the relative motion of spacecraft using Hamiltonian dynamics as well. They develop canonical relative motion elements that they term "epicyclic" elements. These epicyclic elements are solved for by solving the Hamilton-Jacobi equation for the linear part of the Hamiltonian, and the higher order perturbations are analyzed using a variation of parameters procedure. A closed-form solution for particular J_2-invariant orbits is obtained.

Biggs et al. expand on the work of Kasdin and Gurfil by developing a full nonlinear, relative description of satellite motion, but is only valid for motion of the reference trajectory along the geocentric equator (2). Included in this description are the J_2 zonal harmonic and nonlinear gravitational effects. This development is also valid for eccentric motion of the reference satellite, which is of significant value to formation analysis. Newton's method is then used to search for periodic solutions, which led to J_2-invariant motion. A discrete linearization was then performed on the equations of motion, and a linear quadratic regulator was utilized for closed-loop control of the formation.

Summary

Mission design pertaining to distributed satellite systems is currently a study in the trade-offs between fuel requirements and sensor position requirements. Both of these key elements have been studied exhaustively utilizing numerous dynamic representations and control techniques. The search for J_2-invariant orbits which require little to no control usage to maintain any desired formation geometry has shown promising results. This research expands on these ideas to characterize the particular orbits which necessitate the least amount of corrective control to maintain a given formation while also minimizing unnecessary drift in the formation geometry.

III. Methodology

Overview

The purpose of this chapter is to present the theory used during this research. The equations of motion derived in an ECI frame will be presented, and a numerical comparison against an industry standard package is shown. The initial conditions for the formation which guarantee matching periods of the reference trajectory and deputy satellite will be developed. With the equations of motion in hand, the co-state equations of motion will be derived utilizing continuous dynamic optimization theory. A method for solving the resulting two-point boundary value problem will be developed. Finally, a canonical scaling of the entire suite of equations of motion will be performed.

Equations of Motion

The equations of motion for this problem could have been attacked in many ways, with the two most notable solutions using Newtonian and Hamiltonian dynamics. Newtonian dynamics is founded on the force equals mass times acceleration principle, while Hamiltonian dynamics allow the equations of motion to take shape using only energy methods. This research will use Hamiltonian dynamics to derive the equations of motion for the reference trajectory, although both dynamic methods are equally powerful in this particular derivation.

Meirovitch (13:68) introduces the Lagrangian L as the difference between the kinetic and potential energies:

$$L = T - V \tag{3}$$

where T is the kinetic energy and V is the potential energy. In order to solve for the kinetic and potential energies, the position and velocity vectors of the reference trajectory at an instant in time must be defined in the ECI frame:

$$\vec{R} = [X \quad Y \quad Z] \tag{4}$$

$$\dot{\vec{R}} = [\dot{X} \quad \dot{Y} \quad \dot{Z}] \tag{5}$$

The kinetic energy of any object is defined as follows:

$$T = \frac{1}{2} m \dot{R}^2 \tag{6}$$

where m is the mass of the object. Using the previous assumption that all the satellites in the formation have the same ballistic coefficient (same cross-sectional area and mass), the Lagrangian can be described by specific kinetic and potential energies without any loss in generality. The specific kinetic energy can be represented in inertial coordinates as follows:

$$T = \frac{1}{2}\left(\dot{X}^2 + \dot{Y}^2 + \dot{Z}^2\right) \tag{7}$$

The description for the specific potential energy of an orbiting satellite including only the zonal harmonics (ignoring sectoral and tesseral harmonics) is given by Vallado and McClain (22:612):

$$V_{zonal} = \frac{\mu}{R}\left[1 - \sum_{\ell=2}^{\infty} J_\ell \left(\frac{R_\oplus}{R}\right)^\ell P_\ell\left(\sin\phi\right)\right] \tag{8}$$

where $R_\oplus$ is the equatorial radius of the earth of 6378.137 km and the specific gravitational parameter μ ignores the mass of the satellite. In this derivation, only the

second-order zonal harmonic is of interest, so setting l = 2 produces the following simplification:

$$V = -\frac{\mu}{R} + \frac{\mu J_2 R_{\oplus}{}^2}{R^3} P_2\left(\sin\phi\right) \tag{9}$$

where the dimensionless J_2 constant for the earth is 0.00108263 and ϕ is the geocentric latitude. One not-so-minor detail is the fact that all orbiting objects which are not on escape trajectories possess negative potential energies (22:612), resulting in the sign change reflected in Eq. (9). To finish representing the potential energy in inertial coordinates, an inertial description of the second-order Legendre polynomial P_2 must be found. Vallado and McClain (22:517) describe the second-order Legendre polynomial in terms of geocentric latitude as follows:

$$P_2\left(\sin\phi\right) = \frac{1}{2}\left(3\sin^2\phi - 1\right) \tag{10}$$

Vallado and McClain (22:553) also recognize that the geocentric latitude of a satellite can be described using inertial coordinates:

$$\sin\phi = \frac{Z}{R} \tag{11}$$

Substituting these results into Eq. (9), the expanded final form for the potential energy including the J_2 harmonic of an orbiting satellite is given:

$$V = -\frac{u}{R} + \frac{3\mu J_2 R_{\oplus}{}^2 Z^2}{2R^5} - \frac{\mu J_2 R_{\oplus}{}^2}{2R^3} \tag{12}$$

The Lagrangian can now be formed using the kinetic and potential energies. Substituting inertial coordinates in for the radius, the Lagrangian can be represented entirely in inertial coordinates:

$$L = \frac{1}{2}(\dot{X}^2 + \dot{Y}^2 + \dot{Z}^2) + \frac{\mu}{\left(X^2 + Y^2 + Z^2\right)^{1/2}} - \frac{3\mu J_2 R_\oplus{}^2 Z^2}{2\left(X^2 + Y^2 + Z^2\right)^{5/2}} + \frac{\mu J_2 R_\oplus{}^2}{2\left(X^2 + Y^2 + Z^2\right)^{3/2}} \tag{13}$$

Now that the Lagrangian is in hand, the system momenta can be solved for. Given a Lagrangian composed of specific energies, the system momenta should be equal to the inertial velocities. Meirovitch (13:82) defines the generalized system momenta P_i as follows, where in this derivation the generalized coordinates q_i were chosen as the inertial coordinates:

$$P_i = \frac{\partial L}{\partial \dot{q}_i} \tag{14}$$

Performing these partial derivatives reveals that, yes indeed, the system momenta are equivalent to the inertial velocities:

$$P_X = \dot{X} \tag{15}$$

$$P_Y = \dot{Y} \tag{16}$$

$$P_Z = \dot{Z} \tag{17}$$

With the system momenta and the Lagrangian, the system Hamiltonian H can now be derived. Meirovitch (13:94) defines the Hamiltonian as follows:

$$H = \sum_{i=1}^{3}\left(P_i \dot{q}_i\right) - L \tag{18}$$

Meirovitch also states that the system Hamiltonian must not include any generalized velocities in its final form, as they must be substituted for with the system momenta. In this case, the two are equal, so a simple substitution reveals the following Hamiltonian:

$$H = P_X{}^2 + P_Y{}^2 + P_Z{}^2 - L \tag{19}$$

Plugging in the Lagrangian that has already been derived and combining momentum terms, the final system Hamiltonian including the J_2 harmonic for an orbiting satellite is given:

$$H = \frac{1}{2}(P_X{}^2 + P_Y{}^2 + P_Z{}^2) - \frac{\mu}{\left(X^2 + Y^2 + Z^2\right)^{1/2}} + \frac{3\mu J_2 R_\oplus{}^2 Z^2}{2\left(X^2 + Y^2 + Z^2\right)^{5/2}} - \frac{\mu J_2 R_\oplus{}^2}{2\left(X^2 + Y^2 + Z^2\right)^{3/2}} \tag{20}$$

Meirovitch shows that finding Hamilton's equations of motion is a simple matter of taking partial derivatives of the Hamiltonian (13:94). These partial derivates take the following form:

$$\dot{q}_i = \frac{\partial H}{\partial P_i} \tag{21}$$

$$\dot{P}_i = -\frac{\partial H}{\partial q_i} \tag{22}$$

Calculating these partial derivatives, Hamilton's equations of motion including the J_2 harmonic for an orbiting satellite are given:

$$\dot{X} = P_X \tag{23}$$

$$\dot{Y} = P_Y \tag{24}$$

$$\dot{Z} = P_Z \tag{25}$$

$$\dot{P}_X = -\frac{\mu X}{\left(X^2 + Y^2 + Z^2\right)^{3/2}} - \frac{3\mu J_2 R_\oplus{}^2 X}{2\left(X^2 + Y^2 + Z^2\right)^{5/2}} + \frac{15\mu J_2 R_\oplus{}^2 X Z^2}{2\left(X^2 + Y^2 + Z^2\right)^{7/2}} \tag{26}$$

$$\dot{P}_Y = -\frac{\mu Y}{\left(X^2+Y^2+Z^2\right)^{3/2}} - \frac{3\mu J_2 R_\oplus{}^2 Y}{2\left(X^2+Y^2+Z^2\right)^{5/2}} + \frac{15\mu J_2 R_\oplus{}^2 Y Z^2}{2\left(X^2+Y^2+Z^2\right)^{7/2}} \tag{27}$$

$$\dot{P}_Z = -\frac{\mu Z}{\left(X^2+Y^2+Z^2\right)^{3/2}} - \frac{9\mu J_2 R_\oplus{}^2 Z}{2\left(X^2+Y^2+Z^2\right)^{5/2}} + \frac{15\mu J_2 R_\oplus{}^2 Z^3}{2\left(X^2+Y^2+Z^2\right)^{7/2}} \tag{28}$$

Since the momenta are equivalent to the inertial velocities, the derivatives of the momenta $\dot{P}_i$ are equivalent to the inertial accelerations. This is important because the thruster (control) accelerations can simply be added on to the deputy satellite's equations of motion. See Appendix A for a complete listing of the equations of motion.

Validation of the Equations of Motion

Vallado and McClain (22:553-554) similarly derive the accelerations by solving for the gradient of the J_2-simplified disturbing function, reaching the same results that have just been shown using Hamiltonian dynamics. Since this research is *numerically* searching for optimal solutions of the equations of motion utilizing the ODE-45 integration algorithm in Matlab®, it was also desired to compare the equations of motion integrated with Matlab against the numerical integration routines of Satellite Tool Kit® (STK).

It was desired for the two algorithms to differ only to the meter level over one period of the motion. Achieving this result should preclude any questions regarding the validity of the equations of motion and the accuracy of Matlab's ability to numerically propagate them. A comparison of the two algorithms over a 12-hour period is shown in Figure 5. This figure compares the inertial coordinates of a circular orbit with an altitude of 400 km and an inclination of 45 degrees. The HPOP STK numerical propagator was

used, and the gravity model was adjusted to only include J_2 effects. It can be seen that the two numerical schemes remain comparable to the 100-meter level in position after multiple periods of the motion, which is precise enough to validate both the equations of motion and the choice of numerical schemes.

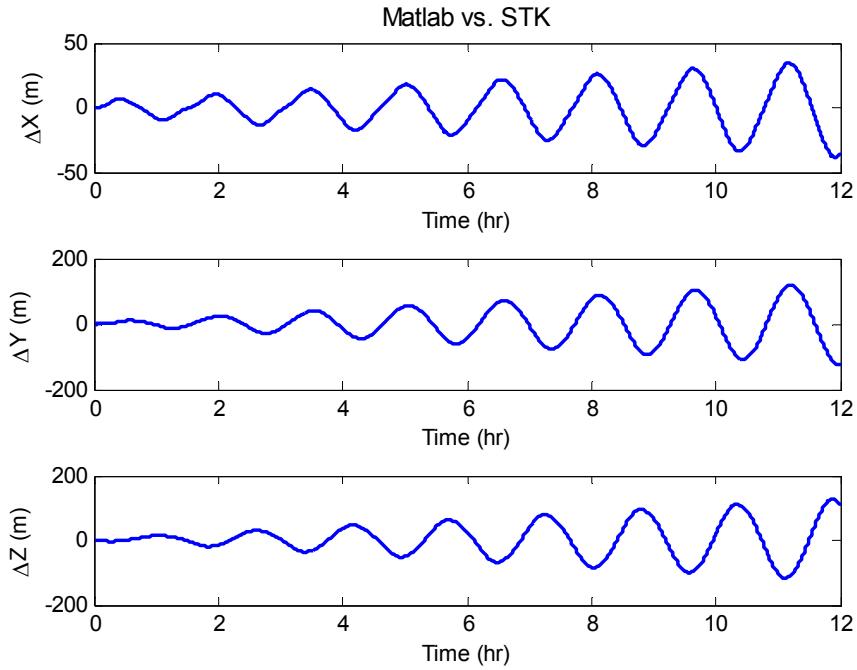

Figure 5. Matlab and STK Numerical Algorithm Comparison

Initial Conditions for Deputy Satellite

Finding or forcing periodic motion drives the selection of the initial conditions for the deputy satellites. If the periods of the reference trajectory and the deputy satellites don't match, analysis over one or multiple periods of the motion becomes subjective on the choice of periods. Also, extrapolating an approximation of the long-term behavior from optimization over limited periods of the motion becomes impossible if the periods

of the reference trajectory and the relative formation trajectory don't match. Essentially, it is desired to find initial conditions for the deputy satellites that guarantee equal periods for both relative and inertial motion.

Sabol et al. (15:272) geometrically derives the following relative initial conditions that induce circular relative motion of the deputy satellite:

$$x_0 = (r_d / 2)\cos\theta \tag{29}$$

$$\dot{x}_0 = -(r_d n / 2)\sin\theta \tag{30}$$

$$y_0 = 2\dot{x}_0 / n \tag{31}$$

$$\dot{y}_0 = -2nx_0 \tag{32}$$

$$z_0 = \pm\sqrt{3}x_0 \tag{33}$$

$$\dot{z}_0 = \pm\sqrt{3}\dot{x}_0 \tag{34}$$

where r_d is the desired radius of the circular formation, n is the mean motion of the reference trajectory, and θ is the phase angle of the deputy within the circle. Sabol et al. also mention that these initial conditions do not produce the same semi-major axis for both the reference and deputy orbits. This fact will result in differing orbital periods, and must be corrected. Sabol et al. does correct the semi-major axes to the same value to match the periods, but does not disclose the methodology in doing so.

If it is assumed that the deputy satellite starts at its apogee point, then the radial velocity $\dot{x}_0$ is known to be zero. The phase angle is set such that any radial velocity is eliminated, revealing that the following derivation is valid only if the phase angle equals 0 or 180 degrees. Figure 6 shows a representation of the relative orbit starting with a

phase of zero degrees. The center cross represents the reference trajectory and the cross on the orbit path represents the starting point (initial conditions) for the deputy satellite.

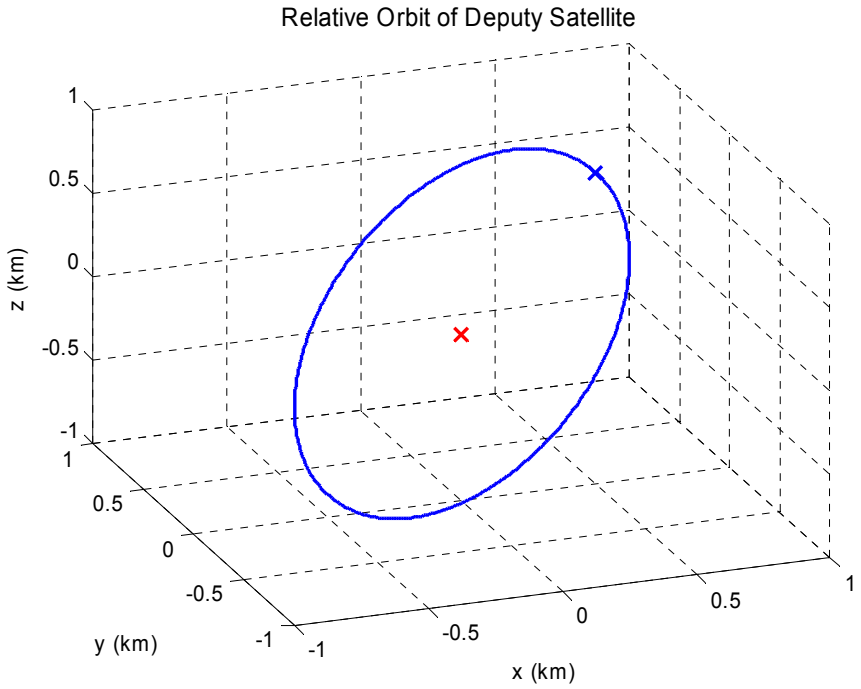

Figure 6. Relative Orbit of Deputy Satellite with Phase = 0 deg

With the assumptions of phase angle equal to 0 or 180 degrees and zero radial velocity, the initial relative positions of the deputy satellite are simplified:

$$x_0 = \pm\frac{r_d}{2} \tag{35}$$

$$y_0 = 0 \tag{36}$$

$$z_0 = \pm\sqrt{3}x_0 = \pm\frac{\sqrt{3}}{2}r_d \tag{37}$$

For a phase angle of zero degrees, the signs of both x_0 and z_0 are positive, and for a phase angle of 180 degrees both signs are negative to maintain the same relative orbit. The following derivation will set the phase angle equal to zero.

Phase Angle of Zero Degrees

With the phase angle set equal to zero, the following are the initial relative positions of the deputy satellite:

$$x_0 = \frac{r_d}{2} \tag{38}$$

$$y_0 = 0 \tag{39}$$

$$z_0 = \frac{\sqrt{3}}{2} r_d \tag{40}$$

The inertial position vector of the deputy satellite can be represented in the Hill frame in the following form:

$$\vec{r} = (R + \frac{1}{2} r_d)\hat{x} + \frac{\sqrt{3}}{2} r_d \hat{z} \tag{41}$$

After simplifying, the magnitude of the inertial position vector is as follows:

$$r = \sqrt{R^2 + R r_d + r_d^{\,2}} \tag{42}$$

In order to match the periods of the reference orbit and the orbit of the deputy satellite, the energies of the orbits must be matched. The energy of the deputy satellite and the energy of the reference orbit, respectively, are as follows:

$$\varepsilon_1 = \frac{1}{2} v^2 - \frac{\mu}{\sqrt{R^2 + R r_d + r_d^{\,2}}} \tag{43}$$

$$\varepsilon = \frac{-\mu}{2R}. \tag{44}$$

The only unknown term in these equations is *v*, the magnitude of the deputy's inertial velocity vector. Setting the two energies equal and solving for *v*, the following result is achieved:

$$v = \sqrt{\frac{2\mu}{\sqrt{R^2 + Rr_d + r_d^{\,2}}} - \frac{\mu}{R}} \tag{45}$$

Now the direction of the velocity must be determined. Referring to Eq. (34), it can be seen that the choice of setting $\dot{x}_0$ equal to zero (at apogee) also implies that $\dot{z}_0$ is equal to zero. Because of this fact, the only necessary correction to the initial conditions given by Sabol et al. is in the in-track velocity $\dot{y}_0$. The resultant initial position and velocity vectors of the deputy satellite from the center of the earth represented in the Hill frame are given:

$$\vec{r} = (R + \frac{1}{2} r_d)\hat{x} + \frac{\sqrt{3}}{2} r_d \hat{z} \tag{46}$$

$$\vec{v} = \sqrt{\frac{2\mu}{\sqrt{R^2 + Rr_d + r_d^{\,2}}} - \frac{\mu}{R}}\ \hat{y} \tag{47}$$

If the phase angle had been set to 180 degrees, only a few sign changes would have affected the result of the previous development.

Phase Angle of 90 Degrees

In order to populate the formation with more than two deputy satellites, as well as study the effects of starting at multiple points in the formation, it is necessary to derive the initial conditions for phases of 90 and 270 degrees. This would permit four deputy

satellites into the formation. The following derivation is for a phase angle of 90 degrees, where just like before, the conversion to 270 degrees is just a matter of sign changes.

Once again starting with the initial conditions from Sabol et al., an initial phase angle of 90 degrees reduces the initial conditions to the following:

$$x_0 = 0 \tag{48}$$

$$\dot{x}_0 = -\frac{r_d n}{2} \tag{49}$$

$$y_0 = -r_d \tag{50}$$

$$\dot{y}_0 = 0 \tag{51}$$

$$z_0 = 0 \tag{52}$$

$$\dot{z}_0 = -\frac{\sqrt{3}}{2} r_d n \tag{53}$$

To solve for initial conditions for a phase angle of 270 degrees, just change all signs to positive and proceed with the following derivation. As before, the periods of the relative orbit and the reference trajectory orbit are not matched. To align the periods, the energies of the orbits must be matched. The inertial position vector of the deputy satellite represented in the Hill frame is as follows:

$$\vec{r} = R\hat{x} - r_d \hat{y} \tag{54}$$

This easily simplifies to solve for the magnitude of the inertial position vector:

$$r = \sqrt{R^2 + {r_d}^2} \tag{55}$$

The energies of both orbits can then be represented as follows:

$$\varepsilon_1 = \frac{1}{2}v^2 - \frac{\mu}{\sqrt{R^2 + r_d{}^2}} \tag{56}$$

$$\varepsilon = \frac{-\mu}{2R}. \tag{57}$$

Solving for the magnitude of the inertial velocity vector of the deputy, the following velocity magnitude will match the energies:

$$v = \sqrt{\frac{2\mu}{\sqrt{R^2 + r_d{}^2}} - \frac{\mu}{R}} \tag{58}$$

Unlike the case for phase equal to zero degrees, where all the velocity was in the relative $\hat{y}$ direction, this case has velocity components in all three relative directions. To solve for the inertial velocity vector, a unit vector for the inertial velocity can be found in the relative frame and multiplied by the necessary magnitude v. The inertial velocity vector can be represented as follows:

$$\dot{\vec{r}} = \frac{{}^{\hat{i}}d}{dt}\left(\vec{r}\right) = \frac{{}^{\hat{i}}d}{dt}\left(R\hat{x} - r_d\hat{y}\right) \tag{59}$$

The inertial derivative of the deputy's position vector has two components, translational (derivative in the relative frame) and angular:

$$\frac{{}^{\hat{i}}d}{dt}\left(R\hat{x} - r_d\hat{y}\right) = \frac{{}^{\hat{o}}d}{dt}\left(R\hat{x} - r_d\hat{y}\right) + \vec{\omega}_{o/i} \times \left(R\hat{x} - r_d\hat{y}\right) \tag{60}$$

where $\vec{\omega}_{o/i}$ is the angular velocity of the relative frame with respect to the inertial frame. In this situation, that's just the mean motion $\vec{n}$ of the reference trajectory, represented in the relative frame as $n\hat{z}$.

After performing the cross product and simplifying terms, the following is the result for the inertial velocity vector represented in the relative Hill frame:

$$\dot{\vec{r}} = \frac{r_d n}{2}\hat{x} + nR\hat{y} - \frac{\sqrt{3}}{2} r_d n\hat{z} \tag{61}$$

The final inertial velocity vector which matches the orbital periods for the reference trajectory and the relative orbit of the deputy satellite is the necessary magnitude v multiplied by the unit vector of the previous result:

$$\vec{v} = v\frac{\dot{\vec{r}}}{\left\|\dot{\vec{r}}\right\|} \tag{62}$$

The previous developments treated each phase angle independently while solving for the resulting initial conditions. Appendix D provides a general derivation for any choice of phase angle within the formation.

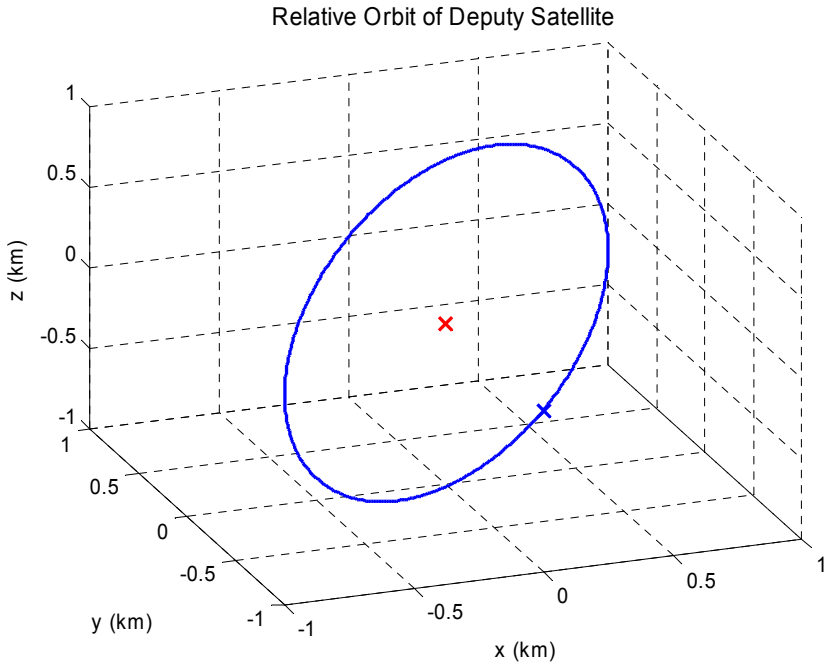

Figure 7. Relative Orbit of Deputy Satellite with Phase = 90 deg

Continuous Dynamic Optimization

The solution methods for dynamic optimization of nonlinear continuous systems with fixed final time and free final state are well documented in Bryson and Ho (3:47-49). Solving for the optimal solution to continuous, dynamic systems is a problem in the calculus of variations, covered by Gelfand (6) in great detail. The following is a brief overview of the setup covered by Bryson and Ho for fixed final time, free final state optimization of dynamic systems. Just a note, do not confuse any of the terminology to follow (such as Hamiltonian, Lagrangian, etc.) with the previous derivation of the equations of motion. Their appearances in this derivation, although based on the same premise, are distinctly different representations.

The continuous dynamic system is generically defined as an n-dimensional set. In this case, there are six inertial states, hence the system is six-dimensional, and they can be represented as follows:

$$\dot{\vec{x}}(t) = f[\vec{x}(t), \vec{u}(t), t] \tag{63}$$

where $\vec{x}\,(t)$ represents the inertial states of the system and $\vec{u}\,(t)$ represents the continuous thrust inputs in the three inertial directions of the deputy satellite shown below:

$$\vec{u} = \begin{bmatrix} u_X \\ u_Y \\ u_Z \end{bmatrix} \tag{64}$$

Given this system, it is desired to minimize an overall performance index J (also known as a cost function) of the following form:

$$J = \phi[\vec{x}(t_f), t_f] + \int_{t_0}^{t_f} L[\vec{x}(t), \vec{u}(t), t]dt \tag{65}$$

In this form, the Lagrangian L is the incremental cost along the trajectory which is integrated over the entire trajectory, and ϕ is the cost associated with the final states of the system.

Next, the constraints of the system must be adjoined to the performance index. In this case, the only constraints imposed on the system are the equations of motion themselves. These constraints are added to the performance index via a vector of Lagrange multipliers λ:

$$J = \phi[\vec{x}(t_f), t_f] + \int_{t_0}^{t_f} \left(L[\vec{x}(t), \vec{u}(t), t] + \vec{\lambda}^T(t)\{f[\vec{x}(t), \vec{u}(t), t] - \dot{\vec{x}}\} \right) dt \tag{66}$$

The transpose on the Lagrange multiplier vector is simply to match dimensions. The performance index can be simplified by introducing the Hamiltonian H, which takes the following form:

$$H[\vec{x}(t), \vec{u}(t), \vec{\lambda}(t), t] = L[\vec{x}(t), \vec{u}(t), t] + \vec{\lambda}^T(t) f[\vec{x}(t), \vec{u}(t), t] \tag{67}$$

After substituting the Hamiltonian into the performance index, integration by parts can be performed to achieve the following result:

$$\begin{aligned} \overline{J} = {} & \phi[\vec{x}(t_f), t_f] - \vec{\lambda}^T(t_f)\vec{x}(t_f) + \vec{\lambda}^T(t_0)\vec{x}(t_0) \\ & + \int_{t_0}^{t_f} \left(H[\vec{x}(t), \vec{u}(t), \vec{\lambda}(t), t] + \dot{\vec{\lambda}}^T(t)\vec{x}(t) \right) dt \end{aligned} \tag{68}$$

Now the variation in the performance index $\bar{J}$ must be taken due to infinitesimal variations in the control vector $\delta\vec{u}$, which also produce variations in the inertial state vector $\delta\vec{x}$. These variations are taken at fixed times t_f and t_0:

$$\delta\bar{J} = \left[\frac{\partial\phi}{\partial\vec{x}} - \vec{\lambda}^T\right]\delta\vec{x}_{t=t_f} + \vec{\lambda}^T\delta\vec{x}_{t=t_0} + \int_{t_0}^{t_f}\left(\left[\frac{\partial H}{\partial\vec{x}} + \dot{\vec{\lambda}}^T\right]\delta\vec{x} + \frac{\partial H}{\partial\vec{u}}\delta\vec{u}\right)dt \tag{69}$$

To force the variations *δx(t)* to vanish, two necessary conditions arise. These necessary conditions are given below:

$$\dot{\vec{\lambda}}^T(t) = -\frac{\partial H}{\partial\vec{x}} \tag{70}$$

$$\vec{\lambda}^T(t_f) = \frac{\partial\phi}{\partial\vec{x}} \tag{71}$$

Eq. (71) is essentially a boundary condition of Eq. (70). With these two necessary conditions in place, the variation of the performance index is reduced to the following form:

$$\delta\bar{J} = \vec{\lambda}^T\delta\vec{x}_{t=t_0} + \int_{t_0}^{t_f}\frac{\partial H}{\partial\vec{u}}\delta\vec{u}\;dt \tag{72}$$

To find a minimum value (extremum) of the performance index, $\delta\bar{J}$ must be zero for any arbitrary value of $\delta\vec{u}$. This is only possible given the following condition, which is commonly known as the optimality condition:

$$\frac{\partial H}{\partial\vec{u}} = 0 \tag{73}$$

Eqs. (70), (71), and (73) complete the first-order solution to the continuous dynamic optimization problem, and are known as the Euler-Lagrange equations in the calculus of variations.

To summarize, the existence of an extremum for the continuous dynamic optimization problem is shown utilizing the calculus of variations. This extremum is found through the choice of an appropriate control vector $\vec{u}$. The equations which produce this extremum, which are shown in full below, are the first-order necessary conditions for an extremum of the chosen performance index (3:49). In order to guarantee that the derived solution is a local extremum, the second-order necessary or sufficient conditions covered by Bryson and Ho must also be validated to avoid saddle and inflection points in the design space (3:50). For the purposes of this research, where the actual value of the performance index subject to changes in the control vector $\delta\vec{u}$ can be analyzed real-time during the iteration process, implementing the second-order conditions would be redundant.

$$\dot{\vec{x}}(t) = f[\vec{x}(t), \vec{u}(t), t] \tag{74}$$

$$\dot{\vec{\lambda}}(t) = -\left(\frac{\partial H}{\partial \vec{x}}\right)^T \tag{75}$$

$$\frac{\partial H}{\partial \vec{u}} = 0 \tag{76}$$

$$\vec{x}(t_0) \quad given \tag{77}$$

$$\vec{\lambda}(t_f) = \left(\frac{\partial \phi}{\partial \vec{x}}\right)^T \tag{78}$$

Performance Index and Co-State Equations of Motion

For this study, it is desired to minimize three quantities. First, the amount of fuel consumed during the control process must be minimized. Second, maintaining

sufficiently little satellite drift from the desired separation of the circular formation is desired. Finally, given the initial conditions of the deputy satellite, it is desired for the final conditions after one orbit to match as closely as possible to the desired initial conditions of the deputy's second orbit. Not matching these conditions precludes the analysis of the long-term behavior of the formation, so it must be added to the performance index.

The first two conditions are constantly evolving over the path of one orbit. For this reason, satellite drift and fuel effects must be integrated over the whole trajectory, and hence make up the Lagrangian of the performance index:

$$L = k_1 \left[\left\| \vec{r} - \vec{R} \right\| - r_d \right]^2 + k_2 \left\| \vec{u} \right\|^2 \tag{79}$$

In the Lagrangian, the constants k_1 and k_2 are weighting factors, which numerically add more effort to minimizing one element of the performance index over another. Given this form of the Lagrangian, and remembering the implementation of the Hamiltonian from Eq. (67), the following is the Hamiltonian expressed in inertial coordinates:

$$\begin{aligned} H = {} & k_1 \left[\sqrt{(X - X_R)^2 + (Y - Y_R)^2 + (Z - Z_R)^2} - r_d \right]^2 + k_2 \left[u_X{}^2 + u_Y{}^2 + u_Z{}^2 \right] \\ & + \begin{bmatrix} \lambda_X & \lambda_Y & \lambda_Z & \lambda_{P_X} & \lambda_{P_Y} & \lambda_{P_Z} \end{bmatrix} \begin{bmatrix} \dot{X} \\ \dot{Y} \\ \dot{Z} \\ \dot{P}_X \\ \dot{P}_Y \\ \dot{P}_Z \end{bmatrix} \end{aligned} \tag{80}$$

where $\vec{r} = (X, Y, Z)$ and $\vec{R} = (X_R, Y_R, Z_R)$. Notice that the equations of motion for the reference trajectory are not included in the Hamiltonian. Since the reference trajectory is

uncontrolled, the Lagrange multipliers for the reference trajectory would have no influence on the motion. This point will become clearer as the derivation progresses. To finalize the Hamiltonian, the equations of motion for the deputy must be substituted in before the partial derivatives can be taken. The Hamiltonian, written fully in inertial coordinates, is given in Appendix B.

The co-state equations of motion, given by Eq. (75), are a simple yet tedious matter of taking partial derivatives of the Hamiltonian. The software package Mathematica® was used to calculate the necessary partial derivatives, and the results are given in Appendix B. These co-state equations almost complete the set of necessary equations of motion to solve the dynamic optimization problem. The only issue that still persists is the existence of more variables than equations.

To alleviate this issue, the optimality condition given in Eq. (76) is used to solve for the control vector $\vec{u}$ in terms of the Lagrange multipliers. The three optimality conditions are given below:

$$\frac{\partial H}{\partial u_X} = 2k_2 u_X + \lambda_{P_X} = 0 \tag{81}$$

$$\frac{\partial H}{\partial u_Y} = 2k_2 u_Y + \lambda_{P_Y} = 0 \tag{82}$$

$$\frac{\partial H}{\partial u_Z} = 2k_2 u_Z + \lambda_{P_Z} = 0 \tag{83}$$

It can be seen that the control inputs are easily solvable in terms of the Lagrange multipliers. This allows for substitution of the results for $\vec{u}$ into the equations of motion, and the problem is reduced to 18 equations of 18 unknown variables, which are the six

states of the reference trajectory, the six states of the deputy, and the six Lagrange multipliers of the deputy. This further vindicates the earlier stated fact that the equations of motion for any uncontrolled trajectory are unnecessary in the Hamiltonian, as the Lagrange multipliers for those equations of motion are of no significance.

The last condition to meet was to have the final conditions of one orbit match the desired initial conditions of the next orbit. Two solutions were attempted to attack this problem. During the derivation of the initial conditions for the deputy satellite, the energies of the reference trajectory and the deputy were set equivalent to match the periods. Initially, it was believed that matching the energies at time t_f would drive the deputy to the new set of desired initial conditions. This methodology was unsuccessful, as it was easy numerically to match the energies, but was failing to drive the final conditions to the desired values. The second method used the known desired initial conditions of the deputy's next orbit as boundary conditions at time t_f. The cost of the performance index at time t_f can be represented as

$$\phi[\vec{x}(t_f), t_f] = k_3 \begin{bmatrix} \{X(t_f) - X_{bc}\}^2 + \{Y(t_f) - Y_{bc}\}^2 + \{Z(t_f) - Z_{bc}\}^2 \\ + \{P_X(t_f) - P_{X_{bc}}\}^2 + \{P_Y(t_f) - P_{Y_{bc}}\}^2 + \{P_Z(t_f) - P_{Z_{bc}}\}^2 \end{bmatrix}, \tag{84}$$

where once again the constant k_3 is a weighting factor and the subscript *bc* signifies the boundary condition states. This method produced promising results, as driving this quantity to zero produced the desired initial conditions of the deputy for successive orbits.

The performance index is now defined in full for this problem. The Euler-Lagrange equations provide final boundary conditions for the Lagrange multipliers given

by Eq. (78), but their initial values which propagate to the final boundary conditions are unknown. This presents a class of problems known as two-point boundary value problems.

Solving the Two-Point Boundary Value Problem

The two-point boundary value problem for this research consists of known initial states which can be propagated forward to find the end states at some chosen period time t_f. With the end states in hand, the boundary conditions for the Lagrange multipliers can be calculated. The initial Lagrange multipliers which result in meeting the final boundary conditions are unknown. Bryson and Ho cover numerous algorithms that can solve this class of problems (3:212-228). The method chosen for this research because of its simplicity is the forward shooting method utilizing direct numerical differentiation.

The forward shooting method uses a transition-matrix algorithm, initialized by guessing the initial values for the Lagrange multipliers. From here, the equations of motion and co-state equations of motion are propagated forward to time t_f and the resulting final Lagrange multipliers are compared against the known final boundary conditions. This comparison is used to form a new guess for the initial Lagrange multipliers, and the process is repeated until the final conditions are matched. Below is the step-by-step approach laid out by Bryson and Ho, modified to solve this particular problem (3:215-217).

Step 1: Guess the unknown initial Lagrange multipliers $\lambda(t_0)$.

Step 2: Integrate Eqs. (74) and (75) forward from t_0 to t_f and record the resulting final Lagrange multipliers $\vec{\varphi}(t_f)$.

Step 3: Determine the transition matrix which relates small changes in the initial guess to small changes in the final conditions

$$\delta\vec{\varphi}(t_f) = \begin{bmatrix} \delta\lambda_X \\ \delta\lambda_Y \\ \delta\lambda_Z \\ \delta\lambda_{P_X} \\ \delta\lambda_{P_Y} \\ \delta\lambda_{P_Z} \end{bmatrix} = \frac{\partial\vec{\varphi}(t_f)}{\partial\vec{\lambda}(t_0)}\delta\vec{\lambda}(t_0) \tag{85}$$

where the transition matrix is given by

$$\frac{\partial\vec{\varphi}(t_f)}{\partial\vec{\lambda}(t_0)} \tag{86}$$

Step 4: Choose $\delta\vec{\varphi}(t_f)$ in order to bring the next iteration closer to the desired values $\vec{\varphi}_{bc}$, given by

$$\delta\vec{\varphi}(t_f) = -\varepsilon\left[\vec{\varphi}(t_f) - \vec{\varphi}_{bc}\right], \qquad 0 < \varepsilon \leq 1 \tag{87}$$

Step 5: With the chosen values of $\delta\vec{\varphi}(t_f)$, the new initial guess for $\vec{\lambda}(t_0)$ can be calculated from Eq. (85) as follows:

$$\delta\vec{\lambda}(t_0) = \left[\frac{\partial\vec{\varphi}(t_f)}{\partial\vec{\lambda}(t_0)}\right]^{-1}\delta\vec{\varphi}(t_f) \tag{88}$$

Step 6: Using the following equation:

$$\vec{\lambda}(t_0)_{new} = \vec{\lambda}(t_0)_{old} + \delta\vec{\lambda}(t_0) \tag{89}$$

repeat Steps 1-5 until $\vec{\varphi}(t_f)$ has the desired values to some specified accuracy.

The transition matrix given by Eq. (86) is formulated utilizing direct numerical differentiation. Direct numerical differentiation requires as many additional integrations of the equations of motion and co-state equations as there are Lagrange multipliers, in this case six. One at a time, each initial Lagrange multiplier $\lambda_i(t_0)$ is changed by some small amount $\delta\lambda_i(t_0)$ from the initial guess. The equations of motion and co-states are integrated, and the resulting change in final conditions $\delta\vec{\varphi}(t_f)$ is recorded and divided by the chosen $\delta\lambda_i(t_0)$. After completing all six integrations, the transition matrix is formed. Bryson and Ho (3:217) cover the process in more detail and also discuss the inherent difficulties with the approach. Lewis and Syrmos provide sample code for solving the two-point boundary value problem using both direct numerical differentiation and another robust algorithm known as the backward-sweep method (10:521-527).

Canonical Formulation

One common difficulty in numerically optimizing dynamic systems is scaling. With the equations of motion and the co-state equations of motion finalized, sample runs were performed to test the code's reliability. Unfortunately, in its current form, the code would only converge for time spans of a few seconds. The numerics of the current formulation, in particular the vastly differing orders of magnitude represented by terms in the equations of motion, made the integration impossible over relatively long time periods. To assuage this problem, a canonical formulation of the problem had to be developed.

For this problem, it was chosen to scale the position (distance) and velocity (speed) units by parameters of the reference trajectory. Distance units (DU) were chosen as the semi-major axis of the two-body motion of the reference trajectory. Speed units, explicitly stated as distance units per time units (DU/TU), were chosen to be the two-body circular orbit velocity of the reference trajectory. Given these parameters, the gravitational parameter μ becomes unity and the two-body period of the motion becomes 2π, cornerstones of the common canonical formulation in orbital dynamics. After scaling all the parameters of the problem, attempts to run the code to convergence over one two-body period of the reference trajectory motion were successful.

IV. Analysis and Results

Chapter Overview

This chapter provides an overview of the critical perturbing effects of the J_2 zonal harmonic and their applications in this research. Due to these effects, the choice of periods of the motion over which to optimize is examined, with the final choice being directly correlated to the perturbing effects on the reference trajectory. In order to gauge the long-term behavior and necessary control histories for the formation, it will be shown that there is an inherent quasi-periodic nature in the relative control histories. This will allow for an approximation of the annual ΔV requirements needed to maintain the desired formation separation. Finally, results of the optimization are presented in a case study format to develop fundamental trends in the ΔV requirements based on differing orbital parameters and initial conditions.

J_2 Effects and the Period of Motion

Deviations from two-body motion must be compensated for in all aspects of this problem. Vallado and McClain (22:612-628) go into great detail examining the perturbing effects of the earth's zonal harmonics, particularly the secular effects as well as the short- and long-period effects. Under two-body conditions, and given the initial conditions already derived, the formation would only deviate slightly from the desired relative radius. With the J_2 perturbation added to the equations of motion, a secular drift is now present in the formation dynamics. Shown in Figure 8 is the two-body and perturbed formation separation over five two-body periods of the motion. The formation

is at an altitude of 400 km and at an inclination of 45 degrees (these will be the baseline orbital parameters for most of the findings for this research), and the desired relative orbit radius is 1 km.

From the figure, it is evident that the secular effects described by Vallado and McClain cause a secular drift in the separation of the deputy from the reference trajectory. The primary mechanism behind this drift is the fact that the derived initial conditions for the formation produce orbits for the reference trajectory and deputy satellite with differing inclinations. These differences in inclination induce different nodal regression rates due to J_2 effects. Meanwhile, the two-body case produces only minimal periodic drift on the order of tenths of a meter. These secular effects induce the need for formation control.

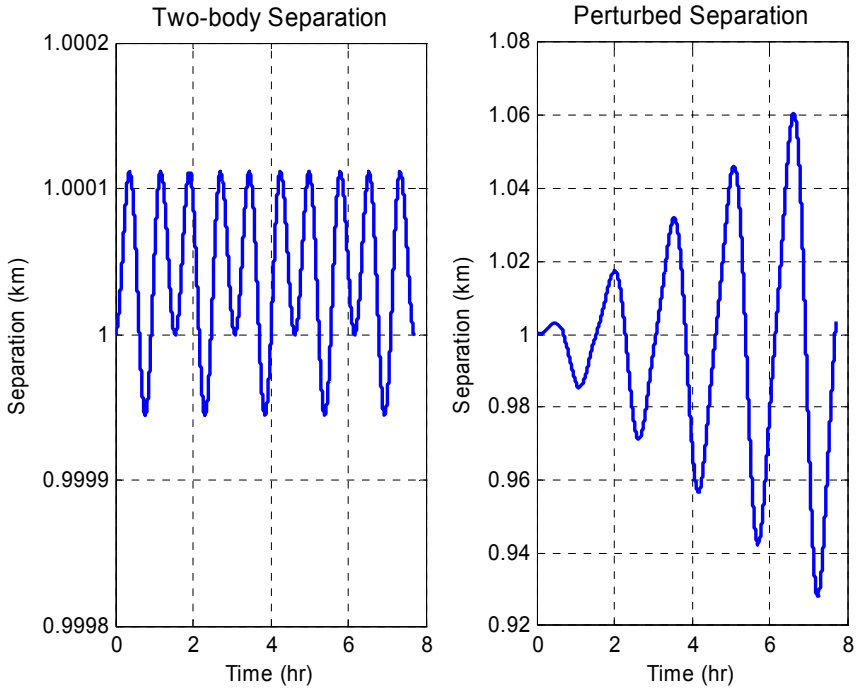

Figure 8. Formation Separation

The choice of periods over which to optimize is significantly affected by these perturbing effects. The desired end product of this research is an estimate of the long-term fuel requirements necessary to maintain a circular formation for multi-year missions, yet it is only practical given the current approach to optimize over short time periods. In order to evaluate long-term requirements based on short-term results, a repeatable control law for successive orbits must be found. The J_2 harmonic is a perturbing force driven by, among other things, geocentric latitude. In order to achieve a periodic solution necessary for the study of long-term behavior, it can be assumed that the mean motion of the formation must be periodic with respect to latitude.

To exploit the symmetries present in the perturbing forces, a good choice for the period of motion would be crossings of the earth's equatorial plane by the reference trajectory. This choice of periods would zero out the latitude at the beginning of each successive orbit, and should result in a periodic control law which would be valid for successive orbits since the perturbing force due to J_2 is symmetric about the equator. This approach would lend itself very well to approximating the long-term fuel requirements associated with the optimal control of the formation.

Given an uncontrolled reference trajectory, another option for optimizing the required control costs is to take advantage of the natural motion of the formation. A look must be taken at the uncontrolled motion of the reference trajectory to find the natural periods existent in the motion. It is expected that the natural motion will deviate from two-body motion due to perturbations, but whether the natural periods of the motion will

match either the two-body period or the desired equatorial crossing period must be determined.

Given once again an orbit of 45-degree inclination and an altitude of 400 km, Figure 9 displays the short-period effect on semi-major axis over five two-body periods of the motion. Under two-body conditions, the circular orbit of the reference trajectory would maintain a constant value for semi-major axis, yielding a constant value for orbital radius. The initial conditions for the deputy satellite would induce slightly elliptical motion. Now with the J_2-perturbation included, both motions are elliptical.

In Figure 9, the dashed line represents the orbital radius of the reference trajectory, and the solid line represents the orbital radius of the deputy satellite. It is this natural periodic motion of the reference trajectory that presents an excellent candidate for the period of motion to optimize over. Table 1 shows the three periods discussed so far for comparison, with the same orbital parameters of 400-km altitude and 45-degree inclination.

Table 1. Periods of Motion

Periods of Motion	Time (sec)
Two-body	5553.62
Equatorial Crossing	5539.64
Natural Period of Semi-major Axis	5543.65

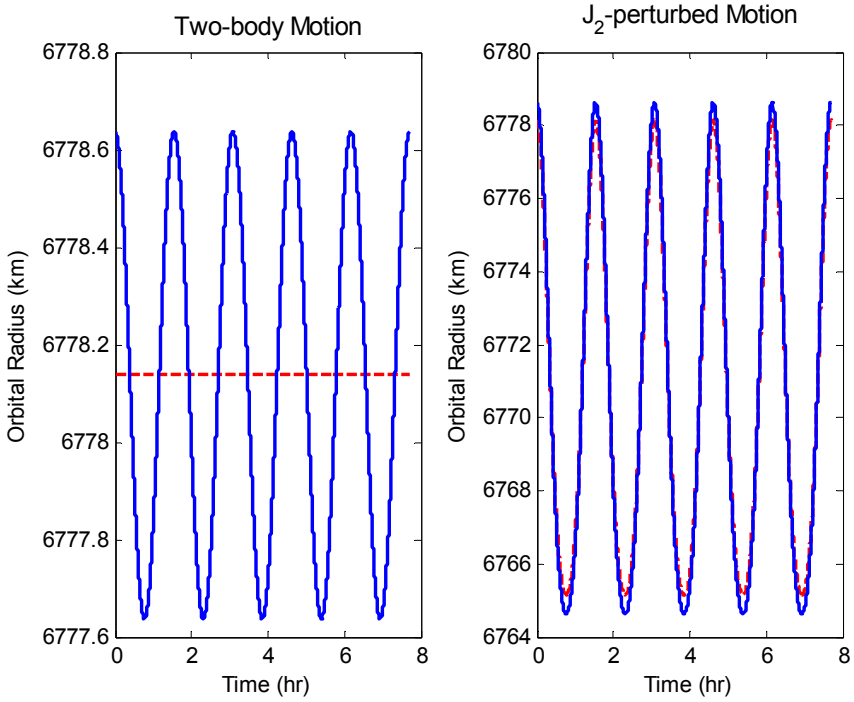

Figure 9. Orbital Radius Comparison

One conclusion drawn from Table 1 is how little the optional periods of the motion differ relative to the length of one orbit, only by a matter of seconds. Despite the small differences, the natural period doesn't match either the two-body period or the equatorial crossing period. These differences have distinct effects on the numerical optimization process, especially when the final boundary conditions for the optimization are calculated. Establishing these boundary conditions for studying successive orbits in the manner derived in Chapter III makes it necessary to choose a natural period of the motion as the period to optimize over. For this reason, the natural period of the semi-major axis of the reference trajectory was chosen as the period of the motion.

Periodic or Quasi-Periodic Solutions

The selection of the period of the motion over which to optimize now poses an uncertainty as to whether the solutions will be periodic over successive orbits. Obviously, control laws in the inertial frame will not be periodic as the orbits precess about the earth. However, the resulting control laws can be described in the Hill frame and studied for periodic nature.

To study the periodic nature of the resulting control laws, successive orbits were run to convergence one at a time given orbital parameters of 400-km altitude and 45-degree inclination. After an optimal control law was found for the first period of the motion, the final states of the system were used as initial conditions for a second orbit and an optimal control law was found for the second period of the motion. Three successive orbits were optimized in this fashion and a comparison of their resultant control histories, represented in the relative Hill frame, is shown in Figure 10.

It is apparent from Figure 10 that the solutions are not perfectly periodic. In fact, there are jump discontinuities in the control laws at the beginning of each successive orbit. Despite these discontinuities, Figure 11 shows that the relative positions within the formation do experience periodic progression, validating the utility of the resulting control laws. These results preclude the precise estimation of the necessary control usage over long time periods. However, only small discrepancies in the control laws exist on the order of 5% between orbits, resulting in a quasi-periodic solution whose results can be extended over any number of orbits to produce a reasonable approximation of the optimal control requirement.

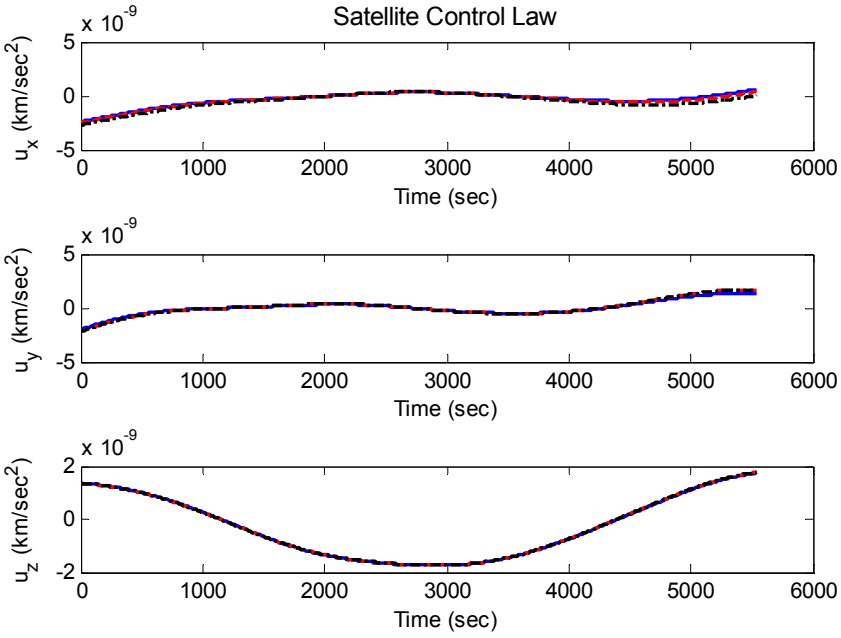

Figure 10. Deputy Satellite Control Histories for Three Successive Orbits

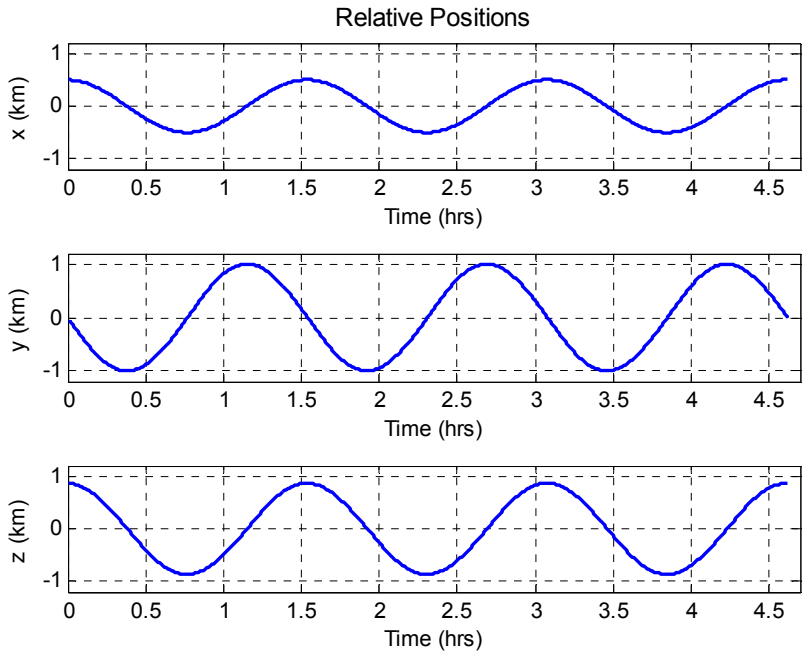

Figure 11. Deputy Satellite Relative Positions for Three Successive Orbits

Optimization Results

Case Study #1

For case study #1, the following table and figures display the results for an orbital altitude of the reference trajectory of 400 km and an initial phase angle of zero degrees at varying inclinations. The relative importance of minimizing satellite separation and control usage was set equal. Differing values for k_1 and k_2 will be treated in a later case study. The results for each run (different inclinations) are accompanied by a figure displaying the relative satellite separation from the reference trajectory and the resultant open-loop control law represented in the Hill frame. In order to calculate the estimates for annual ΔV, it was assumed that attitude control is in place to ensure alignment of the control thrusters of the deputy satellite with the relative Hill frame throughout the orbit. The relative components of the control accelerations (u_x, u_y, and u_z) are integrated over the period of motion and summed to solve for the ΔV per orbit. This ΔV per orbit is then multiplied by the number of orbits completed per year. All of these parameters are summarized in Table 2.

Table 2. Case Study #1

Orbital Parameters		**RESULTS**	
Altitude	400 km		
Formation Radius	1 km	Inclination (deg):	Annual ΔV (m/s):
Phase	0 deg	0	153.58
		30	104.60
Performance Index		45	63.68
k_1	1.0E+03	60	34.63
k_2	1.0E+03	90	27.88
k_3	1.0E+08		

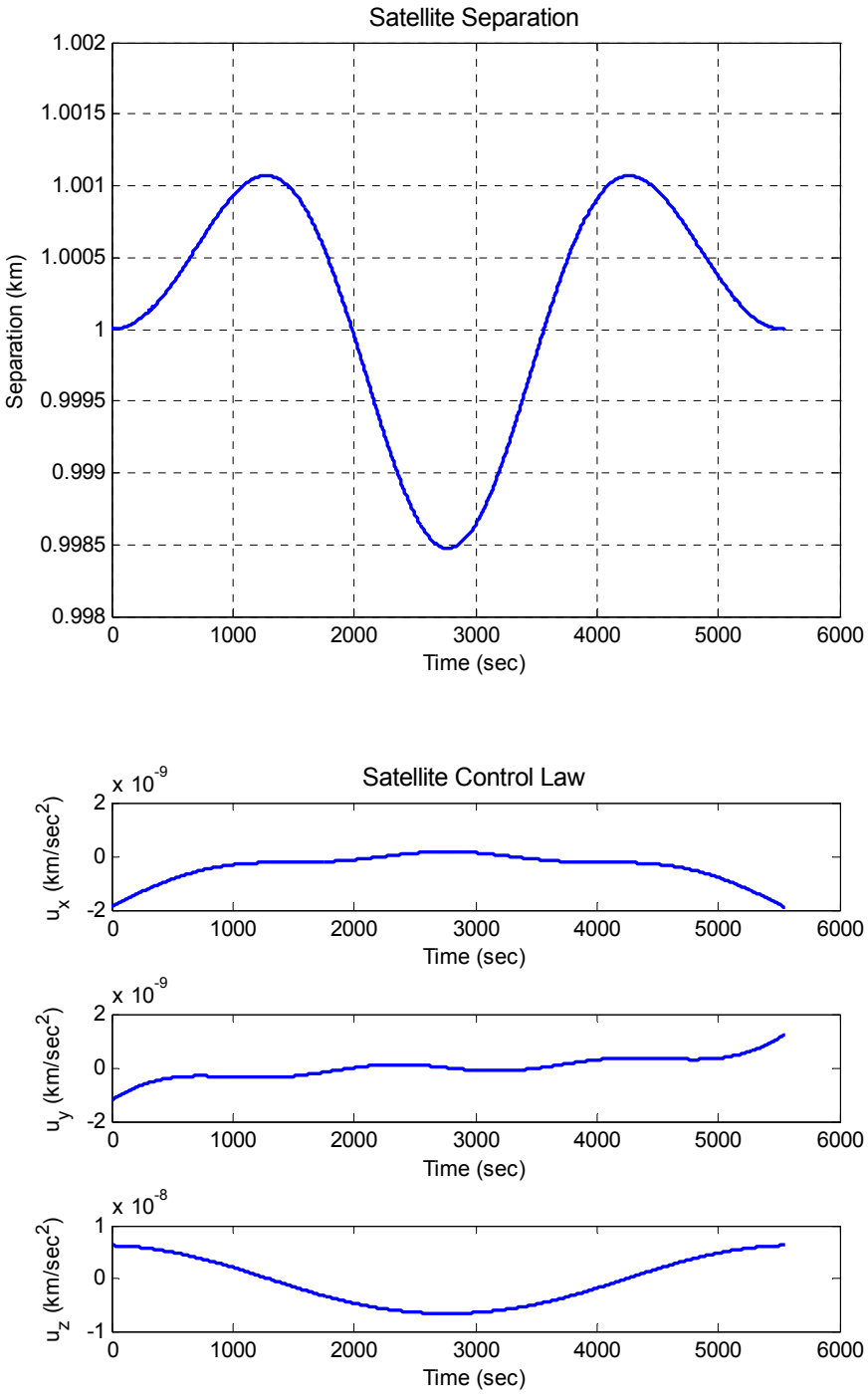

Figure 12. Case Study #1, 0-deg Inclination

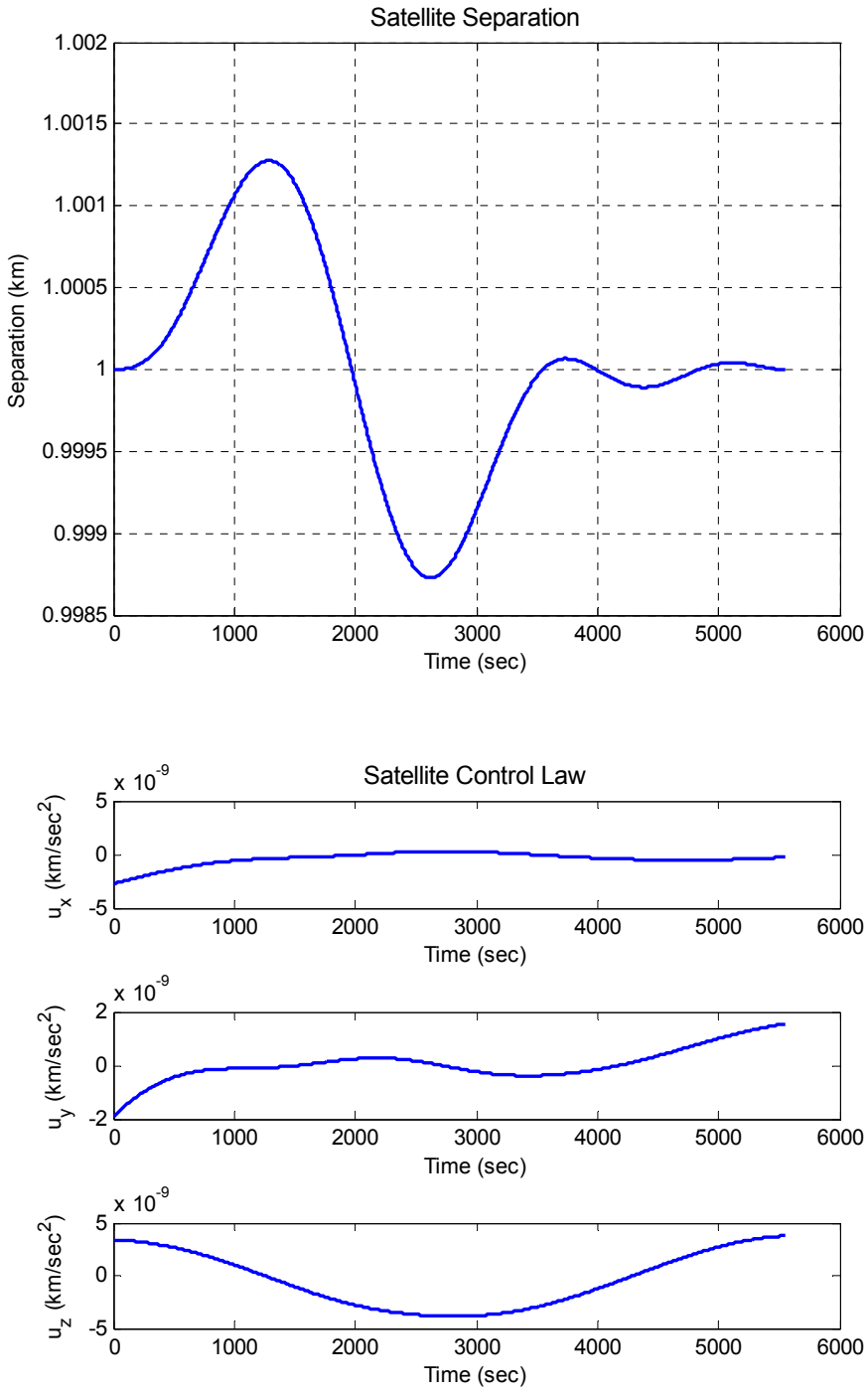

Figure 13. Case Study #1, 30-deg Inclination

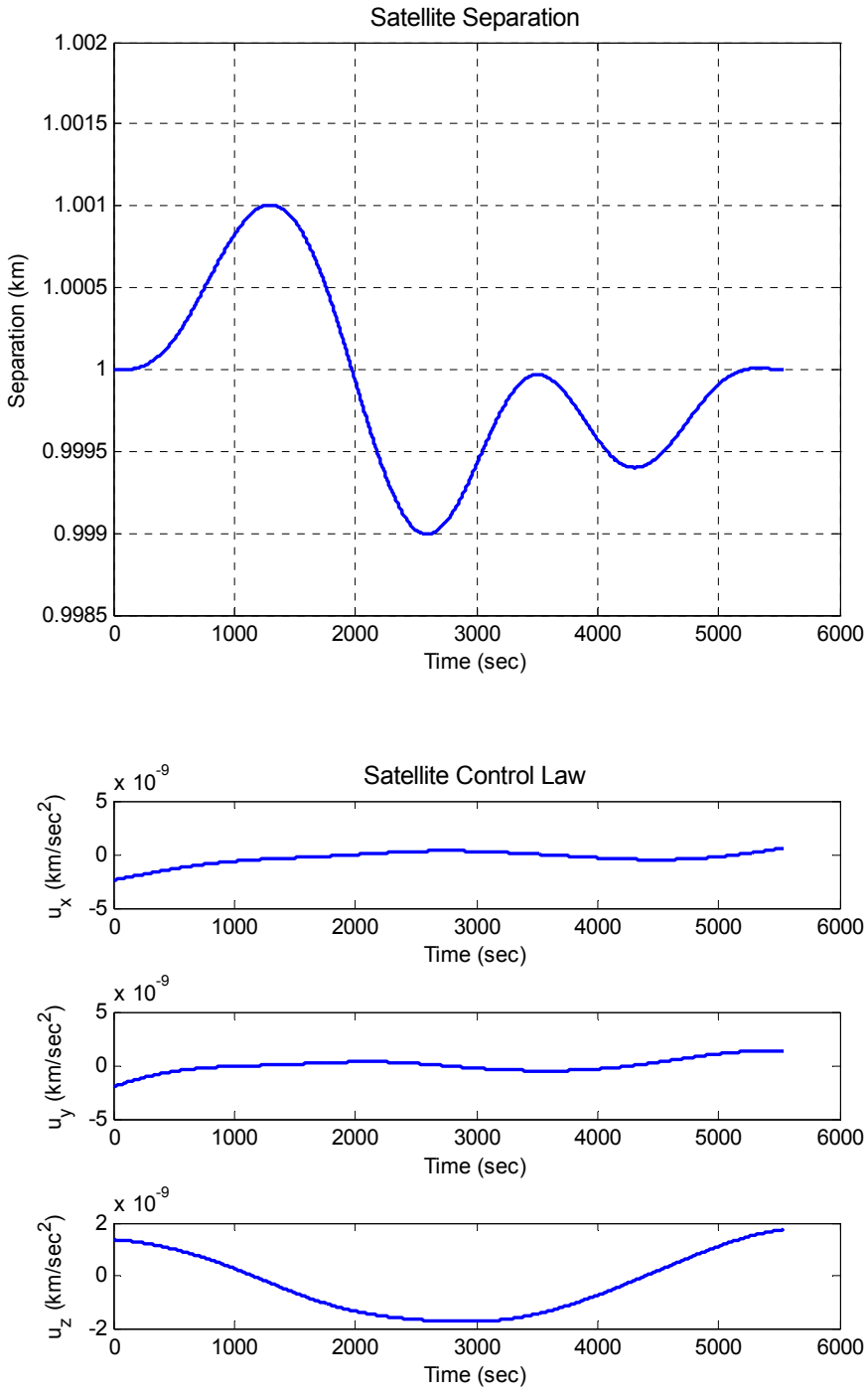

Figure 14. Case Study #1, 45-deg Inclination

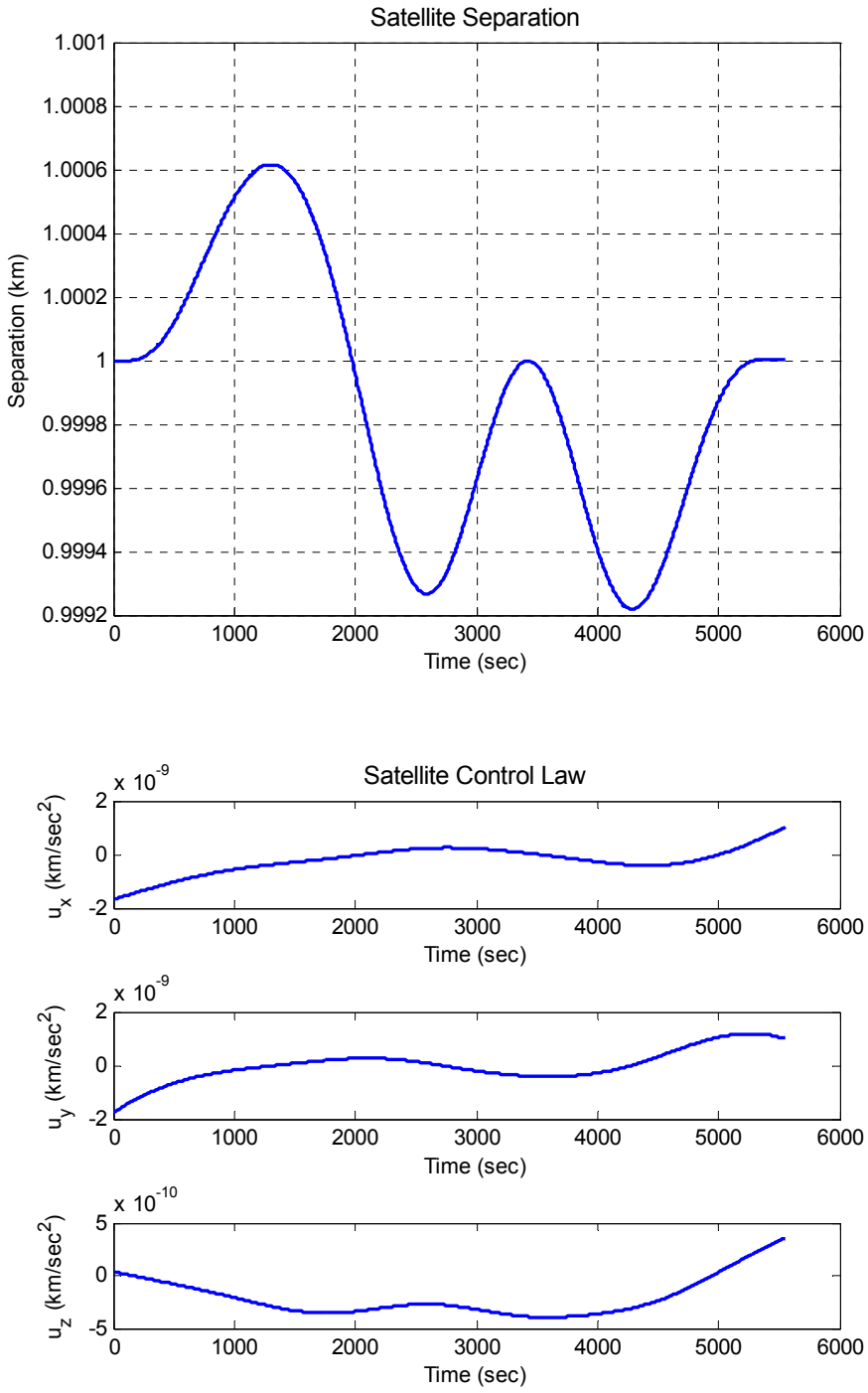

Figure 15. Case Study #1, 60-deg Inclination

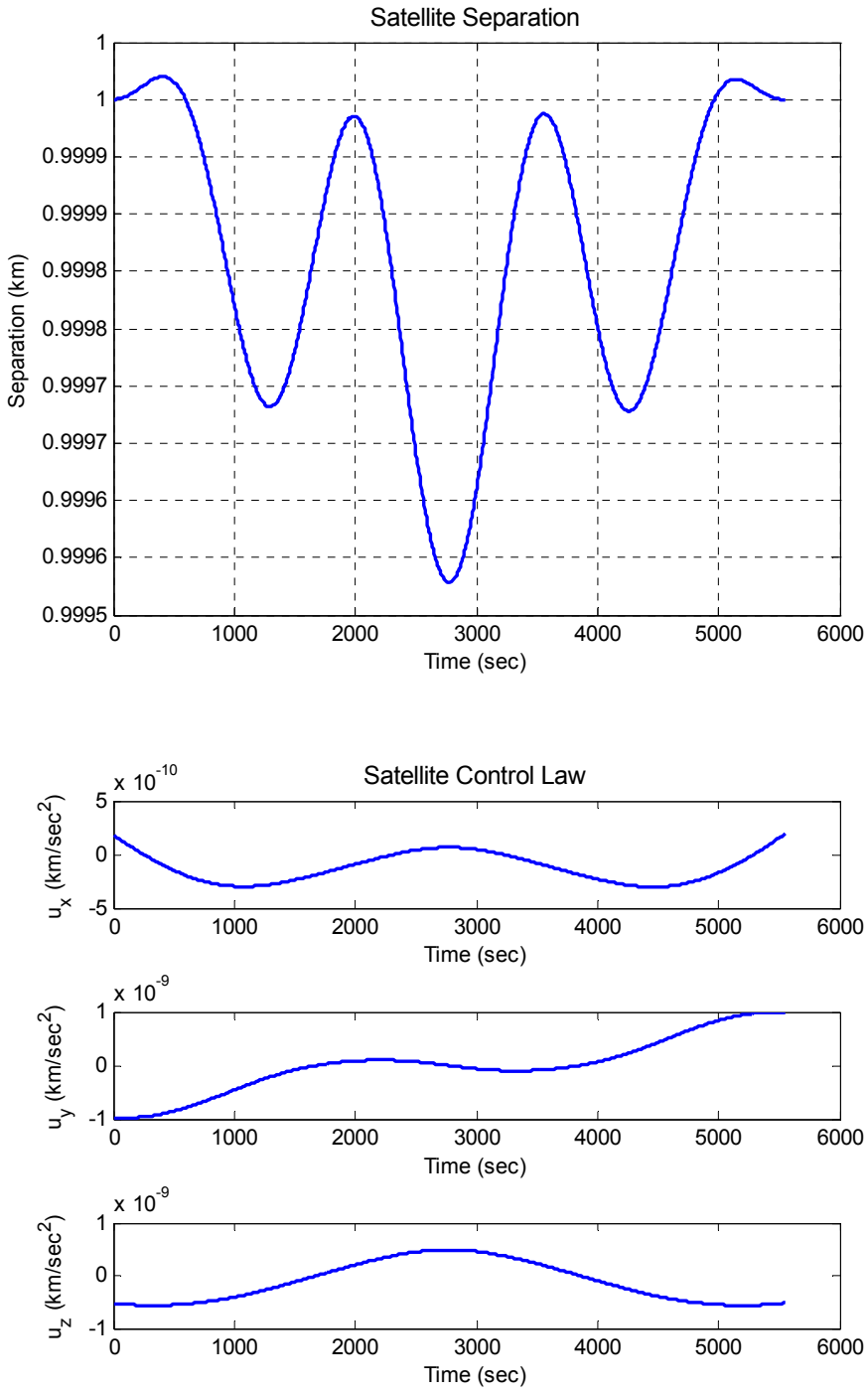

Figure 16. Case Study #1, 90-deg Inclination

The most likely contributor to the resulting trend in ΔV requirements is the differing nodal regression rates of the reference trajectory and the deputy satellite. Given the initial conditions derived for the formation with phase equal zero degrees, Table 3 displays the resulting inclination comparison for the formation.

Table 3. Inclination Comparison for Phase = 0 deg

Formation Inclinations (deg)		
Chief	Deputy	Δi
0	0.007319997	0.00732000
30	30.00000081	0.00000081
45	45.00000047	0.00000047
60	60.00000027	0.00000027
90	90	0

Using these differences in inclination, the differences in the nodal regression rates $\dot{\Omega}$ can be calculated. Vallado and McClain (22:607) give the equation for nodal regression rate in the presence of J_2:

$$\dot{\Omega} = -\frac{3nJ_2R_{\oplus}^{\ 2}}{2a^2(1-e^2)^2}\cos i \tag{90}$$

where the parameter p in Vallado and McClain has been replaced with the equivalent classical orbital elements of semi-major axis a and eccentricity e. To solve for the resulting differences in nodal regression rate due to differences in inclination, the variation of Eq. (90) can be taken:

$$\delta\dot{\Omega} = \frac{3nJ_2R_{\oplus}^{\ 2}}{2a^2(1-e^2)^2}\sin i\ \delta i \tag{91}$$

Plugging in values for the deputy satellite, Figure 17 shows the resulting trend in the difference between the nodal regression rates and how it compares with the trend in annual control cost. It can be seen that as the inclination of the formation increases, the nodal regression difference between the reference trajectory and the deputy satellite approaches zero, which vindicates the apparent minimum in the ΔV requirement at or near a polar configuration.

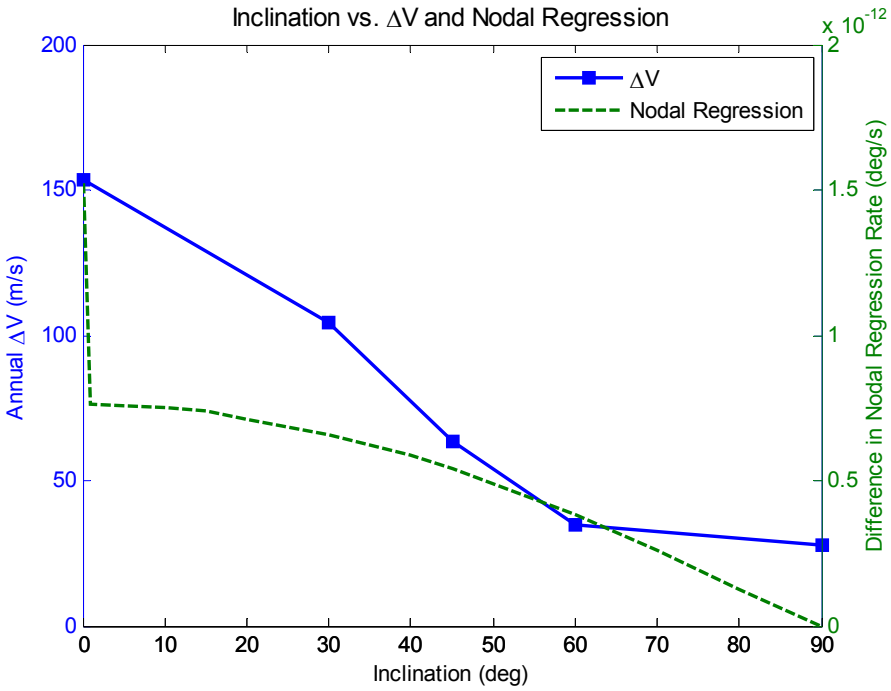

Figure 17. Annual ΔV and Nodal Regression Rates for Phase = 0 deg

Case Study #2

For case study #2, the following table and figures display the results for an orbital altitude of the reference trajectory of 400 km and an initial phase angle of 90 degrees at the same inclinations as Case Study #1. A comparison can then be made between the choice of initial phase angle and the necessary control requirements. The relative importance of minimizing satellite separation and control usage was set equal. All of these parameters are summarized in Table 4.

Table 4. Case Study #2

Orbital Parameters		**RESULTS**	
Altitude	400 km		
Formation Radius	1 km	Inclination (deg):	Annual ΔV (m/s):
Phase	90 deg	0	164.01
		30	85.39
Performance Index		45	33.32
k_1	1.0E+03	60	67.08
k_2	1.0E+03	90	94.50
k_3	1.0E+07		

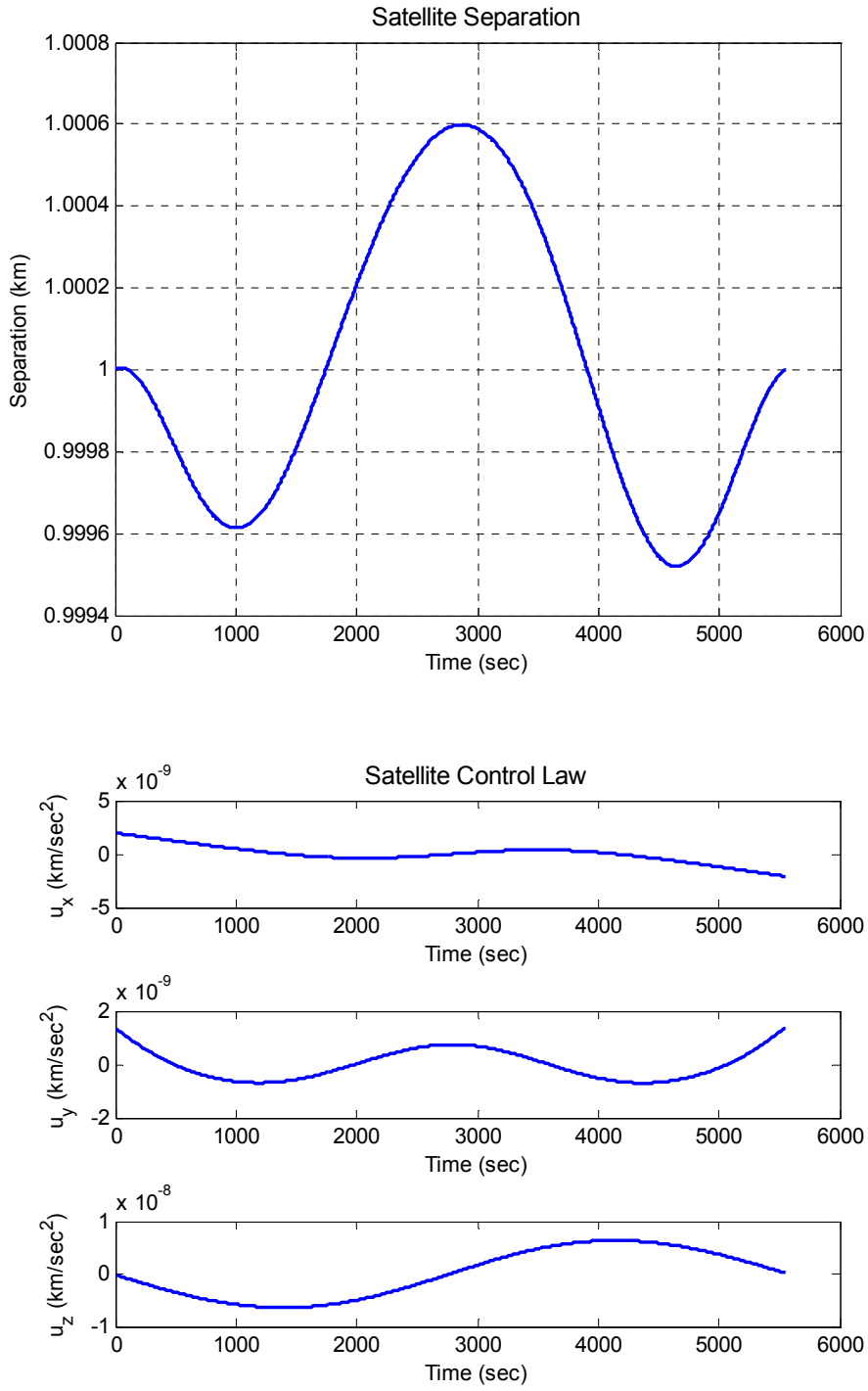

Figure 18. Case Study #2, 0-deg Inclination

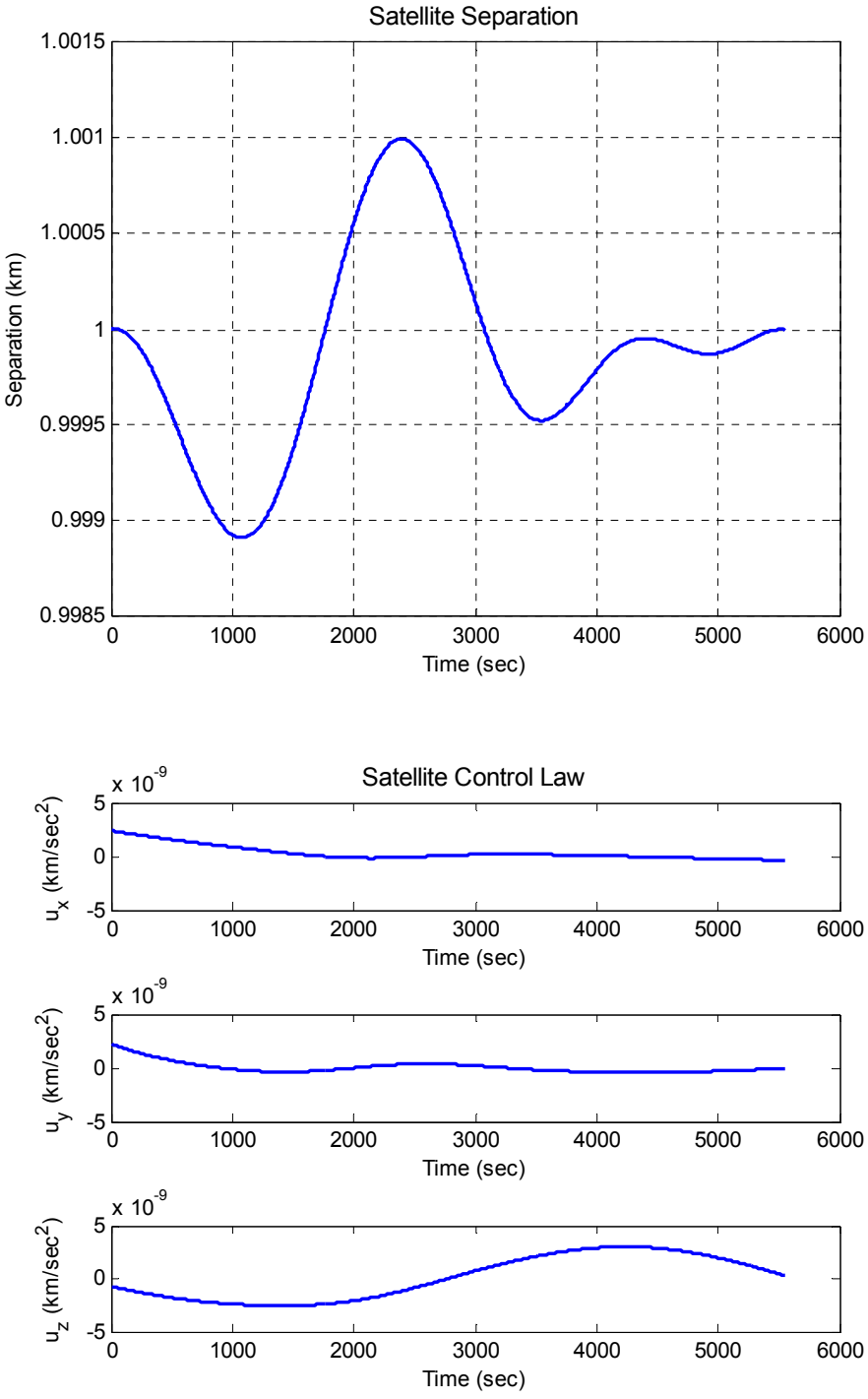

Figure 19. Case Study #2, 30-deg Inclination

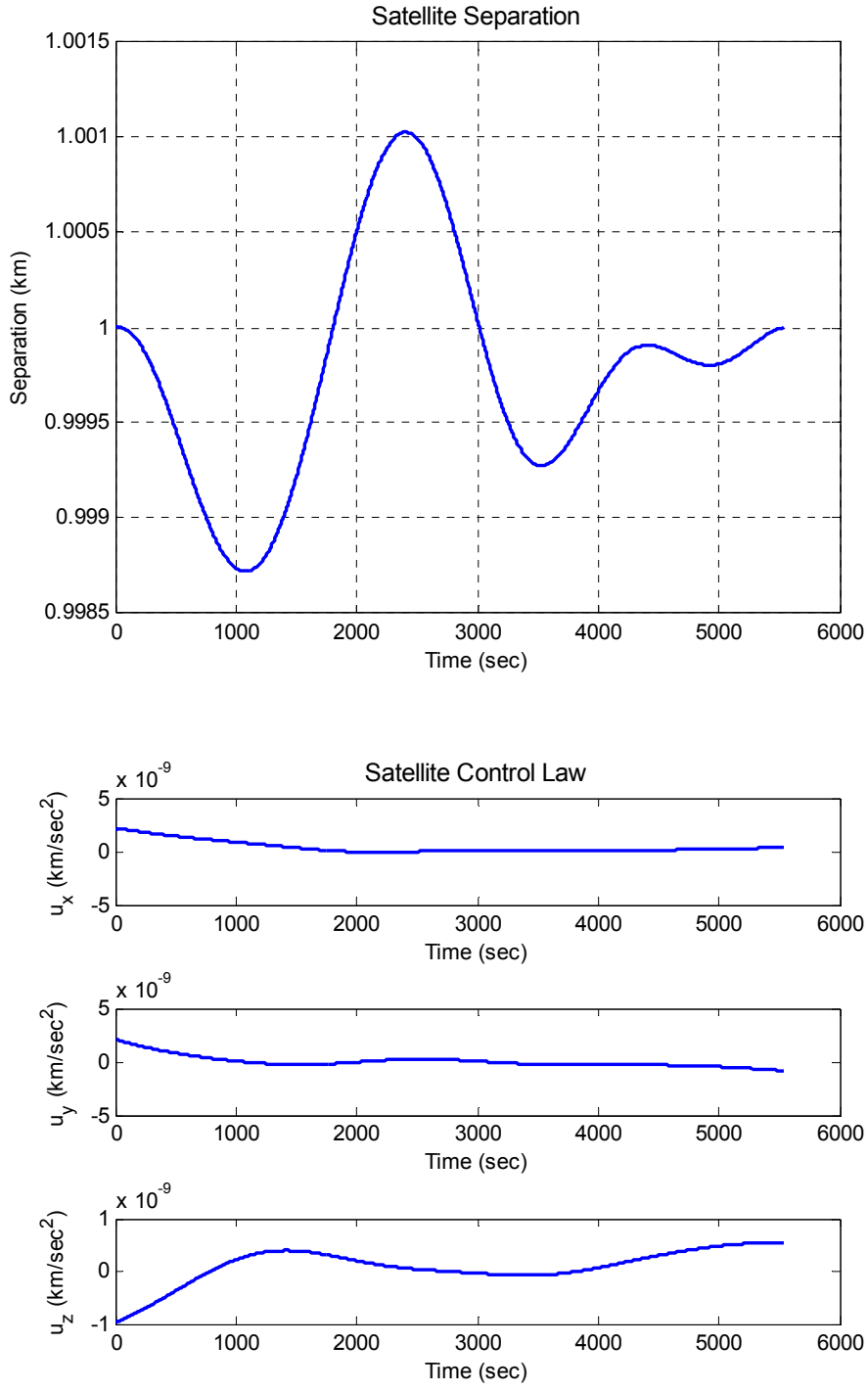

Figure 20. Case Study #2, 45-deg Inclination

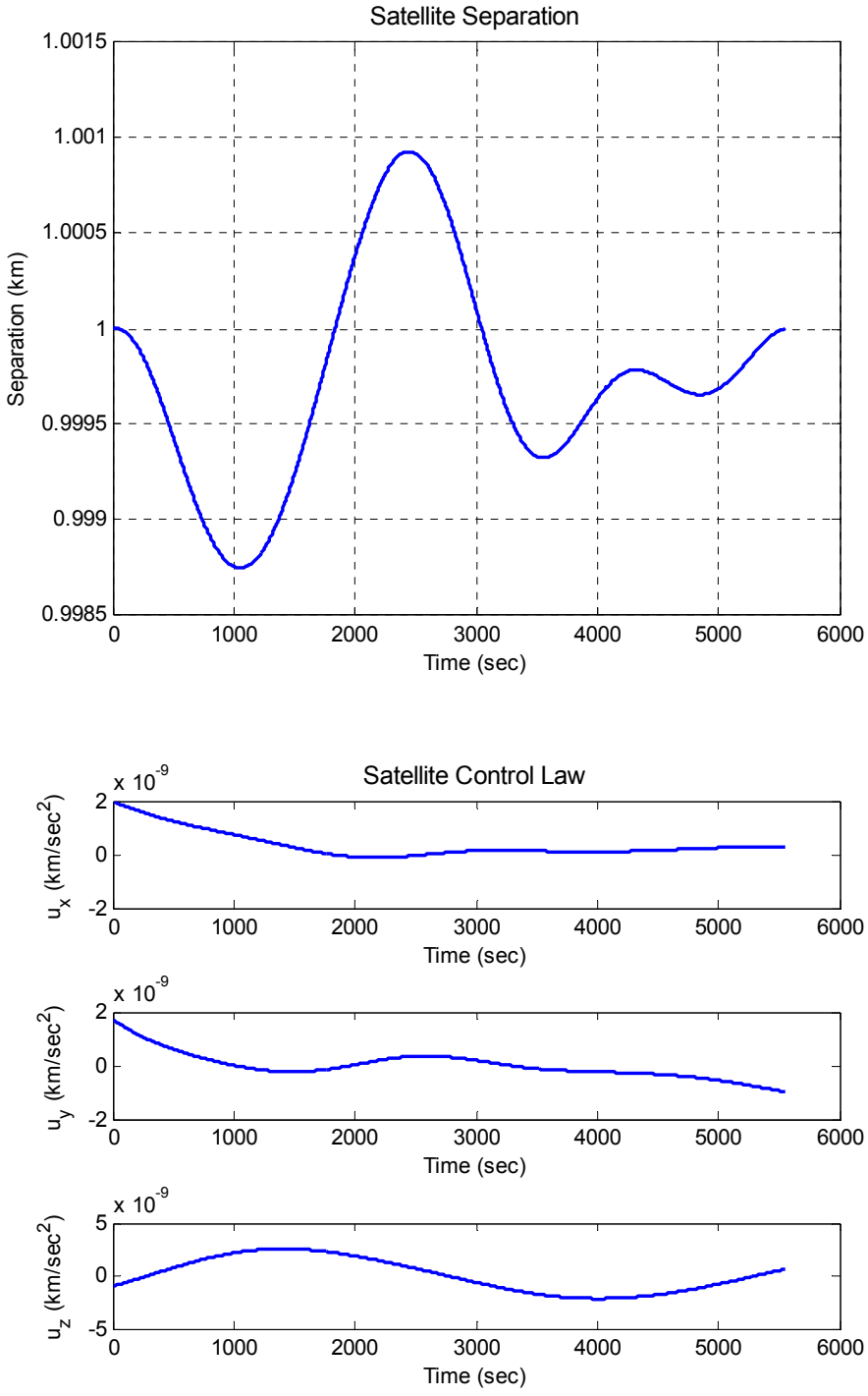

Figure 21. Case Study #2, 60-deg Inclination

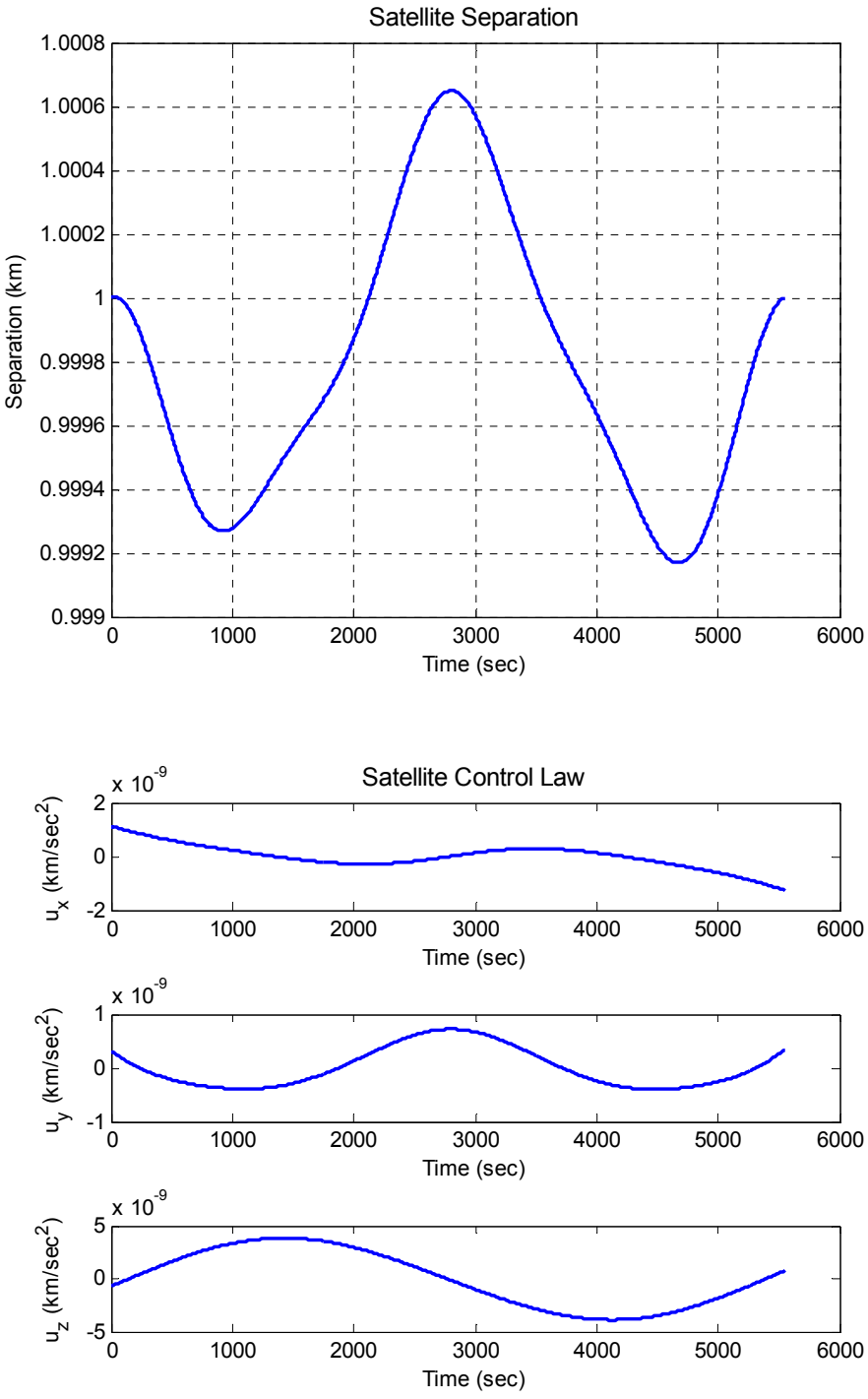

Figure 22. Case Study #2, 90-deg Inclination

In the case of phase angle equal to 90 degrees, the driving force behind the resulting trend line in control cost appears to be the difference in secular drift rates of the argument of perigee ω. Once again, the variation of the secular drift rate can be taken to analyze the difference in drift rates. Vallado and McClain (22:609) give the equation for the secular drift rate of the argument of perigee in the presence of J_2:

$$\dot{\omega} = \frac{3nJ_2R_{\oplus}^{\ 2}}{4a^2(1-e^2)^2}\left(4-5\sin^2 i\right) \tag{92}$$

where once again the parameter *p* has been replaced by the classical orbital elements. Taking the variation of Eq. (92), the following equation shows how variations in inclination produce variations in the drift rate of the argument of perigee:

$$\delta\dot{\omega} = \frac{3nJ_2R_{\oplus}^{\ 2}}{4a^2(1-e^2)^2}\left(4-10\sin i\cos i\ \delta i\right) \tag{93}$$

For the case of phase equal to 90 degrees, the derived initial conditions produce a constant variation in inclination δi equal to 0.0073205 at all reference trajectory inclinations. Therefore, the variations in argument of perigee drift rate are solely dependent on the inclination of the orbit.

A comparison between the trends in annual ΔV requirements and variations in argument of perigee drift rate is shown in Figure 23. For the case of phase angle equal to 90 degrees, this comparison strongly supports a possible minimum at or near 45 degrees of inclination.

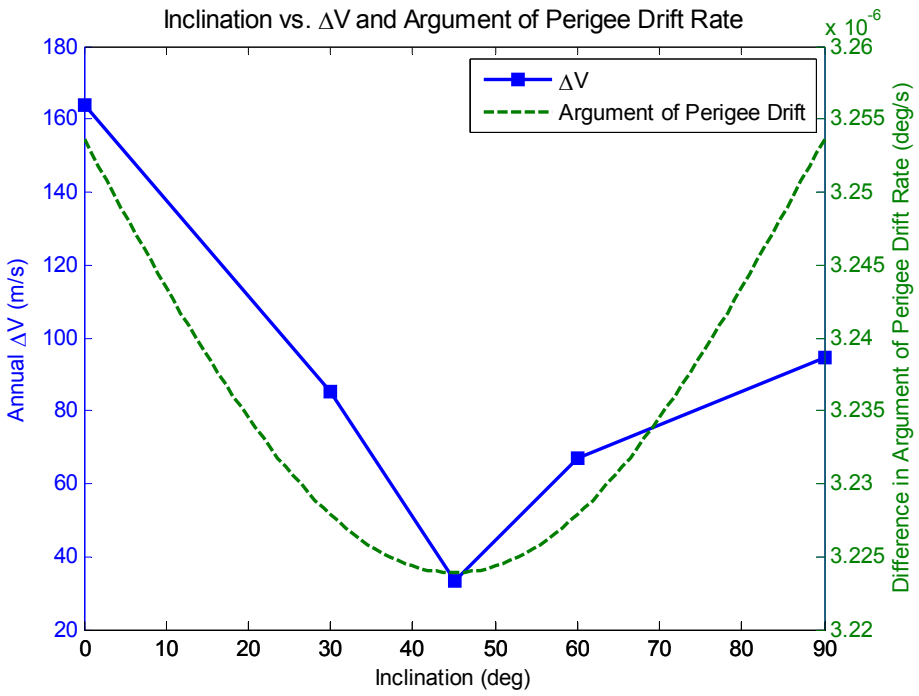

Figure 23. Annual ΔV and Argument of Perigee Drift Rate for Phase = 90 deg

The trend lines for the first two case studies are shown in Figure 24. One obvious conclusion drawn from these results, for the probable reasons given above, is that the optimal fuel requirement is heavily dependent on the choice of initial conditions for the deputy satellite and the inclination of the reference trajectory. Given the limited number of data points, it isn't possible to pinpoint an "optimal" reference trajectory inclination which minimizes fuel requirements for the entire formation. The 0-degree phase condition, as stated earlier, appears to have a minimum at or near 90 degrees of inclination, while the 90-degree phase condition is minimal in the mid-latitude inclinations, with a strong argument that the minimum is at or near 45 degrees. It can also be seen that formations at or near the equator will have the maximum fuel

requirement, which should be expected as the nodal regression of the orbits due to J_2 is strongest at low inclinations. Given the data at hand, the configuration that appears to minimize control cost for the entire formation exists in the inclination range of 45 to 60 degrees, with an estimated control requirement of 40-50 m/s/year per deputy.

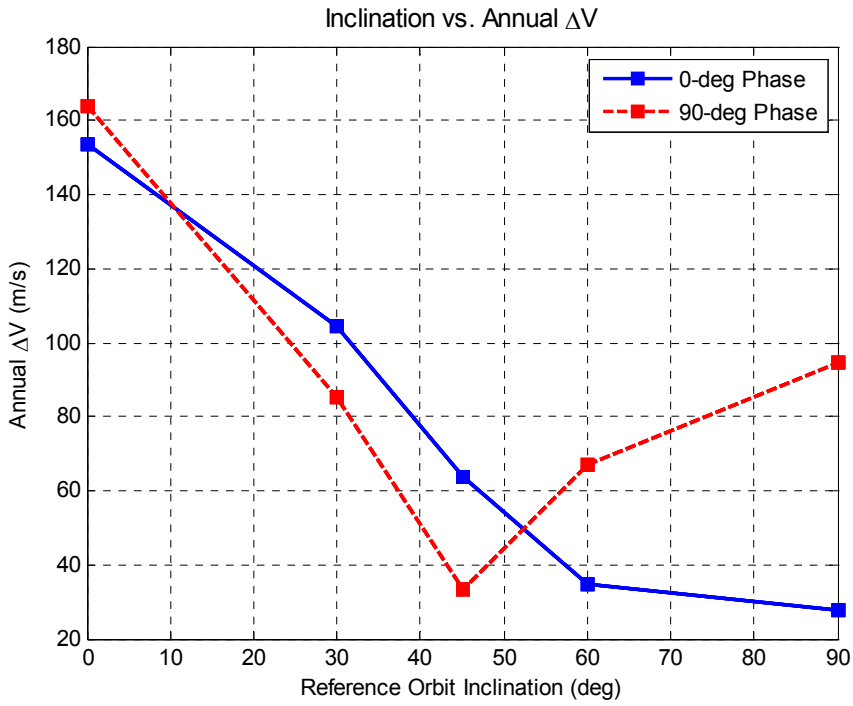

Figure 24. Trends in Annual ΔV Estimates Based on Initial Phase Angle

Case Study #3

For case study #3, the orbital altitude of the formation was modified to study the effects of increasing the altitude on fuel requirements. The altitude of the reference trajectory was increased to 800 km, with the phase angle set back to zero degrees and the radius of the satellite formation remaining at 1 km. The relative importance of minimizing satellite separation and control usage was set equal. For this case study, summarized in Table 5, only two inclinations were chosen to establish the necessary trends, 45 and 90 degrees.

Table 5. Case Study #3

Orbital Parameters		**RESULTS**	
Altitude	800 km		
Formation Radius	1 km		
Phase	0 deg	Inclination (deg):	Annual ΔV (m/s):
		45	47.67
Performance Index		90	20.90
k_1	1.0E+03		
k_2	1.0E+03		
k_3	5.0E+07		

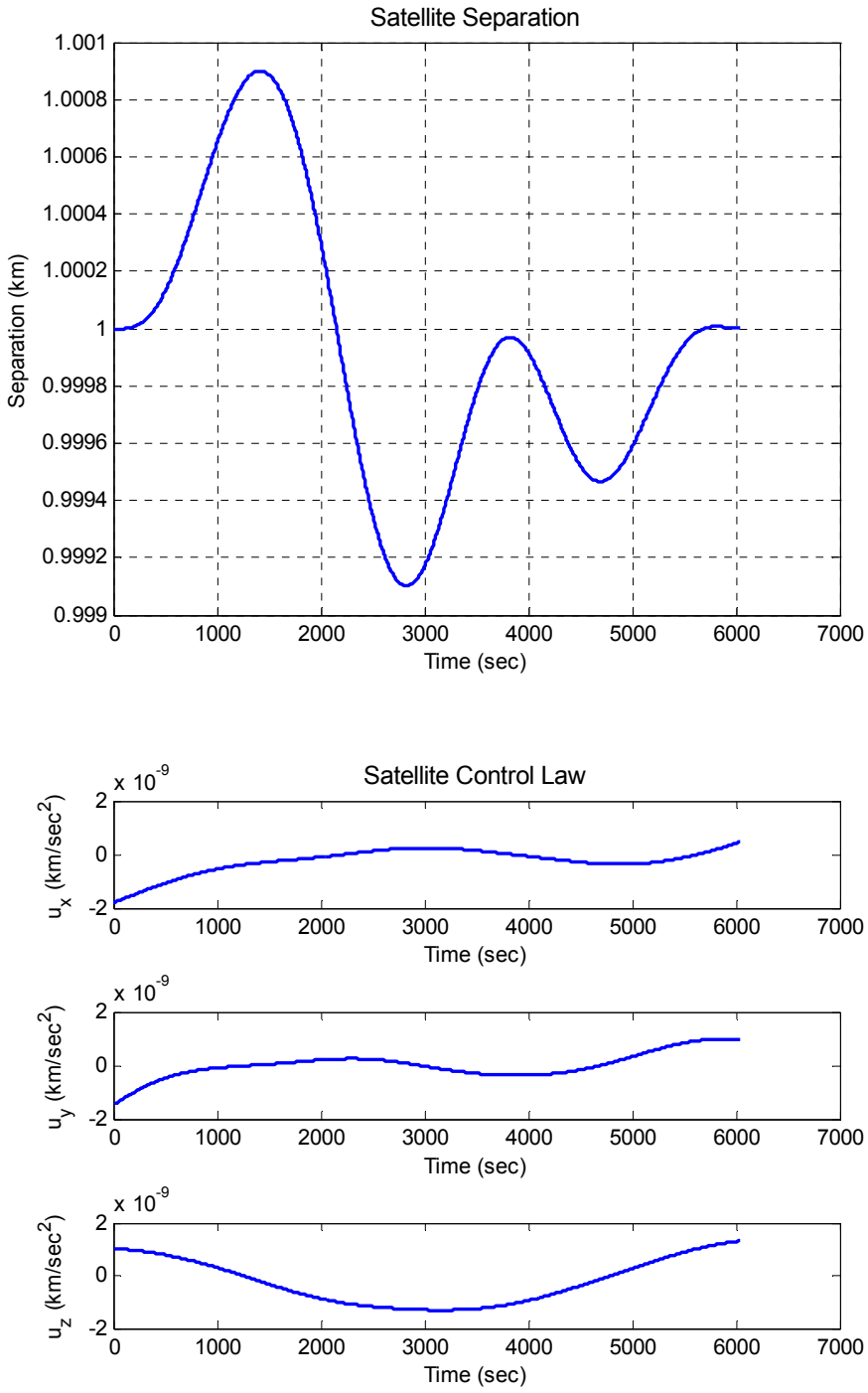

Figure 25. Case Study #3, 45-deg Inclination

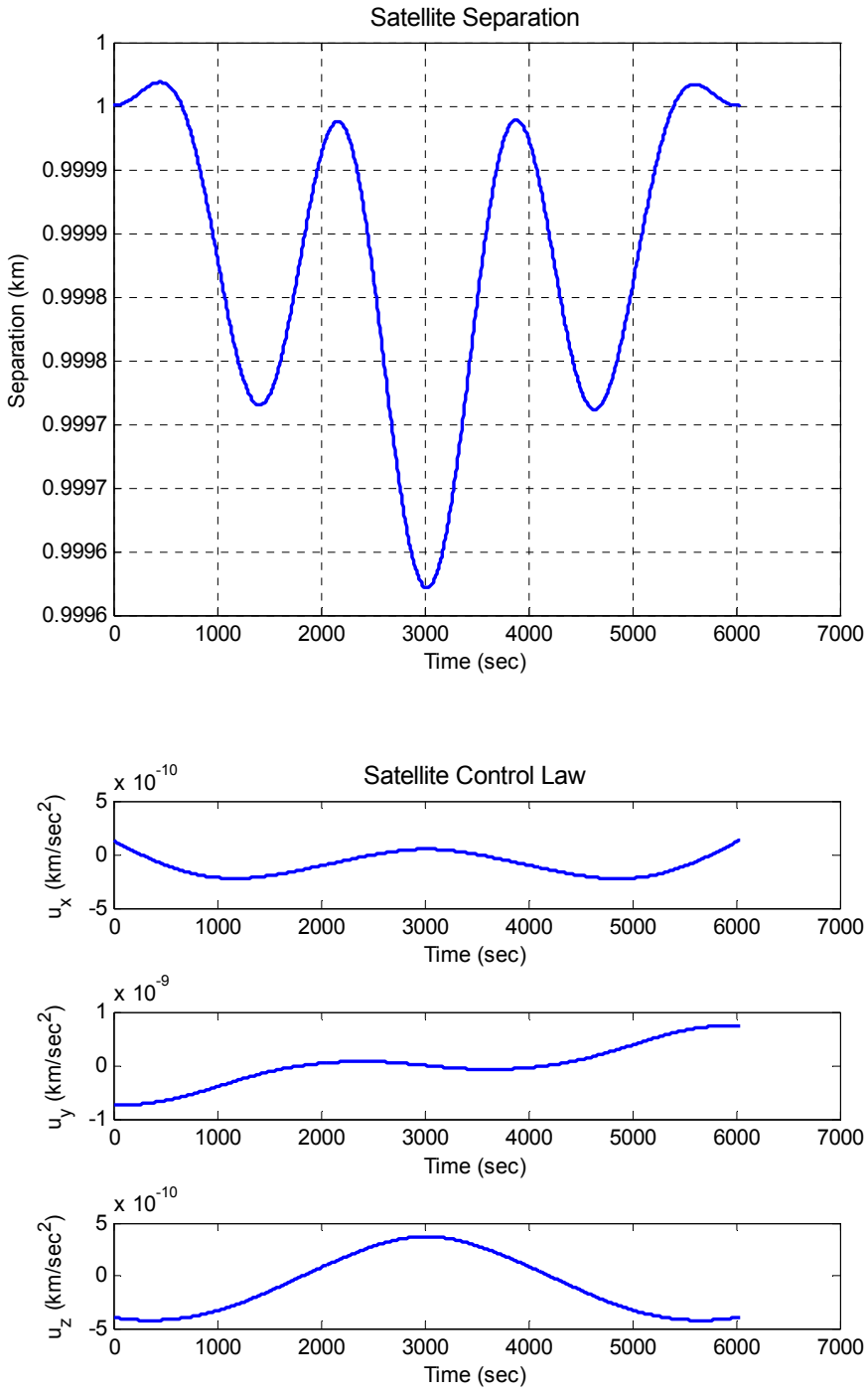

Figure 26. Case Study #3, 90-deg Inclination

Comparing Tables 2 and 5, it can be seen that by increasing the altitude of the formation, the annual ΔV estimate is decreased. As the formation gains altitude, the perturbing part of the potential function given by Eq. (12) is diminished, resulting in less need for control authority to counter the perturbing forces. A comparison of separation profiles for an inclination of 45 degrees is given in Figure 27, which shows less deviation at higher altitudes. A direct comparison of these results can be made with the results from Sabol et al. (15:276-277), who formulated an annual ΔV requirement of approximately 50 m/s/year for an 800-km altitude, polar configuration. Given the results of this study for a similar configuration of approximately 20 m/s/year, it has been shown that it may be possible to improve upon the ΔV requirements found by Sabol et al.

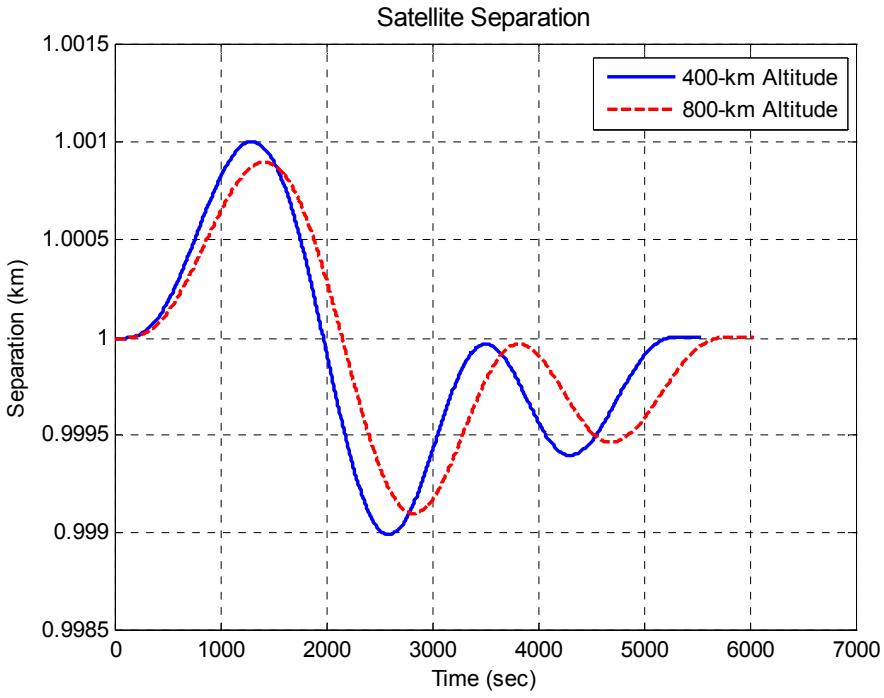

Figure 27. Comparison of Separation Profiles at Different Altitudes

Case Study #4

For case study #4, the radius of the satellite formation was modified to the study the effects of increasing the formation size (aperture size) on fuel requirements. The altitude of the reference trajectory was set to 400 km and the phase angle was zero degrees. The radius of the satellite formation was studied at two and ten kilometers. The relative importance of minimizing satellite separation and control usage was set equal. Table 6 summarizes the results for this case study.

Table 6. Case Study #4

Orbital Parameters		**RESULTS**	
Altitude	400 km		
Inclination	45 deg		
Phase	0 deg	Formation Radius (km):	Annual ΔV (m/s):
		2	125.80
Performance Index		10	617.17
k_1	1.0E+03		
k_2	1.0E+03		
k_3	1.0E+08		

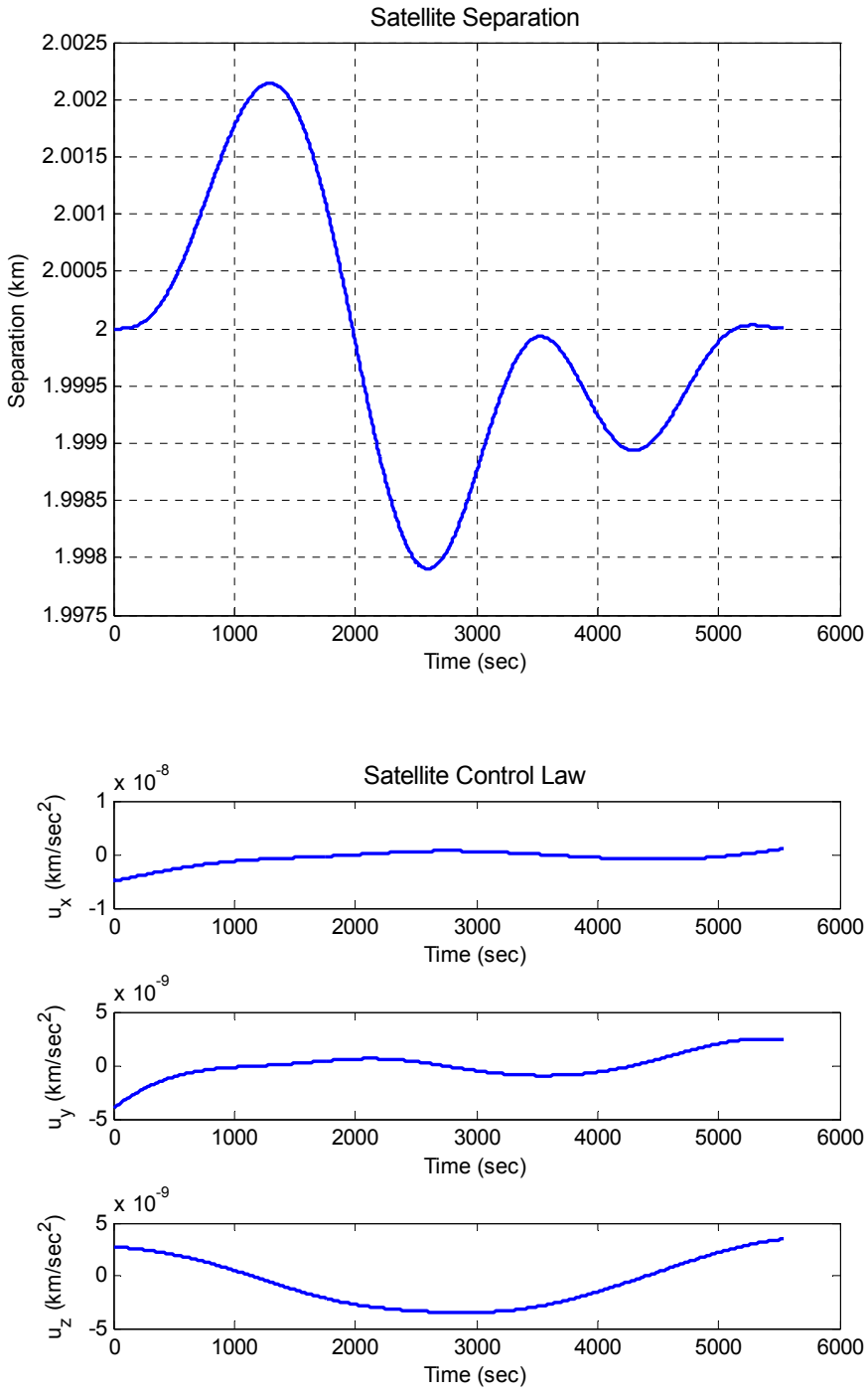

Figure 28. Case Study #4, 2-km Formation Radius

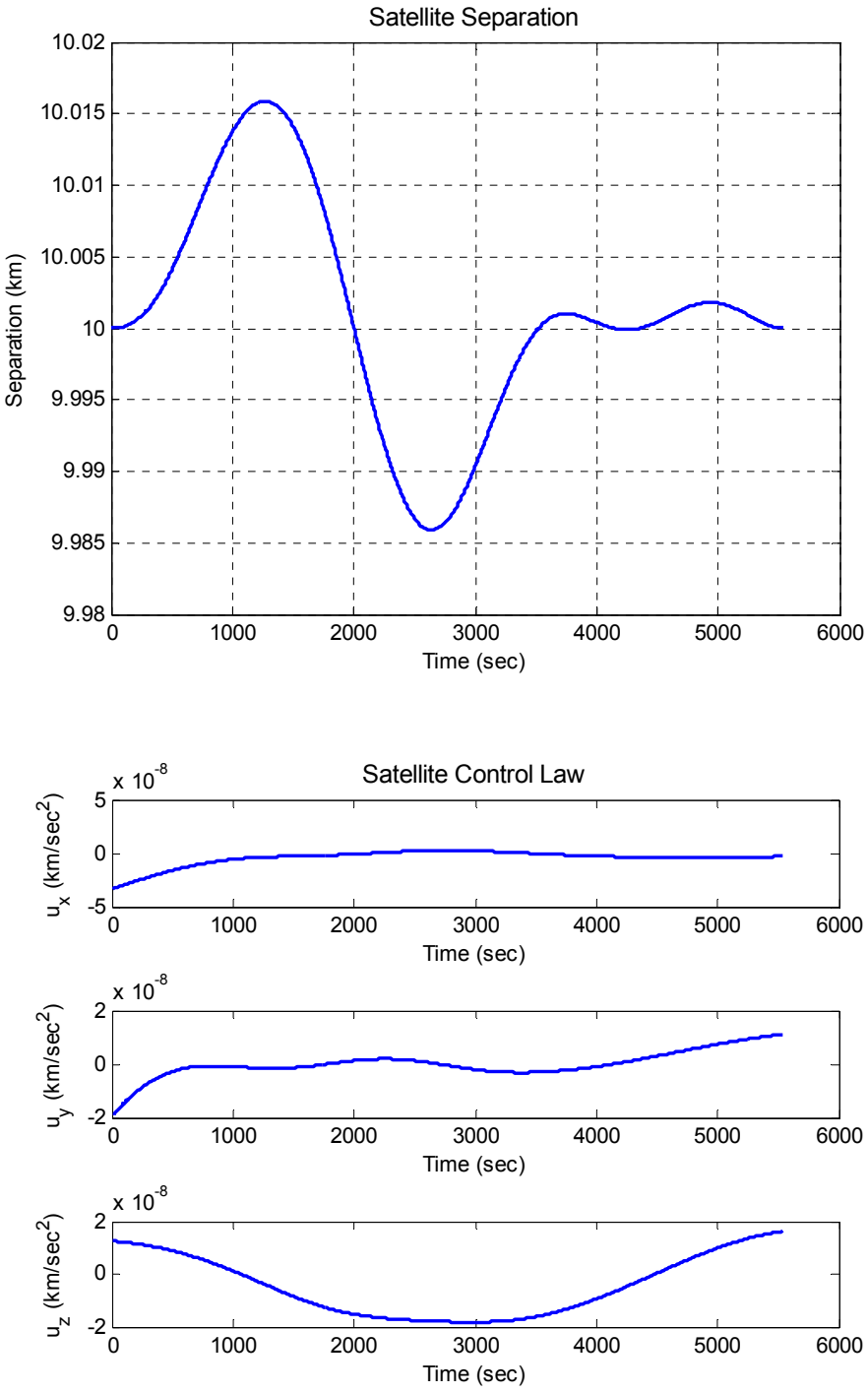

Figure 29. Case Study #4, 10-km Formation Radius

Two interesting trends are formulated from these results. First, despite the limited number of data points, the increase in the annual ΔV requirement appears to have an almost linear relationship with increase in formation size shown by Figure 30. The increase should be expected, for as the formation radius is increased, variations in the perturbing forces discussed in case studies 1 and 2 also increase, requiring more control authority to maintain the formation. Second, comparing percent deviation from the desired formation radius shows that there is an increase in deviation as formation size increases, as well as a change in the profile of the separation. These results are shown in Figure 31.

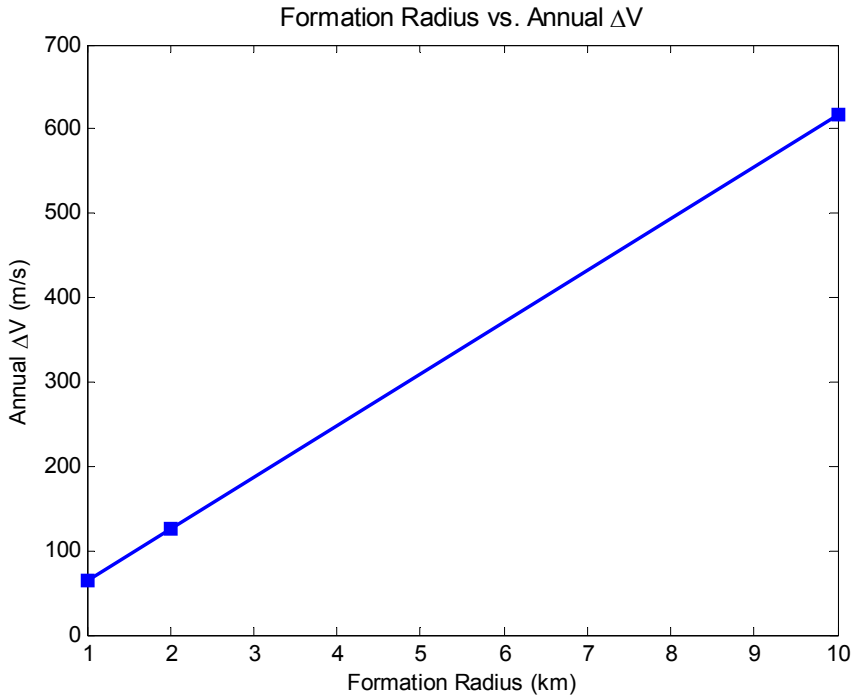

Figure 30. Trends in Annual ΔV Estimates Based on Formation Size

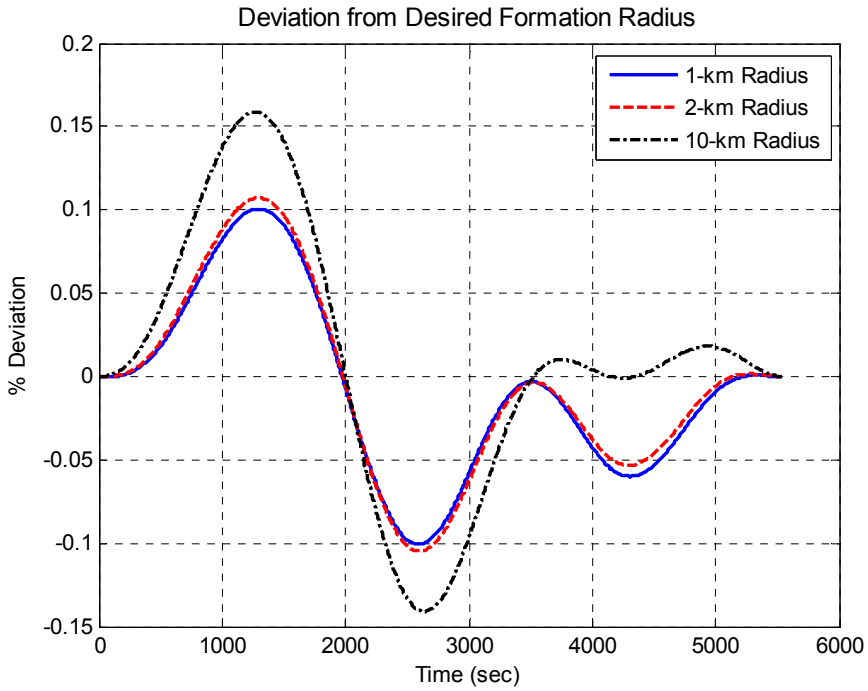

Figure 31. Trends in Percent Deviation from Desired Formation Radius

Change in the Performance Index

All of the previous results have set equal the relative importance between minimizing formation separation and control usage. This set of parameters produced excellent results for both separation and control, but it was desired to see if further minimization of control usage was possible at the expense of the integrity of the circular formation. This last set of results modified the weighting factors of k_1 and k_2 to 100 and 10,000, respectively, which heavily weighted minimizing control usage over satellite drift. An orbital altitude of 400 km and an inclination of 45 degrees were used. The phase angle for the formation was set to zero degrees and the formation radius was 1 km. This choice of parameters resulted in an annual ΔV estimate of 59.62 m/s.

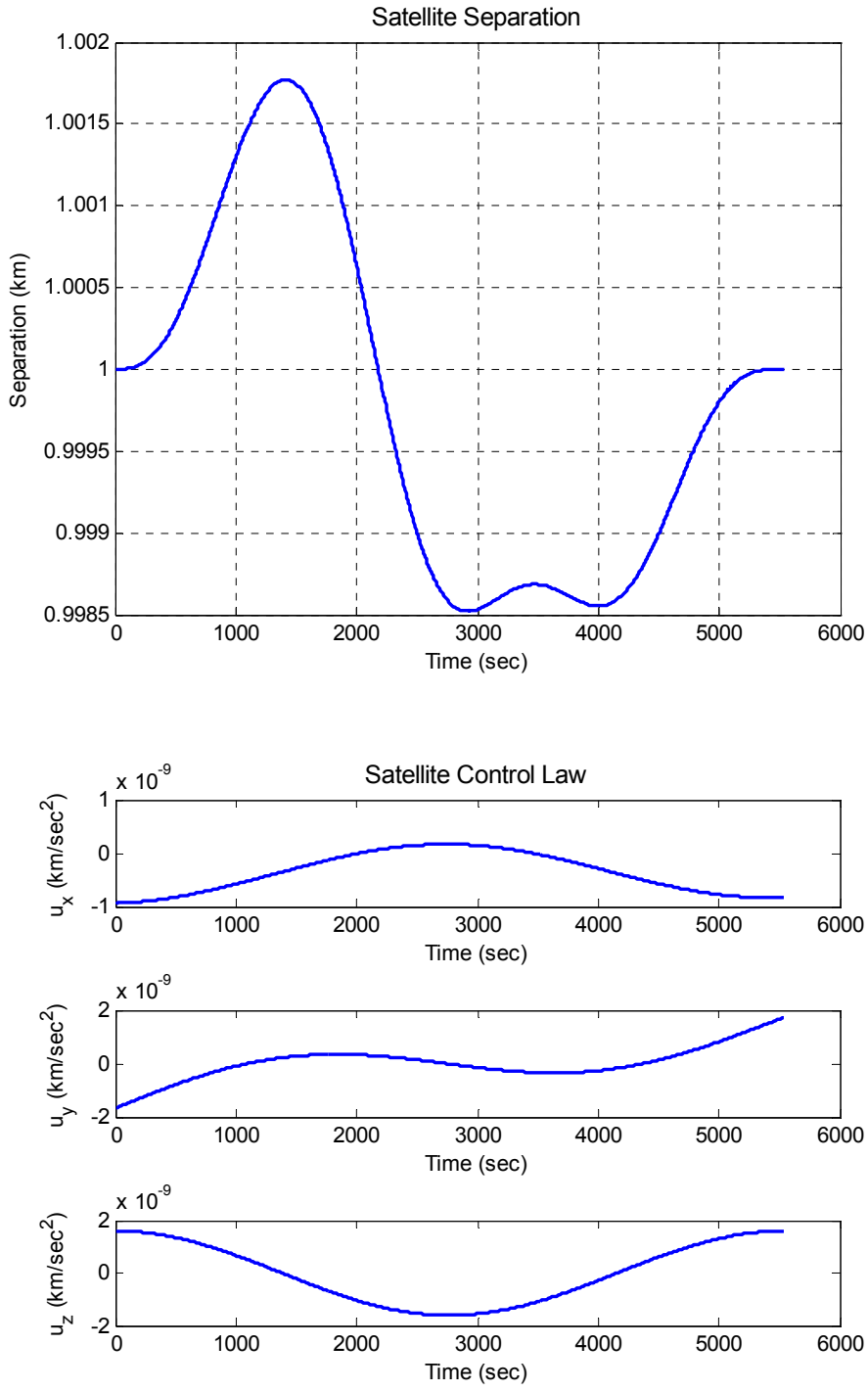

Figure 32. More Weight on Minimizing Control

These results convey the possibility of even further ΔV savings as the performance index is modified to add more weight to minimizing control. This comparison produces a ΔV savings of 4 m/s/year, with the loss in separation precision shown in Figure 33.

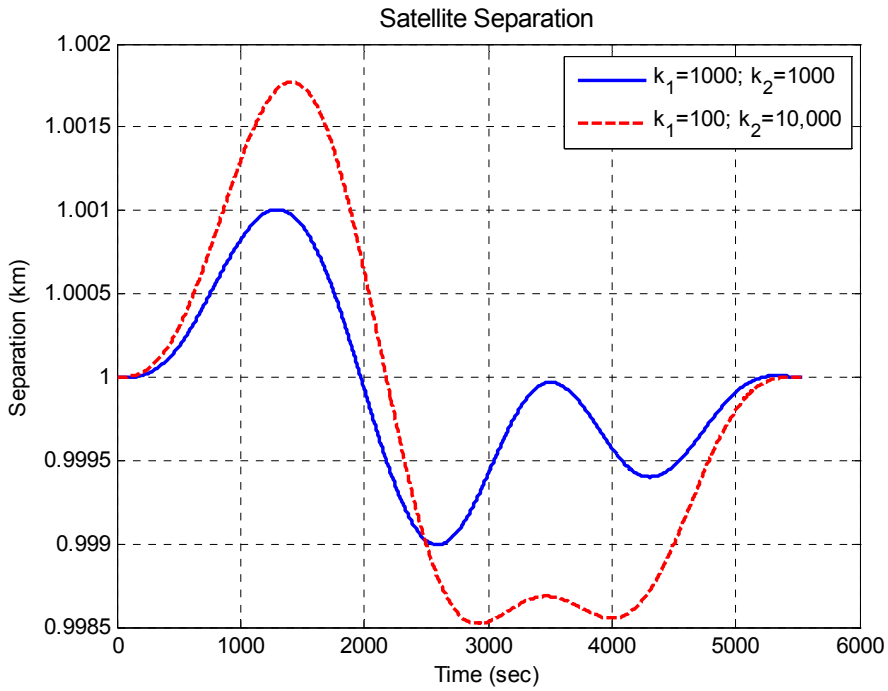

Figure 33. Comparison in Satellite Separation for Modified Performance Index

V. Conclusions and Recommendations

Conclusions of Research

Given the derived initial conditions, the control requirements necessary to maintain the integrity of a circular formation were shown to be highly dependent on the starting phase angle of the deputy satellite within the formation. An initial phase of zero degrees requires less control authority as the inclination of the reference trajectory is increased, reaching an apparent minimum at or near a polar configuration. This was shown to be function of the nodal regression rates within the formation. For an initial phase of 90 degrees, the minimum control costs occur at a mid-latitude configuration, an apparent result of the secular drift rates in the argument of perigee within the formation. At the crossing of the resulting trend lines, it has been shown that for circular, inclined reference trajectories, there exist 1-km circular formation configurations that can be maintained for control costs on the order of 40-50 m/s/year at an altitude of 400 km.

Looking to further minimize the necessary control authority, it was shown that increasing the altitude of the formation from 400 to 800 km results in a 25% savings in annual control costs for both 45 and 90 degree inclinations. The resulting control histories also enhance the separation integrity of the formation. Further increases in altitude should result in similar ΔV savings, where the altitude requirements for an operation are solely restricted by the mission objectives and the capabilities of a given sensor system.

Achieving higher image resolutions requires an increase of the aperture size of the sensor. The results of this research show that as the formation radius is increased to

expand the synthetic aperture of the formation, the control costs are increased on a linear scale. A tenfold increase in the formation radius results in a tenfold increase in annual ΔV costs. At the same time, formation sizes less than 1-km would result in further annual control savings. The selection of the operational formation radius is once again strictly a function of the capabilities of the employed sensor.

Lastly, it was shown that there are alternate performance index configurations that produce further ΔV savings at the expense of the integrity of the circular formation. Selection of the weighting constants for the performance index is an engineering trade-off between the position requirements of the sensor system and minimizing control costs. The savings of the modified performance index are modest, with the example given only achieving a 6% reduction in the annual ΔV costs. Expanding the error tolerances on the precision of the circular formation even further should produce additional ΔV savings.

Recommendations for Future Research

The results of this research portray a promising future for the utilization of satellite formations for remote sensing operations. Expanding upon the findings of this research will be vital to vindicating the utility of satellite formation applications. First and foremost, the results of this research are based on the quasi-periodic solutions of short-term optimization of the formation dynamics, which allow for only the *estimation* of long-term control requirements. To verify the accuracy of these results, a periodic solution must be found, which would require control of the reference trajectory to match the period of the semi-major axis and its equatorial crossing. This is one of many

possible methods of achieving a periodic solution, which would allow for the exact determination of long-term fuel requirements for multi-year formation operations.

This research utilized classical methods for solving for the optimal solution to a nonlinear continuous dynamic system, in particular finding a local minimum given an arbitrary initial guess. At no time were the findings of this research verified as a global minimum in the design space. With that said, the discovery of even further control savings may be possible with further examination of the design space. Alternate methods of solving the optimization problem for this nonlinear continuous dynamic system may also produce or verify a global minimum for this design space.

The initial conditions derived for this research were chosen specifically to match the mean motions of all participants in the formation. This does not preclude the existence of alternate initial conditions which could be better suited for optimizing this particular problem. In addition, the results of this research focused on analyzing initial phase angles of 0 and 90 degrees, while assuming that their 180 and 270 degree counterparts would result in similar control requirements. This must be verified to validate the necessary control requirements for a 4-satellite cluster. Also, if it is desired to include additional satellites into the formation, the initial conditions derived in Appendix D must be used to expand on this research.

Finally, the creation of a closed-loop controller to produce the open-loop control histories found to optimize the formation dynamics must be found. The development of a closed-loop controller is essential to the employment of a satellite cluster for remote sensing and surveillance applications.

Appendix A. Equations of Motion

Equations of Motion for Reference Trajectory

$$\dot{X} = P_X$$
$$\dot{Y} = P_Y$$
$$\dot{Z} = P_Z$$
$$\dot{P}_X = -\frac{\mu X}{\left(X^2+Y^2+Z^2\right)^{3/2}} - \frac{3\mu J_2 R_\oplus{}^2 X}{2\left(X^2+Y^2+Z^2\right)^{5/2}} + \frac{15\mu J_2 R_\oplus{}^2 XZ^2}{2\left(X^2+Y^2+Z^2\right)^{7/2}}$$
$$\dot{P}_Y = -\frac{\mu Y}{\left(X^2+Y^2+Z^2\right)^{3/2}} - \frac{3\mu J_2 R_\oplus{}^2 Y}{2\left(X^2+Y^2+Z^2\right)^{5/2}} + \frac{15\mu J_2 R_\oplus{}^2 YZ^2}{2\left(X^2+Y^2+Z^2\right)^{7/2}}$$
$$\dot{P}_Z = -\frac{\mu Z}{\left(X^2+Y^2+Z^2\right)^{3/2}} - \frac{9\mu J_2 R_\oplus{}^2 Z}{2\left(X^2+Y^2+Z^2\right)^{5/2}} + \frac{15\mu J_2 R_\oplus{}^2 Z^3}{2\left(X^2+Y^2+Z^2\right)^{7/2}}$$

Equations of Motion for Deputy Satellite

$$\dot{X} = P_X$$
$$\dot{Y} = P_Y$$
$$\dot{Z} = P_Z$$
$$\dot{P}_X = -\frac{\mu X}{\left(X^2+Y^2+Z^2\right)^{3/2}} - \frac{3\mu J_2 R_\oplus{}^2 X}{2\left(X^2+Y^2+Z^2\right)^{5/2}} + \frac{15\mu J_2 R_\oplus{}^2 XZ^2}{2\left(X^2+Y^2+Z^2\right)^{7/2}} + u_X$$
$$\dot{P}_Y = -\frac{\mu Y}{\left(X^2+Y^2+Z^2\right)^{3/2}} - \frac{3\mu J_2 R_\oplus{}^2 Y}{2\left(X^2+Y^2+Z^2\right)^{5/2}} + \frac{15\mu J_2 R_\oplus{}^2 YZ^2}{2\left(X^2+Y^2+Z^2\right)^{7/2}} + u_Y$$
$$\dot{P}_Z = -\frac{\mu Z}{\left(X^2+Y^2+Z^2\right)^{3/2}} - \frac{9\mu J_2 R_\oplus{}^2 Z}{2\left(X^2+Y^2+Z^2\right)^{5/2}} + \frac{15\mu J_2 R_\oplus{}^2 Z^3}{2\left(X^2+Y^2+Z^2\right)^{7/2}} + u_Z$$

Appendix B. Optimization Hamiltonian and Co-State Equations of Motion

Optimization Hamiltonian

$$
\begin{aligned}
H = {} & k_1\left[\sqrt{(X-X_R)^2+(Y-Y_R)^2+(Z-Z_R)^2}-r_d\right]^2 \\
& + k_2\left[{u_X}^2+{u_Y}^2+{u_Z}^2\right]+\lambda_X P_X+\lambda_Y P_Y+\lambda_Z P_Z \\
& + \lambda_{P_X}\left[-\frac{\mu X}{\left(X^2+Y^2+Z^2\right)^{3/2}}-\frac{3\mu J_2 {R_\oplus}^2 X}{2\left(X^2+Y^2+Z^2\right)^{5/2}}+\frac{15\mu J_2 {R_\oplus}^2 XZ^2}{2\left(X^2+Y^2+Z^2\right)^{7/2}}+u_X\right] \\
& + \lambda_{P_Y}\left[-\frac{\mu Y}{\left(X^2+Y^2+Z^2\right)^{3/2}}-\frac{3\mu J_2 {R_\oplus}^2 Y}{2\left(X^2+Y^2+Z^2\right)^{5/2}}+\frac{15\mu J_2 {R_\oplus}^2 YZ^2}{2\left(X^2+Y^2+Z^2\right)^{7/2}}+u_Y\right] \\
& + \lambda_{P_Z}\left[-\frac{\mu Z}{\left(X^2+Y^2+Z^2\right)^{3/2}}-\frac{9\mu J_2 {R_\oplus}^2 Z}{2\left(X^2+Y^2+Z^2\right)^{5/2}}+\frac{15\mu J_2 {R_\oplus}^2 Z^3}{2\left(X^2+Y^2+Z^2\right)^{7/2}}+u_Z\right]
\end{aligned}
$$

Co-State Equations of Motion

$$
\begin{aligned}
\dot{\lambda}_X = {} & -\frac{2k_1(X-X_R)\left[\sqrt{(X-X_R)^2+(Y-Y_R)^2+(Z-Z_R)^2}-r_d\right]}{\sqrt{(X-X_R)^2+(Y-Y_R)^2+(Z-Z_R)^2}} \\
& - \lambda_{P_X}\left[\begin{array}{l}\dfrac{-\mu}{(X^2+Y^2+Z^2)^{3/2}}+\dfrac{3\mu X^2}{(X^2+Y^2+Z^2)^{5/2}}-\dfrac{3\mu J_2 {R_\oplus}^2}{2(X^2+Y^2+Z^2)^{5/2}} \\ +\dfrac{15\mu J_2 {R_\oplus}^2 X^2}{2(X^2+Y^2+Z^2)^{7/2}}+\dfrac{15\mu J_2 {R_\oplus}^2 Z^2}{2(X^2+Y^2+Z^2)^{7/2}}-\dfrac{105\mu J_2 {R_\oplus}^2 X^2 Z^2}{2(X^2+Y^2+Z^2)^{9/2}}\end{array}\right] \\
& - \lambda_{P_Y}\left[\frac{3\mu XY}{(X^2+Y^2+Z^2)^{5/2}}+\frac{15\mu J_2 {R_\oplus}^2 XY}{2(X^2+Y^2+Z^2)^{7/2}}-\frac{105\mu J_2 {R_\oplus}^2 XYZ^2}{2(X^2+Y^2+Z^2)^{9/2}}\right] \\
& - \lambda_{P_Z}\left[\frac{3\mu XZ}{(X^2+Y^2+Z^2)^{5/2}}+\frac{45\mu J_2 {R_\oplus}^2 XZ}{2(X^2+Y^2+Z^2)^{7/2}}-\frac{105\mu J_2 {R_\oplus}^2 XZ^3}{2(X^2+Y^2+Z^2)^{9/2}}\right]
\end{aligned}
$$

$$\dot{\lambda}_Y = -\frac{2k_1(Y-Y_R)\left[\sqrt{(X-X_R)^2+(Y-Y_R)^2+(Z-Z_R)^2}-r_d\right]}{\sqrt{(X-X_R)^2+(Y-Y_R)^2+(Z-Z_R)^2}}$$
$$-\lambda_{P_X}\left[\frac{3\mu XY}{(X^2+Y^2+Z^2)^{5/2}}+\frac{15\mu J_2 {R_\oplus}^2 XY}{2(X^2+Y^2+Z^2)^{7/2}}-\frac{105\mu J_2 {R_\oplus}^2 XYZ^2}{2(X^2+Y^2+Z^2)^{9/2}}\right]$$
$$-\lambda_{P_Y}\left[\begin{array}{l}\frac{-\mu}{(X^2+Y^2+Z^2)^{3/2}}+\frac{3\mu Y^2}{(X^2+Y^2+Z^2)^{5/2}}-\frac{3\mu J_2 {R_\oplus}^2}{2(X^2+Y^2+Z^2)^{5/2}}\\ +\frac{15\mu J_2 {R_\oplus}^2 Y^2}{2(X^2+Y^2+Z^2)^{7/2}}+\frac{15\mu J_2 {R_\oplus}^2 Z^2}{2(X^2+Y^2+Z^2)^{7/2}}-\frac{105\mu J_2 {R_\oplus}^2 Y^2Z^2}{2(X^2+Y^2+Z^2)^{9/2}}\end{array}\right]$$
$$-\lambda_{P_Z}\left[\frac{3\mu YZ}{(X^2+Y^2+Z^2)^{5/2}}+\frac{45\mu J_2 {R_\oplus}^2 YZ}{2(X^2+Y^2+Z^2)^{7/2}}-\frac{105\mu J_2 {R_\oplus}^2 YZ^3}{2(X^2+Y^2+Z^2)^{9/2}}\right]$$

$$\dot{\lambda}_Z = -\frac{2k_1(Z-Z_R)\left[\sqrt{(X-X_R)^2+(Y-Y_R)^2+(Z-Z_R)^2}-r_d\right]}{\sqrt{(X-X_R)^2+(Y-Y_R)^2+(Z-Z_R)^2}}$$
$$-\lambda_{P_X}\left[\frac{3\mu XZ}{(X^2+Y^2+Z^2)^{5/2}}+\frac{45\mu J_2 {R_\oplus}^2 XZ}{2(X^2+Y^2+Z^2)^{7/2}}-\frac{105\mu J_2 {R_\oplus}^2 XZ^3}{2(X^2+Y^2+Z^2)^{9/2}}\right]$$
$$-\lambda_{P_Y}\left[\frac{3\mu YZ}{(X^2+Y^2+Z^2)^{5/2}}+\frac{45\mu J_2 {R_\oplus}^2 YZ}{2(X^2+Y^2+Z^2)^{7/2}}-\frac{105\mu J_2 {R_\oplus}^2 YZ^3}{2(X^2+Y^2+Z^2)^{9/2}}\right]$$
$$-\lambda_{P_Z}\left[\begin{array}{l}\frac{-\mu}{(X^2+Y^2+Z^2)^{3/2}}+\frac{3\mu Z^2}{(X^2+Y^2+Z^2)^{5/2}}-\frac{9\mu J_2 {R_\oplus}^2}{2(X^2+Y^2+Z^2)^{5/2}}\\ +\frac{45\mu J_2 {R_\oplus}^2 Z^2}{(X^2+Y^2+Z^2)^{7/2}}-\frac{105\mu J_2 {R_\oplus}^2 Z^4}{2(X^2+Y^2+Z^2)^{9/2}}\end{array}\right]$$

$$\dot{\lambda}_{P_X} = -\lambda_X$$

$$\dot{\lambda}_{P_Y} = -\lambda_Y$$

$$\dot{\lambda}_{P_Z} = -\lambda_Z$$

Appendix C. Discrete vs. Continuous Control Performance

One question that still exists pertains to the performance of the continuous control laws against a more realistic control history employed with current spacecraft propulsion systems. A discrete zero-order hold control law employs a constant acceleration magnitude over a specified time step, which differs from an impulsive control law which employs instantaneous boosts of acceleration at specified instances in time. It was desired to compare continuous control with a similar discrete zero-order hold control law, which also served as further validation of the equations of motion.

When integrating equations of motion in Matlab, error tolerances can be provided to enhance the accuracy of the results, and in this case extremely low error tolerances were provided to amplify the continuous nature of this system of equations. Despite this fact, the output results are provided to the user in vector form using discrete time steps, which are rarely the time steps Matlab utilized during the integration process, especially if error tolerances are provided for increased accuracy. In this case, the resulting control input vector $\vec{u}(t)$ is calculated in Matlab using a relatively small time step, but can only be provided as a finite vector to the user. For this reason, a comparison of the performance of a discrete zero-order hold control input against the resulting continuous control law should better convey the accuracy and the reliability of the formulated control histories.

The following figures show a comparison of the continuous control law against two discrete zero-order hold control laws, one at an approximate 1.1-second hold and the second at an approximate 5.5-second hold.

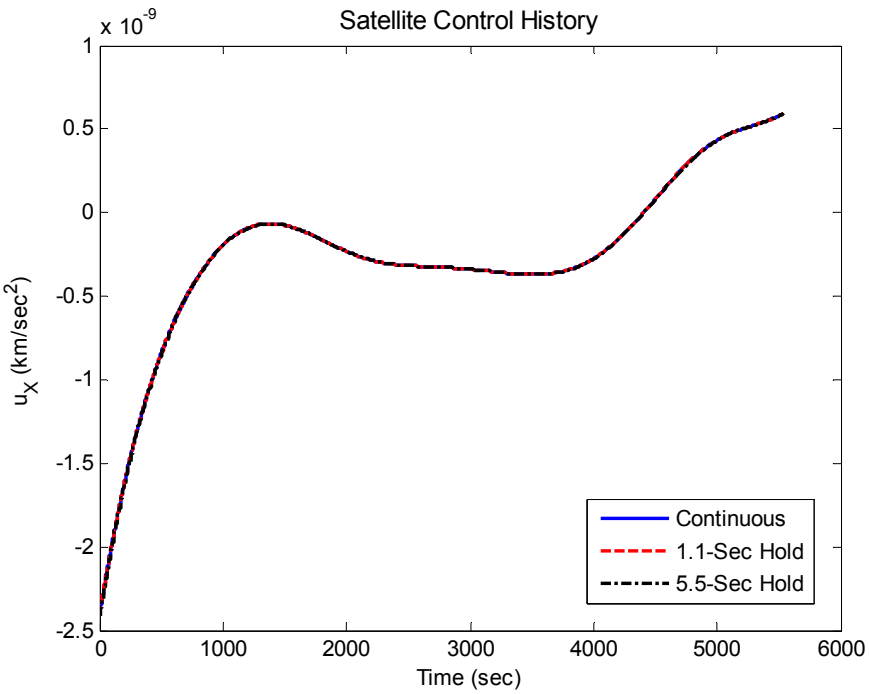

Figure 34. Comparison of Discrete vs. Continuous Control Histories

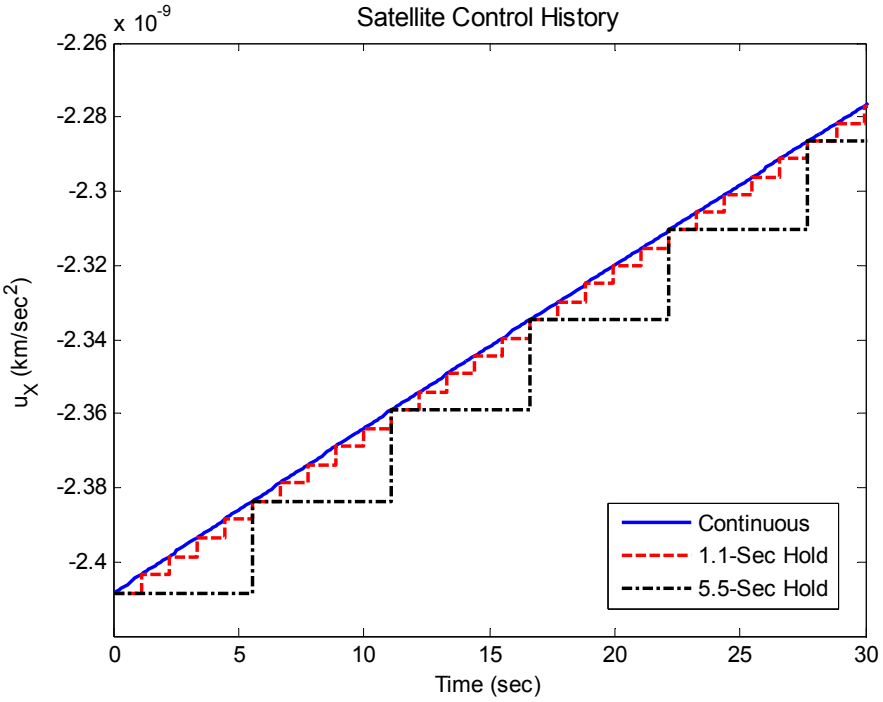

Figure 35. Zoom-In View of Figure 34

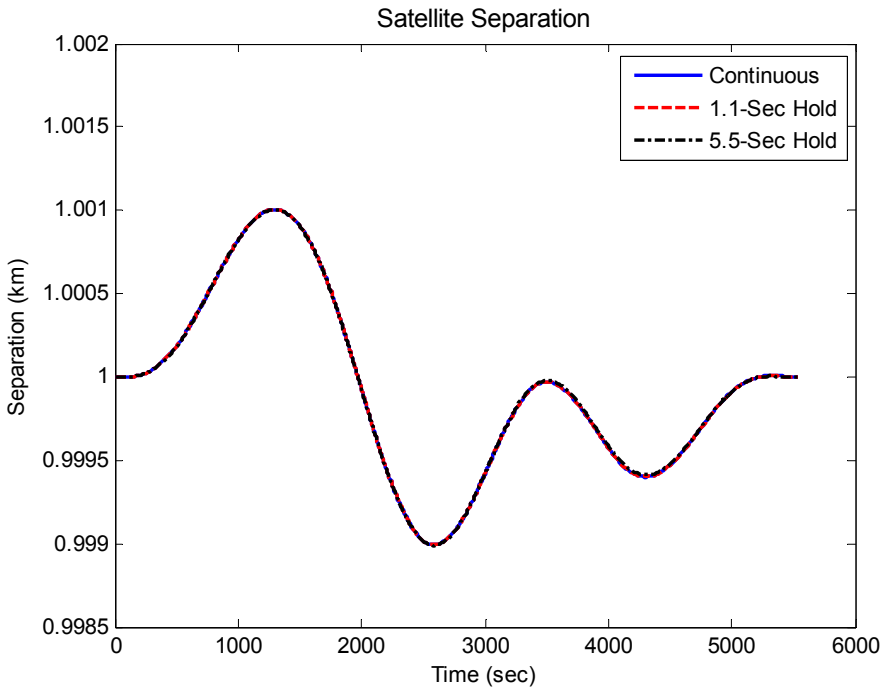

Figure 36. Comparison of Discrete vs. Continuous Satellite Drift

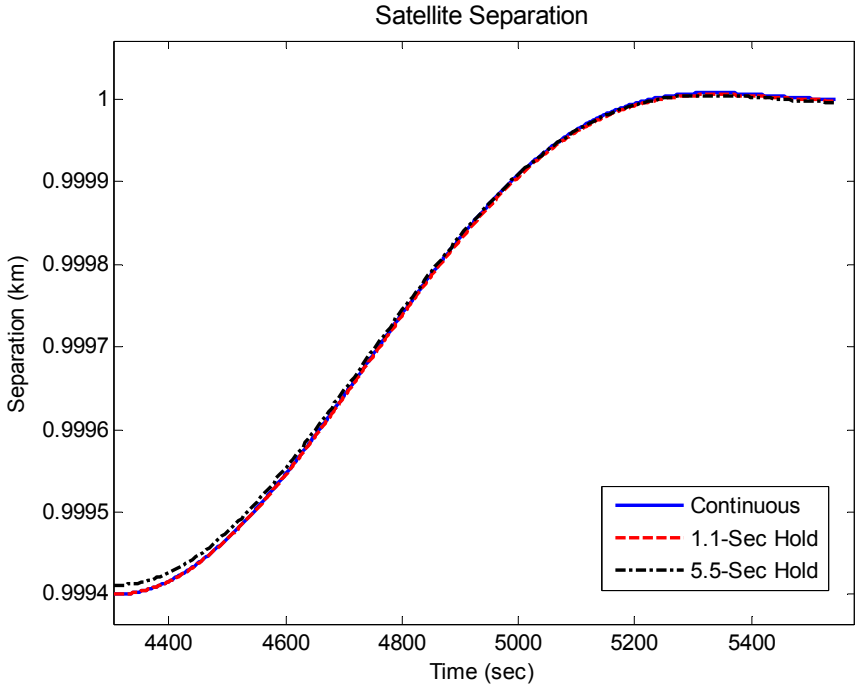

Figure 37. Zoom-In View of Figure 36

This particular example is for a formation altitude of 400 km and an inclination of 45 degrees. The initial phase angle of the deputy satellite is zero degrees. Figure 34 shows the inertial-X component of the control acceleration vector, with Figure 35 zooming in on the first 30 seconds to show the discrepancy between the continuous control and the two zero-order hold controllers. Figures 36 and 37 show that there is very little deviation in the separations given a zero-order hold controller. This leads to the conclusion that the formation sensitivity to differing control algorithms is relatively small. Obviously, as the hold time is increased, deviation from the desired formation dynamics will also increase, evident from the 5.5 second hold shown in Figure 37.

Appendix D. General Derivation of the Initial Conditions Given Any Phase Angle

The derivation of the initial conditions for the deputy satellite can be generalized for any initial phase angle. As before, the relative initial conditions developed by Sabol el al. (15:272-273) provide a starting point for the derivation:

$$x_0 = (r_d / 2)\cos\theta \tag{94}$$

$$\dot{x}_0 = -(r_d n / 2)\sin\theta \tag{95}$$

$$y_0 = 2\dot{x}_0 / n \tag{96}$$

$$\dot{y}_0 = -2nx_0 \tag{97}$$

$$z_0 = \pm\sqrt{3}x_0 \tag{98}$$

$$\dot{z}_0 = \pm\sqrt{3}\dot{x}_0 \tag{99}$$

The inertial position vector of the deputy satellite can be represented in the relative Hill frame as follows:

$$\vec{r} = (R + x_0)\hat{x} + y_0\hat{y} + z_0\hat{z} \tag{100}$$

The inertial velocity vector of the deputy satellite can be expressed in the relative Hill frame in the following form:

$$\dot{\vec{r}} = \frac{^{\hat{i}}d}{dt}(\vec{r}) = \frac{^{\hat{o}}d}{dt}(\vec{r}) + \vec{\omega}_{o/i} \times \vec{r} \tag{101}$$

where once again $\vec{\omega}_{o/i}$ is the angular velocity of the relative frame with respect to the inertial frame, and can be represented in the relative frame as $n\hat{z}$. Plugging Eqs. (94)-(100) into Eq. (101) produces the following inertial velocity vector:

$$\dot{\vec{r}} = \frac{r_d n}{2}\sin\theta\hat{x} + \left(nR - \frac{r_d n}{2}\cos\theta\right)\hat{y} \mp \frac{\sqrt{3}r_d n}{2}\sin\theta\hat{z} \tag{102}$$

Now that the direction of the inertial velocity vector is found, the magnitude must be adjusted to match the energies of the reference trajectory and the deputy satellite. The magnitude is solved for by equating the energies, which produces the following result:

$$v = \sqrt{2\left(\varepsilon + \frac{\mu}{\|\vec{r}\|}\right)} \tag{103}$$

This magnitude is then multiplied by the unit vector in the inertial velocity direction to solve for the initial velocity vector:

$$\vec{v} = v\frac{\dot{\vec{r}}}{\|\dot{\vec{r}}\|} \tag{104}$$

Appendix E. Matlab Optimization Code

```
%%%%%%%%%%%%%%%%%%%%%%%%%%%%%%%%%%%%%%%%%%%%%%%%%%%%%%%%%%%%%%%%%%%%%%%%%%%%
%optimize.m
%
%This script accepts user-defined initial conditions for the states
%of two satellites in a circular formation, and then uses continuous
%dynamic optimization to minimize the control input while maintaining
%a circular formation.  The equations of motion for both satellites,
%along with the co-state equations derived from the user-defined
%performance index, must be provided in the script states_eom.m.
%
%Capt Jason Baldwin
%1 Feb 07
%%%%%%%%%%%%%%%%%%%%%%%%%%%%%%%%%%%%%%%%%%%%%%%%%%%%%%%%%%%%%%%%%%%%%%%%%%%%
clc; clear all; close all;
global k1 k2 k3 Rdes optim_on control_on plot_optim output_optim Re mu J2
global DU DUTU X_bc

%%%%%%%%%%%%%%%%%%%%%%%%%%%%%%%%%%%%%%%%%%%%%%%%%%%%%%%%%%%%%%%%%%%%%%%%%%%%
%Given the following performance index ...
%
% J = k3*(X-X_BC)^2 + integral ( k1{|R-Rref|-Rdes}^2 + k2|u|^2 )
%
%The user must supply the weighting factors k1(sat sep), k2(control),
%and k3(difference between end state and desired end state)
%%%%%%%%%%%%%%%%%%%%%%%%%%%%%%%%%%%%%%%%%%%%%%%%%%%%%%%%%%%%%%%%%%%%%%%%%%%%
k1 = 1e3;
k2 = 1e3;
k3 = 1e8;

%%%%%%%%%%%%%%%%%%%%%%%%%%%%%%%%%%%%%%%%%%%%%%%%%%%%%%%%%%%%%%%%%%%%%%%%%%%%
%Establish initial guess for lagrange multipliers
%%%%%%%%%%%%%%%%%%%%%%%%%%%%%%%%%%%%%%%%%%%%%%%%%%%%%%%%%%%%%%%%%%%%%%%%%%%%
lam_ini = zeros(6,1);

%For simulation, add capability to turn optimization (control) off
%0 = control off; 1 = control on
optim_on = 1;
control_on = 1;
output_optim = 1;

%Switch for J2 perturbation -- 0 = off; 1 = on
J2 = 1;

%%%%%%%%%%%%%%%%%%%%%%%%%%
%Define Earth constants
%%%%%%%%%%%%%%%%%%%%%%%%%%
mu = 398600.4418;       %Earth gravity constant
Re = 6378.137;          %Earth equatorial radius

%%%%%%%%%%%%%%%%%%%%%%%%%%%%
%Define constants of motion
%%%%%%%%%%%%%%%%%%%%%%%%%%%%
r = 400;                        %Altitude of circular reference orbit (km)
n = sqrt(mu/(Re+r)^3);          %Mean motion of reference orbit (rad/s)

%%%%%%%%%%%%%%%%%%%%%%%%%%%%%%%%%%%%%%%%%%%%%%%%%%%%%%%%%%%%%%%%%%%%%%%%%%%%
```

```
%Input desired orbital elements for formation orbit
%%%%%%%%%%%%%%%%%%%%%%%%%%%%%%%%%%%%%%%%%%%%%%%%%%%
a = Re + r;             %semi-major axis (km)
e = 0;                  %eccentricity
i = 45;                  %inclination (deg)
Om = 0;                 %longitude of ascending node (deg)
w = 0;                  %argument of perigee (deg)
nu = 0;                 %true anomaly (deg)
phase = 0;             %phase angle of relative orbit (deg) (0 or 90)
Rdes = 1;               %Desired relative orbit radius (km)

%%%%%%%%%%%%%%%%%%%%%%%%%%%%%%%%%%%%%%%%%%%%%%%%%%%%%%%%%
%Input desired initial coordinates of deputy satellite in
%relative frame for phase = 0 deg
%%%%%%%%%%%%%%%%%%%%%%%%%%%%%%%%%%%%%%%%%%%%%%%%%%%%%%%%%
if phase == 0
    x0 = a + Rdes/2;
    y0 = 0;
    z0 = sqrt(3)/2*Rdes;
    px0 = 0;
    py0 = sqrt(2*mu/sqrt(a^2+a*Rdes+Rdes^2) - mu/a);
    pz0 = 0;
    X_rel_0 = [x0 y0 z0 px0 py0 pz0]';
end

%%%%%%%%%%%%%%%%%%%%%%%%%%%%%%%%%%%%%%%%%%%%%%%%%%%%%%%%%
%Input desired initial coordinates of deputy satellite in
%relative frame for phase = 90 deg
%%%%%%%%%%%%%%%%%%%%%%%%%%%%%%%%%%%%%%%%%%%%%%%%%%%%%%%%%
if phase == 90
    x0 = a;
    px0 = -0.5*n*Rdes;
    y0 = 2*px0/n;
    py0 = sqrt(mu/a);
    z0 = 0;
    pz0 = -sqrt(3)/2*n*Rdes;
    %Calculate the unit vector for velocity
    vhat = [-px0; py0; pz0]/norm([px0; py0; pz0]);
    %Calculate the necessary magnitude for energy matching
    K = sqrt(2*mu/sqrt(a^2+Rdes^2) - mu/a);
    %Calculate initial velocities
    vvec = K*vhat;
    px0 = vvec(1);
    py0 = vvec(2);
    pz0 = vvec(3);
    X_rel_0 = [x0 y0 z0 px0 py0 pz0]';
end

%%%%%%%%%%%%%%%%%%%%%%%%%%%%%%%%%%%%%%%%%%%%%%%%%%%%%%%%%%
%Convert the orbital elements into earth-centered inertial
%radius and velocity
%%%%%%%%%%%%%%%%%%%%%%%%%%%%%%%%%%%%%%%%%%%%%%%%%%%%%%%%%%

%Convert degrees to radians
i = i*pi/180;
Om = Om*pi/180;
w = w*pi/180;
nu = nu*pi/180;

%Calculate semi-latus rectum and radius magnitude
p = a*(1-e^2);
```

```
r_mag = p/(1+e*cos(nu));

%Calculate radius and velocity vectors in perifocal coordinates
rad = [r_mag*cos(nu); r_mag*sin(nu); 0];
vel = sqrt(mu/p)*[-sin(nu); e+cos(nu); 0];

%Calculate the rotation matrix from perifocal to inertial
R11 = cos(Om)*cos(w) - sin(Om)*sin(w)*cos(i);
R12 = -cos(Om)*sin(w) - sin(Om)*cos(w)*cos(i);
R13 = sin(Om)*sin(i);
R21 = sin(Om)*cos(w) + cos(Om)*sin(w)*cos(i);
R22 = -sin(Om)*sin(w) + cos(Om)*cos(w)*cos(i);
R23 = -cos(Om)*sin(i);
R31 = sin(w)*sin(i);
R32 = cos(w)*sin(i);
R33 = cos(i);

R_pi = [R11 R12 R13; R21 R22 R23; R31 R32 R33];

%Calculate the inertial radius and velocity vectors of formation center
r_chief = R_pi*rad;
v_chief = R_pi*vel;

%Set the initial state vector of formation center
Xref_0 = [r_chief' v_chief']';

%Calculate the state vector of deputy in inertial coordinates
C_IR = rel_to_inert(Xref_0);
C = [C_IR zeros(3,3); zeros(3,3) C_IR];
X_0 = C*X_rel_0;

%%%%%%%%%%%%%%%%%%%%%%%%%%%%%%%%%%%%%%%%
%Switch everything to canonical units
%%%%%%%%%%%%%%%%%%%%%%%%%%%%%%%%%%%%%%%%
DU = a;                 %Canonical position unit
TU = sqrt(mu)/a^(3/2);  %Canonical time unit
DUTU = sqrt(mu/a);      %Canonical velocity unit
a = 1;
mu = 1;
Re = Re/DU;
Rdes = Rdes/DU;
Xref_0(1:3) = Xref_0(1:3)/DU;
Xref_0(4:6) = Xref_0(4:6)/DUTU;
X_0(1:3) = X_0(1:3)/DU;
X_0(4:6) = X_0(4:6)/DUTU;
X_rel_0(1:3) = X_rel_0(1:3)/DU;
X_rel_0(4:6) = X_rel_0(4:6)/DUTU;

%%%%%%%%%%%%%%%%%%%%%%%%%%%%%%%%%%%%%%%%%%%%%%%%%%%%%%%%%%%%%%%%%%%%%%%%%%%%
%Calculate the time between consecutive crossings of the argument
%of apogee.  Also, at t = 1 period, define the reference states at
%that time to be used in calculating our boundary conditions
%%%%%%%%%%%%%%%%%%%%%%%%%%%%%%%%%%%%%%%%%%%%%%%%%%%%%%%%%%%%%%%%%%%%%%%%%%%%
T_2body = 2*pi/sqrt(mu)*a^(3/2);
T = 1.01*T_2body;
div = 1e4;
kill = 0;
tspan = 0:T/div:T;
options = odeset('RelTol',1e-13,'AbsTol',1e-13);
[t,xf] = ode45(@inertialJ2_eom,tspan,Xref_0,options);
len = length(t);
```

```
xref = xf(:,1);
yref = xf(:,2);
zref = xf(:,3);
ref_mag = sqrt(xref.^2+yref.^2+zref.^2);
for i = len:-1:1
    if ref_mag(i)-ref_mag(i-1) > 0
        new_x0 = [xf(i-2,1) xf(i-2,2) xf(i-2,3) ...
                  xf(i-2,4) xf(i-2,5) xf(i-2,6)];
        tspan2 = t(i-2):abs(t(i+2)-t(i-2))/div:t(i+2);
        [t2,xf2] = ode45(@inertialJ2_eom,tspan2,new_x0,options);
        len2 = length(t2);
        xref2 = xf2(:,1);
        yref2 = xf2(:,2);
        zref2 = xf2(:,3);
        ref_mag2 = sqrt(xref2.^2+yref2.^2+zref2.^2);
        for j = len2:-1:1
            if ref_mag2(j)-ref_mag2(j-1) > 0
                new_x0 = [xf2(j-2,1) xf2(j-2,2) xf2(j-2,3) ...
                          xf2(j-2,4) xf2(j-2,5) xf2(j-2,6)];
                tspan3 = t2(j-2):abs(t2(j+2)-t2(j-2))/div:t2(j+2);
                [t3,xf3] = ode45(@inertialJ2_eom,tspan3,new_x0,options);
                len3 = length(t3);
                xref3 = xf3(:,1);
                yref3 = xf3(:,2);
                zref3 = xf3(:,3);
                ref_mag3 = sqrt(xref3.^2+yref3.^2+zref3.^2);
                for k = len3:-1:1
                    if ref_mag3(k)-ref_mag3(k-1) > 0
                        T_period = t3(k);
                        Xref_bc = xf3(k,1);
                        Yref_bc = xf3(k,2);
                        Zref_bc = xf3(k,3);
                        PXref_bc = xf3(k,4);
                        PYref_bc = xf3(k,5);
                        PZref_bc = xf3(k,6);
                        kill = 1;
                        break;
                    end
                end
            end
            if kill == 1
                break;
            end
        end
    end
    if kill == 1
        break;
    end
end

%%%%%%%%%%%%%%%%%%%%%%%%%%%%%%%%%%%%%%%%%%%%%%%%%%%%%%%%%%%%%%%%%%%%%%%%%%%
%Calculate the final boundary conditions for the deputy satellite
%%%%%%%%%%%%%%%%%%%%%%%%%%%%%%%%%%%%%%%%%%%%%%%%%%%%%%%%%%%%%%%%%%%%%%%%%%%
%Calculate transformation matrix
Ref_bc = [Xref_bc; Yref_bc; Zref_bc; PXref_bc; PYref_bc; PZref_bc];
C_IR = rel_to_inert(Ref_bc);
R_bc = [C_IR zeros(3,3); zeros(3,3) C_IR];

%Calculate new initial conditions based on new altitude
if phase == 0
    a2 = norm([Xref_bc Yref_bc Zref_bc]);
```

```
    x0 = a2 + Rdes/2;
    y0 = 0;
    z0 = sqrt(3)/2*Rdes;
    px0 = 0;
    py0 = sqrt(2*mu/sqrt(a2^2+a2*Rdes+Rdes^2) - mu/a2);
    pz0 = 0;
    X_rel_bc = [x0 y0 z0 px0 py0 pz0]';
    X_bc = R_bc*X_rel_bc;
end

if phase == 90
    a2 = norm([Xref_bc Yref_bc Zref_bc]);
    n2 = sqrt(mu/(a2)^3);
    x0 = a2;
    px0 = -0.5*n2*Rdes;
    y0 = 2*px0/n2;
    py0 = sqrt(mu/a2);
    z0 = 0;
    pz0 = -sqrt(3)/2*n2*Rdes;
    %Calculate the unit vector for velocity
    vhat = [-px0; py0; pz0]/norm([px0; py0; pz0]);
    %Calculate the necessary magnitude for energy matching
    K = sqrt(2*mu/sqrt(a2^2+Rdes^2) - mu/a2);
    %Calculate initial velocities
    vvec = K*vhat;
    px0 = vvec(1);
    py0 = vvec(2);
    pz0 = vvec(3);
    X_rel_bc = [x0 y0 z0 px0 py0 pz0]';
    X_bc = R_bc*X_rel_bc;
end

%%%%%%%%%%%%%%%%%%%%%%%%%%%%%%%%%%%%%%%%%%%%%%%%%%%%%%%%%%%%%%%%
%Call two-point boundary value problem function to solve
%for the initial lagrange multipliers which minimize
%performance index
%%%%%%%%%%%%%%%%%%%%%%%%%%%%%%%%%%%%%%%%%%%%%%%%%%%%%%%%%%%%%%%%
%Set the number of time steps and the time span for integration
tsteps = 1e3;
Tspan = 0:T_period/tsteps:T_period;
if optim_on == 1
    [lambda_0,lambda_f,lambda_bc] = tpbvp(X_0,Xref_0,lam_ini,Tspan);
end

%Integrate once with converged solution
x_0 = [Xref_0' X_0' lambda_0']';
[t,states] = ode45(@states_eom,Tspan,x_0,options);

%Unpack final results and convert to metric units
Xref = states(:,1)*DU;
Yref = states(:,2)*DU;
Zref = states(:,3)*DU;
PXref = states(:,4)*DUTU;
PYref = states(:,5)*DUTU;
PZref = states(:,6)*DUTU;

X = states(:,7)*DU;
Y = states(:,8)*DU;
Z = states(:,9)*DU;
PX = states(:,10)*DUTU;
PY = states(:,11)*DUTU;
```

```
PZ = states(:,12)*DUTU;

lamX = states(:,13)*DUTU^2/DU;
lamY = states(:,14)*DUTU^2/DU;
lamZ = states(:,15)*DUTU^2/DU;
lamPX = states(:,16)*DUTU^2/DU;
lamPY = states(:,17)*DUTU^2/DU;
lamPZ = states(:,18)*DUTU^2/DU;

t = t/TU;
a = a*DU;

%%%%%%%%%%%%%%%%%%%%%%%%%%%%%%%%%%%%%%%%%%%%%%%%%%%%%%%%%%%%%%%%%%%%%%%%%%%%
%                      Plot final results                                    %
%%%%%%%%%%%%%%%%%%%%%%%%%%%%%%%%%%%%%%%%%%%%%%%%%%%%%%%%%%%%%%%%%%%%%%%%%%%%
%Plotting Code Omitted

%%%%%%%%%%%%%%%%%%%%%%%%%%%%%%%%%%%%%%%%%%%%%%%%%%%%%%%%%%%%%%%%%%%%%%%%%%%%
%%%%%%%%%%%%%%%%%%%%%%%%%%%%%%%%%%%%%%%%%%%%%%%%%%%%%%%%%%%%%%%%%%%%%%%%%%%%

function [lambda_initial,lambda_final,lam_f] = tpbvp(x,xref,lam_0,T)
%%%%%%%%%%%%%%%%%%%%%%%%%%%%%%%%%%%%%%%%%%%%%%%%%%%%%%%%%%%%%%%%%%%%%%%%%%%%
%tpbvp.m
%
%This script solves the two-point boundary value problem for
%the minimum control input to maintain circular formation for
%two satellites.  This script uses the "shooting" method to
%solve the two-point boundary value problem.
%
%1Lt Jason Baldwin
%27 Sep 06
%%%%%%%%%%%%%%%%%%%%%%%%%%%%%%%%%%%%%%%%%%%%%%%%%%%%%%%%%%%%%%%%%%%%%%%%%%%%
global k1 k2 k3 Rdes plot_optim output_optim mu X_bc
options = odeset('RelTol',1e-13,'AbsTol',1e-13);
itr = 0;
maxitr = 1e5;
e_tol = 5e-4;
eps = 3e-6;

%Display column headings for optimization output
if output_optim == 1
    fprintf(1, '\r\r%65s', 'OPTIMIZATION RESULTS')
    fprintf(1, '\r\r%23s %15s %15s %15s %15s %20s', ...
            'Final State','Satellite','Control','Cost Function',...
            'Jacobian','Final Boundary')
    fprintf(1, '\r%7s %15s %15s %15s %15s %15s %20s', ...
            'Iter','Difference','Separation','Magnitude','J',...
            'Min Singl Val','Conditions Error')
    fprintf(1, '\r%7s %15s %15s %15s %15s %15s %20s', ...
            '----','-----------','----------','---------',...
            '-------------','-------------','----------------')
end

while itr < maxitr

    %Propagate EOM to calculate the states and co-states
    x_0 = [xref' x' lam_0']';
    [t,states] = ode45(@states_eom,T,x_0,options);
    m = length(t);

    %Unpack the states for ease of calculations
```

```
Xref = states(:,1);
Yref = states(:,2);
Zref = states(:,3);
PXref = states(:,4);
PYref = states(:,5);
PZref = states(:,6);

X = states(:,7);
Y = states(:,8);
Z = states(:,9);
PX = states(:,10);
PY = states(:,11);
PZ = states(:,12);

lamX = states(:,13);
lamY = states(:,14);
lamZ = states(:,15);
lamPX = states(:,16);
lamPY = states(:,17);
lamPZ = states(:,18);

%Calculate the final conditions on the Lagrange Multipliers (LMs)
%Difference between final states and desired final states
lam_xf = 2*(X(m)-X_bc(1));
lam_yf = 2*(Y(m)-X_bc(2));
lam_zf = 2*(Z(m)-X_bc(3));
lam_pxf = 2*(PX(m)-X_bc(4));
lam_pyf = 2*(PY(m)-X_bc(5));
lam_pzf = 2*(PZ(m)-X_bc(6));
lam_f = k3*[lam_xf lam_yf lam_zf lam_pxf lam_pyf lam_pzf]';

%Calculate errors in final LMs
cur_lms = [lamX(m) lamY(m) lamZ(m) lamPX(m) lamPY(m) lamPZ(m)]';
cur_error = cur_lms - lam_f;

%Calculate the transition matrix (Jacobian)
for j=1:6
    temp = lam_0(j);
    delta_lam = eps*abs(temp);
    if delta_lam == 0
        delta_lam = eps;
    end
    lam_0(j) = temp + delta_lam;
    x_0 = [xref' x' lam_0']';
    [t,states] = ode45(@states_eom,T,x_0,options);
    new_lms = [states(m,13) states(m,14) states(m,15)...
               states(m,16) states(m,17) states(m,18)]';
    for i=1:6
        Jacb(i,j) = (new_lms(i) - cur_lms(i))/delta_lam;
    end
    lam_0(j) = temp;
end

%%%%%%%%%%%%%%%%%%%%%%%%%%%%%%%%
%Output the optimization results
%%%%%%%%%%%%%%%%%%%%%%%%%%%%%%%%
if output_optim == 1
    %Calculate the final state difference at final time
    dx = (X(m)-X_bc(1))^2;
    dy = (Y(m)-X_bc(2))^2;
    dz = (Z(m)-X_bc(3))^2;
```

```
        dpx = (PX(m)-X_bc(4))^2;
        dpy = (PY(m)-X_bc(5))^2;
        dpz = (PZ(m)-X_bc(6))^2;
        delta_state = k3*(dx+dy+dz+dpx+dpy+dpz);

        %Calculate the satellite separation and control magnitude
        delta_X = (X - Xref);
        delta_Y = (Y - Yref);
        delta_Z = (Z - Zref);
        ux = -lamPX/(2*k2);
        uy = -lamPY/(2*k2);
        uz = -lamPZ/(2*k2);
        for i=1:length(t)
            delta_r(i) = (norm([delta_X(i) delta_Y(i) delta_Z(i)]) - Rdes)^2;
            u_mag(i) = norm([ux(i) uy(i) uz(i)])^2;
        end
        delta_pos = k1*trapz(t,delta_r);
        u = k2*trapz(t,u_mag);

        %Output the results
        fprintf(1, '\r%7.0f %15.5e %15.5e %15.5e %15.5e %15.5e %20.5e', ...
                itr, delta_state, delta_pos, u, delta_state+delta_pos+u, ...
                max(svd(Jacb)), norm(cur_error))
    end

    %Compare errors with tolerance and break if within tolerance
    if norm(cur_error) < e_tol
        lambda_initial = lam_0;
        lambda_final = cur_lms;
        fprintf(1,'\r\rThe solution converged in %3d iterations.\r\r',itr)
        break;
    end

    %Choose change in final LMs that drives LMs to desired boundary
    %condition
    delta_mu = -eps*(cur_lms - lam_f);

    %Calculate the change in the initial LMs using Jacobian
    delta_lam_0 = inv(Jacb)*delta_mu;

    %Calculate the new initial guess for the LMs
    lam_0 = lam_0 + delta_lam_0;

    %Increase iteration count
    itr=itr+1;
end

if itr == maxitr
    fprintf(1,'\r\rThe maximum number of iterations were exceeded.\r\r')
end

%%%%%%%%%%%%%%%%%%%%%%%%%%%%%%%%%%%%%%%%%%%%%%%%%%%%%%%%%%%%%%%%%%%%%%%%%%%%%%%%
%%%%%%%%%%%%%%%%%%%%%%%%%%%%%%%%%%%%%%%%%%%%%%%%%%%%%%%%%%%%%%%%%%%%%%%%%%%%%%%%

function [xdot] = states_eom(t,state)
%%%%%%%%%%%%%%%%%%%%%%%%%%%%%%%%%%%%%%%%%%%%%%%%%%%%%%%%%%%%%%%%%%%%%%%%%%%%%%%%
%This function is called by ode45 to propagate the states of
%a satellite formation to include the reference satellite, the
%deputy satellite, and the lagrange multipliers determined by
%the specified performance index
%
```

```
%1Lt Jason Baldwin
%27 Sep 06
%%%%%%%%%%%%%%%%%%%%%%%%%%%%%%%%%%%%%%%%%%%%%%%%%%%%%%%%%%%%%%%%%%%%%%%


global k1 k2 Rdes optim_on control_on Re mu J2

%Unpack the state vector
Xref = state(1);
Yref = state(2);
Zref = state(3);
PXref = state(4);
PYref = state(5);
PZref = state(6);

X = state(7);
Y = state(8);
Z = state(9);
PX = state(10);
PY = state(11);
PZ = state(12);

lamX = state(13);
lamY = state(14);
lamZ = state(15);
lamPX = state(16);
lamPY = state(17);
lamPZ = state(18);

if optim_on == 0 && control_on == 0
    lamX = 0;
    lamY = 0;
    lamZ = 0;
    lamPX = 0;
    lamPY = 0;
    lamPZ = 0;
end

%Set the necessary Earth constants
if J2 == 0              %J2 perturbation constant
    J_2 = 0;
else
    J_2 = 0.00108263;
end

%Calculate the inertial position derivatives of reference satellite
xdot(1) = PXref;
xdot(2) = PYref;
xdot(3) = PZref;

%Calculate the inertial velocity derivatives of reference satellite
xdot(4) = 15*mu*J_2*Re^2*Xref*Zref^2/(2*(Xref^2+Yref^2+Zref^2)^(7/2))...
          - 3*mu*J_2*Re^2*Xref/(2*(Xref^2+Yref^2+Zref^2)^(5/2))...
          - mu*Xref/((Xref^2+Yref^2+Zref^2)^(3/2));
xdot(5) = 15*mu*J_2*Re^2*Yref*Zref^2/(2*(Xref^2+Yref^2+Zref^2)^(7/2))...
          - 3*mu*J_2*Re^2*Yref/(2*(Xref^2+Yref^2+Zref^2)^(5/2))...
          - mu*Yref/((Xref^2+Yref^2+Zref^2)^(3/2));
xdot(6) = 15*mu*J_2*Re^2*Zref^3/(2*(Xref^2+Yref^2+Zref^2)^(7/2))...
          - 9*mu*J_2*Re^2*Zref/(2*(Xref^2+Yref^2+Zref^2)^(5/2))...
          - mu*Zref/((Xref^2+Yref^2+Zref^2)^(3/2));
```

```
%Calculate the inertial position derivatives of deputy satellite
xdot(7) = PX;
xdot(8) = PY;
xdot(9) = PZ;

%Calculate the inertial velocity derivatives of deputy satellite
xdot(10) = 15*mu*J_2*Re^2*X*Z^2/(2*(X^2+Y^2+Z^2)^(7/2))...
          - 3*mu*J_2*Re^2*X/(2*(X^2+Y^2+Z^2)^(5/2))...
          - mu*X/((X^2+Y^2+Z^2)^(3/2))...
          - lamPX/(2*k2);
xdot(11) = 15*mu*J_2*Re^2*Y*Z^2/(2*(X^2+Y^2+Z^2)^(7/2))...
          - 3*mu*J_2*Re^2*Y/(2*(X^2+Y^2+Z^2)^(5/2))...
          - mu*Y/((X^2+Y^2+Z^2)^(3/2))...
          - lamPY/(2*k2);
xdot(12) = 15*mu*J_2*Re^2*Z^3/(2*(X^2+Y^2+Z^2)^(7/2))...
          - 9*mu*J_2*Re^2*Z/(2*(X^2+Y^2+Z^2)^(5/2))...
          - mu*Z/((X^2+Y^2+Z^2)^(3/2))...
          - lamPZ/(2*k2);

%Calculative the time derivatives of the lagrange multipliers
xdot(13) = -2*k1*(X-Xref)*(sqrt((X-Xref)^2+(Y-Yref)^2+(Z-Zref)^2)-Rdes)/...
               sqrt((X-Xref)^2+(Y-Yref)^2+(Z-Zref)^2)...
            - lamPX*(3*X^2*mu/((X^2+Y^2+Z^2)^(5/2))...
               - mu/((X^2+Y^2+Z^2)^(3/2))...
               - 105*X^2*Z^2*Re^2*mu*J_2/(2*(X^2+Y^2+Z^2)^(9/2))...
               + 15*X^2*Re^2*mu*J_2/(2*(X^2+Y^2+Z^2)^(7/2))...
               + 15*Z^2*Re^2*mu*J_2/(2*(X^2+Y^2+Z^2)^(7/2))...
               - 3*Re^2*mu*J_2/(2*(X^2+Y^2+Z^2)^(5/2)))...
            - lamPY*(3*X*Y*mu/((X^2+Y^2+Z^2)^(5/2))...
               - 105*X*Y*Z^2*Re^2*mu*J_2/(2*(X^2+Y^2+Z^2)^(9/2))...
               + 15*X*Y*Re^2*mu*J_2/(2*(X^2+Y^2+Z^2)^(7/2)))...
            - lamPZ*(3*X*Z*mu/((X^2+Y^2+Z^2)^(5/2))...
               - 105*X*Z^3*Re^2*mu*J_2/(2*(X^2+Y^2+Z^2)^(9/2))...
               + 45*X*Z*Re^2*mu*J_2/(2*(X^2+Y^2+Z^2)^(7/2)));

xdot(14) = -2*k1*(Y-Yref)*(sqrt((X-Xref)^2+(Y-Yref)^2+(Z-Zref)^2)-Rdes)/...
               sqrt((X-Xref)^2+(Y-Yref)^2+(Z-Zref)^2)...
            - lamPY*(3*Y^2*mu/((X^2+Y^2+Z^2)^(5/2))...
               - mu/((X^2+Y^2+Z^2)^(3/2))...
               - 105*Y^2*Z^2*Re^2*mu*J_2/(2*(X^2+Y^2+Z^2)^(9/2))...
               + 15*Y^2*Re^2*mu*J_2/(2*(X^2+Y^2+Z^2)^(7/2))...
               + 15*Z^2*Re^2*mu*J_2/(2*(X^2+Y^2+Z^2)^(7/2))...
               - 3*Re^2*mu*J_2/(2*(X^2+Y^2+Z^2)^(5/2)))...
            - lamPX*(3*X*Y*mu/((X^2+Y^2+Z^2)^(5/2))...
               - 105*X*Y*Z^2*Re^2*mu*J_2/(2*(X^2+Y^2+Z^2)^(9/2))...
               + 15*X*Y*Re^2*mu*J_2/(2*(X^2+Y^2+Z^2)^(7/2)))...
            - lamPZ*(3*Y*Z*mu/((X^2+Y^2+Z^2)^(5/2))...
               - 105*Y*Z^3*Re^2*mu*J_2/(2*(X^2+Y^2+Z^2)^(9/2))...
               + 45*Y*Z*Re^2*mu*J_2/(2*(X^2+Y^2+Z^2)^(7/2)));

xdot(15) = -2*k1*(Z-Zref)*(sqrt((X-Xref)^2+(Y-Yref)^2+(Z-Zref)^2)-Rdes)/...
               sqrt((X-Xref)^2+(Y-Yref)^2+(Z-Zref)^2)...
            - lamPZ*(3*Z^2*mu/((X^2+Y^2+Z^2)^(5/2))...
               - mu/((X^2+Y^2+Z^2)^(3/2))...
               - 105*Z^4*Re^2*mu*J_2/(2*(X^2+Y^2+Z^2)^(9/2))...
               + 45*Z^2*Re^2*mu*J_2/((X^2+Y^2+Z^2)^(7/2))...
               - 9*Re^2*mu*J_2/(2*(X^2+Y^2+Z^2)^(5/2)))...
            - lamPX*(3*X*Z*mu/((X^2+Y^2+Z^2)^(5/2))...
               - 105*X*Z^3*Re^2*mu*J_2/(2*(X^2+Y^2+Z^2)^(9/2))...
               + 45*X*Z*Re^2*mu*J_2/(2*(X^2+Y^2+Z^2)^(7/2)))...
            - lamPY*(3*Y*Z*mu/((X^2+Y^2+Z^2)^(5/2))...
```

```
                - 105*Y*Z^3*Re^2*mu*J_2/(2*(X^2+Y^2+Z^2)^(9/2))...
                + 45*Y*Z*Re^2*mu*J_2/(2*(X^2+Y^2+Z^2)^(7/2)));

xdot(16) = -lamX;
xdot(17) = -lamY;
xdot(18) = -lamZ;

xdot = xdot';

%%%%%%%%%%%%%%%%%%%%%%%%%%%%%%%%%%%%%%%%%%%%%%%%%%%%%%%%%%%%%%%%%%%%%%%%%%%%%%%%
%%%%%%%%%%%%%%%%%%%%%%%%%%%%%%%%%%%%%%%%%%%%%%%%%%%%%%%%%%%%%%%%%%%%%%%%%%%%%%%%

function [C] = rel_to_inert(inertial_vec)
%This function takes as input a position/velocity (6x1) vector of a
%reference trajectory in inertial coordinates and calcuates the
%transformation matrix (C) for a relative-to-inertial transformation.
%Since the transformation matrix is orthonormal, the inertial-to-relative
%transformation is just the transpose of C.  This transformation matrix
%is valid for both elliptical and circular motion of the reference
%trajectory.

%Unpack the inertial vector
X = inertial_vec(1);
Y = inertial_vec(2);
Z = inertial_vec(3);
PX = inertial_vec(4);
PY = inertial_vec(5);
PZ = inertial_vec(6);

rvec = [X; Y; Z];
rdotvec = [PX; PY; PZ];

%Elliptical/Circular reference motion transformation
x_hat = [X/norm(rvec); Y/norm(rvec); Z/norm(rvec)];
y_hat_p = [PX/norm(rdotvec); PY/norm(rdotvec); ...
           PZ/norm(rdotvec)];
z_hat = cross(x_hat,y_hat_p);
y_hat = cross(z_hat,x_hat);

C = [x_hat y_hat z_hat];

%%%%%%%%%%%%%%%%%%%%%%%%%%%%%%%%%%%%%%%%%%%%%%%%%%%%%%%%%%%%%%%%%%%%%%%%%%%%%%%%
%%%%%%%%%%%%%%%%%%%%%%%%%%%%%%%%%%%%%%%%%%%%%%%%%%%%%%%%%%%%%%%%%%%%%%%%%%%%%%%%
```

Bibliography

1. Alfriend, K. T., & Schaub, H. (2000). Dynamics and Control of Spacecraft Formations: Challenges and Some Solutions. *Advances in the Astronautical Sciences, 106*, 205-223.

2. Biggs, J. D., Becerra, V. M., Nasuto, S. J., Ruiz, V. F., & Holderbaum, W. (2005). *A Search for Invariant Relative Satellite Motion.* Contract 18875/05/NL/MV. Department of Cybernetics, The University of Reading, European Space Agency Advanced Concepts Team

3. Bryson, A. E., & Ho, Y. (1969). *Applied Optimal Control; Optimization, Estimation, and Control*. Columbus, Ohio: Ginn & Co.

4. Burns, R., McLaughlin, C. A., Leitner, J., & Martin, M. (2000). TechSat 21: Formation Design, Control, and Simulation. *2000 IEEE Aerospace Conference, Mar 18-25 2000,* 19-25.

5. Clohessy, W. H., & Wiltshire, R. S. (1960). Terminal Guidance System for Satellite Rendezvous. *Journal of the Aerospace Sciences, 27*(9), 653-658.

6. Gelfand, I. M., & Fomin, S. V. (1963). *Calculus of Variations* (Rev. English ed.). Englewood Cliffs, N.J.: Prentice-Hall.

7. Hill, G. W. (1878). Researches in the Lunar Theory. *American Journal of Mathematics, Vol. 1*(No. 1), 5-26.

8. Kasdin, N. J., & Gurfil, P. (2003). Canonical Modelling of Relative Spacecraft Motion Via Epicyclic Orbital Elements. *AIAA Guidance, Navigation, and Control Conference and Exhibit; Austin, TX; USA; 11-14 Aug. 2003, AIAA Paper 2003-5591*

9. Kechichian, J. A. (1998). Motion in General Elliptic Orbit with Respect to a Dragging and Precessing Coordinate Frame. *Journal of the Astronautical Sciences, 46*(1), 25-45.

10. Lewis, F. L., & Syrmos, V. L. (1995). *Optimal Control* (2nd ed.). New York: Wiley.

11. Lovell, T. A., & Tragesser, S. G. (2004). Guidance for Relative Motion of Low Earth Orbit Spacecraft Based on Relative Orbit Elements. *Collection of Technical Papers - AIAA/AAS Astrodynamics Specialist Conference, Aug 16-19 2004, 2,* 644-658.

12. Martin, M., & Kilberg, S. (2001). TechSat 21 and Revolutionizing Space Missions Using Microsatellites. *Fifteenth AIAA/USU Conference on Small Satellites, Logan, UT; UNITED STATES; 13-16 Aug. 2001*

13. Meirovitch, L. (1970). *Methods of Analytical Dynamics*. New York: McGraw-Hill.

14. Miller, D. W., & Sedwick, R. J. (2001). *Grand Challenges in Space Technology: Distributed Satellite Systems*. Massachusetts Inst of Tech, Cambridge Space Systems Lab.

15. Sabol, C., Burns, R., & McLaughlin, C. A. (2001). Satellite Formation Flying Design and Evolution. *Journal of Spacecraft and Rockets, 38*(2), 270-278.

16. Schaub, H., & Alfriend, K. T. (2001). J_2-invariant Relative Orbits for Spacecraft Formations. *Celestial Mechanics and Dynamical Astronomy, 79*(2), 77-95.

17. Schaub, H., Vadali, S. R., Junkins, J. L., & Alfriend, K. T. (2001). Spacecraft Formation Flying Control Using Mean Orbit Elements. *Journal of the Astronautical Sciences, 48*(1), 69-87.

18. Schweighart, S. A., & Sedwick, R. J. (2002). High-fidelity Linearized J_2 Model for Satellite Formation Flight. *Journal of Guidance, Control, and Dynamics, 25*(6), 1073-1080.

19. Sedwick, R. J., Kong, E. M. C., & Miller, D. W. (1998). Exploiting Orbital Dynamics and Micropropulsion for Aperture Synthesis Using Distributed Satellite Systems - Applications to TechSat 21. *AIAA Paper 1998-5289*

20. Sparks, A. (2000). Satellite Formationkeeping Control in the Presence of Gravity Perturbations. *2000 American Control Conference, Jun 28-Jun 30 2000,* 844-848.

21. Vadali, S. R., Schaub, H., & Alfriend, K. T. (1999). Initial Conditions and Fuel-optimal Control for Formation Flying of Satellites. *AIAA Paper 1999-4265*

22. Vallado, D. A., & McClain, W. D. (1997). *Fundamentals of Astrodynamics and Applications*. New York: The McGraw-Hill Companies, Inc.

23. Wiesel, W. E. (2002). Relative Satellite Motion About an Oblate Planet. *Journal of Guidance, Control, and Dynamics, 25*(4), 776-785.

REPORT DOCUMENTATION PAGE

Form Approved
OMB No. 074-0188

1. REPORT DATE *(DD-MM-YYYY)*	2. REPORT TYPE	3. DATES COVERED *(From – To)*
22-03-2007	Master's Thesis	June 2006 – March 2007

4. TITLE AND SUBTITLE

Optimal Control of a Circular Satellite Formation Subject to Gravitational Perturbations

5a. CONTRACT NUMBER

5b. GRANT NUMBER

5c. PROGRAM ELEMENT NUMBER

6. AUTHOR(S)

Baldwin, Jason L., Captain, USAF

5d. PROJECT NUMBER

5e. TASK NUMBER

5f. WORK UNIT NUMBER

7. PERFORMING ORGANIZATION NAMES(S) AND ADDRESS(S)

Air Force Institute of Technology
Graduate School of Engineering and Management (AFIT/EN)
2950 Hobson Way, Building 640
WPAFB OH 45433-7765

8. PERFORMING ORGANIZATION REPORT NUMBER

AFIT/GA/ENY/07-M02

9. SPONSORING/MONITORING AGENCY NAME(S) AND ADDRESS(ES)

N/A

10. SPONSOR/MONITOR'S ACRONYM(S)

11. SPONSOR/MONITOR'S REPORT NUMBER(S)

12. DISTRIBUTION/AVAILABILITY STATEMENT

APPROVED FOR PUBLIC RELEASE; DISTRIBUTION UNLIMITED.

13. SUPPLEMENTARY NOTES

14. ABSTRACT

Satellite formations, otherwise known in the space community as satellite clusters or distributed satellite systems, have been studied extensively over the last 10 to 15 years. For use in remote sensing applications, formations consisting of smaller, simpler satellites provide numerous advantages over individual satellites. The image resolution capabilities of small-satellite formations constitute a significant technological leap in the ability to synthesize critical information. This research utilizes the nonlinear satellite dynamics, including gravitational perturbations, to search for the optimal fuel cost for maintaining a circular formation. The system dynamics were developed in an earth-centered inertial coordinate frame using the methods of Hamiltonian dynamics. Continuous dynamic optimization theory was used to minimize fuel requirements, resulting in a continuous thrust, open-loop control law. The uncontrolled reference trajectory off which the formation is based was restricted to a circular, inclined orbit. Given initial conditions which match the mean motion of every member of the formation, it is shown that 1-km circular formation configurations can be maintained for control costs on the order of 40-50 m/s/year at an altitude of 400 km. Additionally, further fuel savings are possible with modifications to orbit altitude, formation radius, and variations in the defined performance index.

15. SUBJECT TERMS

Satellites(Artificial); Formations; Control; Hamiltonian Function

16. SECURITY CLASSIFICATION OF: U			17. LIMITATION OF ABSTRACT	18. NUMBER OF PAGES	19a. NAME OF RESPONSIBLE PERSON
a. REPORT	b. ABSTRACT	c. THIS PAGE			Titus, Nathan A., Lt Col, ENY
U	U	U	UU	112	19b. TELEPHONE NUMBER *(Include area code)* (937) 255-3636, ext 7469 (nathan.titus@afit.edu)